## NOTICE

The quality of this microform is heavily dependent upon the quality of the original thesis submitted for microfilming. Every effort has been made to ensure the highest quality of reproduction possible.

If pages are missing, contact the university which granted the degree.

Some pages may have indistinct print especially if the original pages were typed with a poor typewriter ribbon or if the university sent us an inferior photocopy.

Reproduction in full or in part of this microform is governed by the Canadian Copyright Act, R.S.C. 1970, c. C-30, and subsequent amendments.

## AVIS

La qualité de cette microforme dépend grandement de la qualité de la thèse soumise au microfilmage. Nous avons tout fait pour assurer une qualité supérieure de reproduction.

S'il manque des pages, veuillez communiquer avec l'université qui a conféré le grade.

La qualité d'impression de certaines pages peut laisser à désirer, surtout si les pages originales ont été dactylographiées à l'aide d'un ruban usé ou si l'université nous a fait parvenir une photocopie de qualité inférieure.

La reproduction, même partielle, de cette microforme est soumise à la Loi canadienne sur le droit d'auteur, SRC 1970, c. C-30, et ses amendements subséquents.



Canada

# Advances in PATH LOSS Algorithm in the Antenna-to-Antenna Propagation with Graphics (AAPG) EMC Analysis Program

Marc J.L. Drolet

A Thesis

in

The Department

of

Electrical and Computer Engineering

Presented in Partial Fulfillment of the Requirements
for the Degree of Master of Engineering at
Concordia University
Montreal, Quebec, Canada

August 1989

ISBN 0-315-51361-6

**ABSTRACT**

**Advances in PATH LOSS Algorithm in
The Antenna-to-Antenna Propagation with Graphics (AAPG)
EMC Analysis Program**

Marc J.L. Drolet

This thesis deals with Electromagnetic Compatibility (EMC) on aircraft. Due to the very high number of emitting and recepting systems on board aircraft, it is of prime importance to design and utilize computer codes which will help EMC Engineers ensure the compatibility of all systems.

These computer programs must be subject to constant review in order to ensure that the latest algorithms and mathematical formulations are utilized. With the increasing complexity of airframes, the review of the EMC softwares become vital for the survival of test pilots and the development projects.

This thesis provides a description of one very important EMC computer code, AAPG, and introduces new algorithms which enhance the precision of the numbers presented to the EMC analysts. Each of the five improvement areas are supported by comparison data and examples of path changes which provide a full appreciation of the modification results.

**Acknowledgements**

I wish to thank Dr. S. Kubina, my supervisor, for his guidance in selecting the topic, providing challenging discussions and for his precious encouragements.

I am also indebted to Dr. C. Trueman, Mr. Deboroto Chatterjee and Mr. Tom Roobereck for the many enlightening discussions which greatly helped in the advancement of this task.

Sincere appreciation is also extended to Mr. David Gaudine and Mr. Mike Marak for their guidance in the system software implementation and hardware hook-ups necessary to run the codes.

My appreciation must also be extended to all the members of the Concordia University EMC laboratory for their friendship and for sharing the pressure and the fun throughout the program, in particular Mr. Vincenzo Tarantino and Constinos Christopoulos for their assistance in the software validation and the selection of the software to type the formulas.

Finally, I must very particularly thank Mrs. Patricia Kierans for her invaluable assistance in typing this thesis and for her support she gave me during my stay at Concordia University.

# TABLE OF CONTENTS


| | | | Page |
|---|---|---|---|
| Abstract | | | iii |
| Acknowledgements | | | iv |
| Table of Contents | | | v |
| List of Figures | | | viii |
| List of Tables | | | xii |
| CHAPTER 1. | | INTRODUCTION | 1 |
| | 1.1 | General Overview | 1 |
| | 1.2 | Philosophy of Software Analysis | 2 |
| | 1.3 | Scope of the Thesis | 3 |
| | 1.4 | Main Contribution of the Work | 5 |
| CHAPTER 2. | | GTD THEORY | 6 |
| | 2.1 | Historic Data | 6 |
| | 2.2 | Geometrical Theory of Diffraction | 8 |
| | 2.3 | Asymptotic Solution of Maxwell's Equations | 12 |
| | 2.4 | Reflection | 19 |
| | 2.5 | Diffraction | 20 |
| | 2.6 | Edge Diffraction | 25 |
| | 2.7 | Surface Shading | 30 |
| | 2.8 | UTD Convex Surface Diffraction | 35 |
| CHAPTER 3. | | ANTENNA TO ANTENNA PROPAGATION WITH GRAPHICS (AAPG) | 45 |

3.1 Introduction . . . . . 45

3.2 Structure of AAPG . . . . . 46

3.3 Input Data File . . . . . 48

3.4 Parameters Computation . . . . . 51

3.5 Using AAPG . . . . . 53

3.6 Validation . . . . . 58

CHAPTER 4. WING DIFFRACTION POINT IMPROVEMENT . . 64

4.1 Introduction . . . . . 64

4.2 Modified Wing Edge Diffraction Point Algorithm . . . . . 66

4.3 Results . . . . . 72

4.4 Summary . . . . . 74

CHAPTER 5. CYLINDRICAL/CONICAL SPIRAL INTERCEPTION POINT . . . . . 83

5.1 Introduction . . . . . 83

5.2 Formal Versus New Approach . . . . . 84

5.3 Optimization Technique . . . . . 86

5.4 Results . . . . . 86

5.5 Validity . . . . . 87

CHAPTER 6. PATH IMPROVEMENT IN THE CONE REGION . . . . . 92

6.1 Introduction . . . . . 92

6.2 Line of Sight Verification . . . . . 94

6.3 Results . . . . . 101

6.4 Path Intercepting Fuselage Geometry . 101

6.5 Path Improvement . . . . . 107

CHAPTER 7. CONICAL PATH DISTANCE CALCULATION IMPROVEMENT . . . . . 113

| | | |
|---|---|---|
| 7.1 | Introduction | 113 |
| 7.2 | Geodesic Deviation Using 2-D Mapping | 114 |
| 7.3 | Durface of Revolution | 116 |
| 7.4 | Mathematical Formulation | 118 |
| 7.5 | Software Implementation | 120 |
| 7.6 | Results | 121 |
| CHAPTER 8. | CONICAL SPIRAL SHADING CALCULATION | 125 |
| 8.1 | Introduction | 125 |
| 8.2 | Arbitrary Curved Surface Diffraction Loss | 126 |
| 8.3 | The Ray Curvature on a Cone | 131 |
| 8.4 | New Conical Spiral Loss Implementation | 134 |
| 8.5 | Conical Spiral Shading Results | 135 |
| CHAPTER 9. | SUMMARY AND CONCLUSION | 142 |
| 9.1 | Summary and Conclusion | 142 |
| 9.2 | Suggestions for Future Work | 144 |
| BIBLIOGRAPHY | | 146 |
| APPENDIX A | Flowchart Subroutine WNGEDG | 151 |
| APPENDIX B | Modified Subroutine WNGEDG Listing. | 153 |
| APPENDIX C | Conical/Cylindrical Spiral Cross Over Point Improvement Flowchart | 158 |
| APPENDIX D | Conical/Cylindrical Spiral Modification Listing | 159 |
| APPENDIX E | Subroutine CONINT Flowchart | 160 |
| APPENDIX F | Subroutine CONE Listing | 161 |
| APPENDIX G | Conical Spiral Distance Calculation | 163 |
| APPENDIX H | Subroutine DCON Listing | 164 |
| APPENDIX J | Conical Shading Flowchart | 166 |
| APPENDIX K | Subroutine Loss Listing | 167 |

## LIST OF FIGURES


| Figure | | Page |
|---|---|---|
| 2.1 | The Eikonal of a Ray System | 10 |
| 2.2 | Incident, Reflected and Diffracted Rays | 11 |
| 2.3 | A Smooth Curved Surface Near The Point P | 23 |
| 2.4 | Locus of the Rays Diffracted by a Wedge | 25 |
| 2.5 | Edge Diffraction Angles | 30 |
| 2.6 | Surface Shading | 31 |
| 2.7 | Surface Shading Source Location | 32 |
| 2.8 | Incident, Reflected and Diffracted Field | 37 |
| 2.9 | Plots of Transition Functions | 40 |
| 3.1 | Structure of AAPG | 48 |
| 3.2 | Interference Interaction Reduction | 49 |
| 3.3 | AAPG Coordinate System | 50 |
| 3.4 | AAPG Menus | 55 |
| 3.5 | Frequency Coincidence Data Summary | 59 |
| 3.6a | Frequency Coincidence Path Plot | 60 |
| 3.6b | Data Plot/Power vs Frequency | 60 |
| 3.7a | Antenna Location Diagram | 61 |
| 3.7b | Antenna Pattern Diagram | 61 |
| 3.8 | EMI Margin | 62 |
| 3.9 | Antenna Positioning Input | 62 |
| 3.10 | New EMI Margin | 63 |
| 3.11 | Quantitative KC-135B Aircraft Validation of the Free-Space and Curved-Surface Losses Computed by AAPG | 63 |

4.1 Unmodified Path - Top View . . . . . 75

4.2 Major Points Identification . . . . . 75

4.3 Modified Path - Top View . . . . . 76

4.4 Unmodified Path - Left Wing Case . . . . . 76

4.5 Unmodified Path - Left Wing Case - All View . . 77

4.6 Modified Path - Left Wing Case . . . . . 77

4.7 Modified Path - Left Wing Case - All View . . . 78

4.8 Unmodified Path - Right Wing Case . . . . . 78

4.9 Unmodified Path - Right Wing Case - All View . . 79

4.10 Modified Path - Right Wing Case . . . . . 79

4.11 Modified Path - Right Wing Case - All View . . . 80

4.12 Unmodified Path - Different Wing Edge Case . . . 80

4.13 Unmodified Path - Different Wing Edge Case - All View . . . . . 81

4.14 Modified Path - Different Wing Edge Case . . . . 81

4.15 Modified Path - Different Wing Edge Case - All View . . . . . 82

5.1 Cross Point Approximation . . . . . 85

5.2 Unmodified Path EMI . . . . . 88

5.3 Modified Path EMI . . . . . 88

5.4 Unmodified Path - All View . . . . . 89

5.5 Modified Path - All View . . . . . 89

5.6 Unmodified Path EMI . . . . . 90

5.7 Modified Path EMI . . . . . 90

5.8 Unmodified Path - All View . . . . . 91

5.9 Modified Path - All View . . . . . 91

6.1 Demonstration of Incorrect Algorithm . . . . . 93

6.2 Incorrect Algorithm - All View . . . . . 94

| | | |
|---|---|---|
| 6.3 | Cone Coordinates | 96 |
| 6.4 | Intercept Line | 96 |
| 6.5 | The Intercept Line on the Y Axis | 98 |
| 6.6 | Line of Sight Modified Path | 99 |
| 6.7 | Line of Sight Modified Path - All View | 99 |
| 6.8 | Unmodified Path | 100 |
| 6.9 | Modified Path | 100 |
| 6.10 | Tangent Points Angle Definitions | 103 |
| 6.11 | Cone Radius Calculation - Side View | 105 |
| 6.12 | Unmodified Path - Case 1 | 108 |
| 6.13 | Unmodified Path - Case 1 - All View | 109 |
| 6.14 | Modified Path - Case 1 | 109 |
| 6.15 | Modified Path - Case 1 - All View | 110 |
| 6.16 | Unmodified Path - Case 2 | 110 |
| 6.17 | Unmodified Path - Case 2 - All View | 111 |
| 6.18 | Modified Path - Case 2 | 111 |
| 6.19 | Modified Path - Case 2 - All View | 112 |
| 7.1 | Cylinder Developed Into a Rectangular Plane | 115 |
| 7.2 | Cone and Its Unrolled Plane | 116 |
| 7.3 | Side View of a Three-Dimensional Cone Illustrating the Nose of an Aircraft | 117 |
| 7.4 | The Three-Dimensional Cone Mapped Into Two-Dimensions | 118 |
| 7.5 | Conical Spiral Distance Comparison | 123 |
| 7.6 | Front View of a Conical Spiral Path | 123 |
| 7.7 | Conical Spiral | 124 |
| 8.1 | Geodesic on a Convex Surface | 129 |
| 8.2 | 3-D and Developed Cone | 132 |

| | | |
|---|---|---|
| 8.3 | Coupling Coefficient S., Between Two Circumferential Slots on a Cone as a Function of Frequency . . . . . | 137 |
| 8.4 | Unmodified Path - Case 1 . . . . . | 137 |
| 8.5 | Modified Path - Case 1 . . . . . | 138 |
| 8.6 | Conical Path - Case 1 - All View . . . . . | 138 |
| 8.7 | Unmodified Path - Case 2 . . . . . | 139 |
| 8.8 | Modified Path - Case 2 . . . . . | 139 |
| 8.9 | Conical Path - Case 2 - All View . . . . . | 140 |
| 8.10 | Unmodified Path - Case 3 . . . . . | 140 |
| 8.11 | Modified Path - Case 3 . . . . . | 141 |
| 8.12 | Conical Path - Case 3 - All View . . . . . | 142 |

# LIST OF TABLES

Page

2.1 Transition Function Values . . . . . 29

# CHAPTER I

# INTRODUCTION

## 1.1 General Overview

The number and the increasing complexity and density of electronic systems have placed special demands upon those responsible for achieving electromagnetic compatibility (EMC) within the host weapon platforms. Aircraft are prime examples of where the systems' density has reached a dangerous level making the platforms vulnerable to electromagnetic interference (EMI).

Many lives have been lost due to EMI. The Black Hawk Helicopters incidents [1] where 22 American servicemen lost their lives in five crashes directly attributed to EMI, is an astonishing example of EMC related problems.

The achievement of EMC means that equipments, subsystems and the complete system, perform in their operational electromagnetic environment at design levels of efficiency, without causing or suffering unacceptable degradation due to EMI.

The process of achieving EMC requires careful attention to potential EMI problems at the design stage and throughout

the life cycle of the system or platform.

The high complexity along with the increasing number of systems on board the aircraft, force the engineering staff to develop tools such as computer codes to assist them in the verification of EMC.

## 1.2 Philosophy of Software Analysis

There are several problems associated with ensuring systems compatibility on board an electronic platform. In addition to the high cost of EMC tests and to the fact that problems are frequently identified too late in a program, the methods utilized for EMC analysis do not account for the amount of energy coupled between equipments on the system and cannot provide the engineering staff with a precise electromagnetic path between these equipments [2].

Systematic and orderly software analysis is vital to anticipate EMC problems and to efficiently solve them [3]. During the design and test phase of any platform containing numerous electronic systems, a complete EMC analysis must become mandatory in order to calculate with precision the electromagnetic fields propagating between systems and to provide a graphical view of the coupling path.

The quality of the work to effectuate the EMC analysis

will depend on the exactness of all calculations and the accuracy of the electromagnetic paths provided to the EMC engineers.

For these reasons, it becomes of utmost importance to revise and update the computer codes so as to meet the challenge of changing technology and to provide those responsible for systems compatibility with reliable tools.

## 1.3 Scope of the Thesis

In this thesis one of the valuable computer codes will be considered, the Antenna-To-Antenna Propagation with Graphics (AAPG), which uses the potential of interactive computer graphics to present EMI margins between systems on aircraft.

In Chapter 2 the concept used within the code, the Geometrical Theory of Diffraction (GTD), is reviewed. This is fundamental to the study since all electromagnetic field loss calculation is based on GTD. The complete development of the key mathematical formulation is covered, to obtain a full understanding of the most recent approach to field calculation.

In Chapter 3 an overview of the computer code AAPG is presented. A description of the software program structure

along with an operational approach is provided. Chapter 4 shows an area of difficulty experienced with AAPG where the code cannot locate the optimum wing diffraction point whenever a propagation path intercepts a wing structure. A refinement technique which will provide a better edge diffraction point is considered, and the validity shown with examples.

Chapter 5 concentrates on propagation paths between two antennas which are located on the two different structures forming the body of the aircraft, the cylindrical and the conical geometry. It will be shown that the cross-over-point, on the line separating the cylinder and the cone, does not provide the user with the shortest path. An iterative technique is presented along with examples of the improvement.

Chapter 6 analyzes the behaviour of the electromagnetic path between antennas located on or around the conical portion of the airframe. The difficulty that the present version of AAPG experiences in dealing with such cases will be covered. A new approach in the determination of the path algorithm is introduced which illustrates the improvement supported by examples.

Chapter 7 covers the calculation of the conical path distances. A study of the present version method to

evaluate the distance of conical spirals show that it will not provide the users with the true geodesic measurements. A new algorithm and examples of improvements are introduced.

Chapter 8 evaluates the way AAPG effectuates the electromagnetic shading loss calculation. A state-of-the-art approach to evaluate shading loss on the cone is developed. This technique is implemented in the code and examples of this improvement are documented.

Chapter 9 summarizes the thesis work and suggests ideas for further work in order to improve a unique tool precious to the industry.

## 1.4 Main Contribution of the Work

The Canadian Defence Department and the United States Department of Defence both have recognized the high value of AAPG. The code is extensively utilized and constant revision of the algorithms is necessary in order to provide the users with an accurate tool.

The improvement presented in this work is being processed in new versions of the code which will be introduced to both Defence Departments and industry thus giving the EMC Engineering staff a better tool to accomplish their vital analysis.

# CHAPTER 2

# GTD THEORY

## 2.1 Historic Data

It was Maxwell who showed before 1873 that the propagation of light could be viewed as an electromagnetic phenomenon. Since the wavelength of light waves is usually small compared to objects with which it interacts, the analytical treatment of light wave propagation is much different than that employed to analyze lower frequency propagation where the size of a scattering surface is comparable to the wavelength.

The problem of observing systems on board aircraft is the treatment of electromagnetic problems, for situations where the wavelength is small compared to the geometrical dimensions of the scatterer. In such cases high-frequency methods must be employed since it is not practical to use moment methods or eigen function expansions. This is due to the poor rate of convergence of both of these techniques when dealing with an electrically large scatterer [4].

The Geometrical Theory of Diffraction which has its origin in Geometrical optics or ray optics can better be understood by an analysis of its position in the historical context of high frequency solutions.

It was known long before the 1800's that light propagated from the source to the eye. The laws of reflection and refraction were also known in the 1600's with the work from Fermat and in the early 1800's with Young's publications. In fact, Young's diffraction experiments were the first attempt to explain diffraction by means of rays.

However, it was not until Maxwell gathered together the vector field equations and the scientist began to integrate them with the Helmholtz wave equation, that the true nature of high frequency radiation was understood.

After 1864 when Maxwell demonstrated the existence of an electromagnetic wave and in 1887 when Hertz experimentally verified the existence of the electromagnetic wave predicted by Maxwell, the work in high frequency phenomena accelerated.

In 1896 Sommerfeld published his classic work on diffraction by a half plane screen. Soon after, in 1938 Pauli extended Sommerfeld's solution to a satisfactory asymptotic expression of the diffraction from a wedge. It

represents an improvement over Summerfeld's expression in that it can be made finite at transition boundaries.

Starting in approximately 1950 Keller developed the so called Geometrical Theory of Diffraction as a natural extension of Geometrical Optics. However, his diffraction coefficients suffered, as did Summerfelds' asymptotic expression from singularities at boundaries.

Subsequently, in around 1970, Kouyoumjian generalized the results of Pauli to develop the modern G.T.D. or the "Uniform Geometric Theory of Diffraction" which is commonly utilized presently. Keller's work [5] and Kouyoumjian's improvements [7] are summarized in the next section. A study of the GTD formulation must be done in order to evaluate the "shading" effect in AAPG.

## 2.2 Geometrical Theory of Diffraction (GTD)

The Geometrical Theory of Diffraction conceived by J.B. Keller in the 1950's is an analytical technique in the prediction of high frequency diffraction phenomena.

Basically, GTD is an extension of Geometrical Optics by the inclusion of additional diffracted rays to describe the diffracted field [5].

The diffraction coefficient is introduced in the geometrical theory of diffraction in order to relate the field of the ray incident at the edge to the field of the edge diffracted ray.

The diffraction coefficient is analogous to the reflection coefficient used to relate incident and reflected fields. This diffraction coefficient is found from an asymptotic solution to the pertinent diffraction problem.

The fundamental of geometrical optics on which GTD is based, is that light propagation is a local phenomenon due to the very short wavelength of light.

Geometrical optics, although dealing with polarization and phase information is unable to handle the intensity of reflected and refracted rays at boundaries.

In a homogeneous medium, light energy moves along ray paths that are straight lines. Normal to these ray paths are a family of surfaces called the "eikonal" of the ray system. For a plane wave the eikonal surfaces are planes perpendicular to the ray paths as shown in Figure 2.1. For a spherical source the eikonal surfaces are spherical surfaces perpendicular to the ray paths as shown in Figure 2.1.

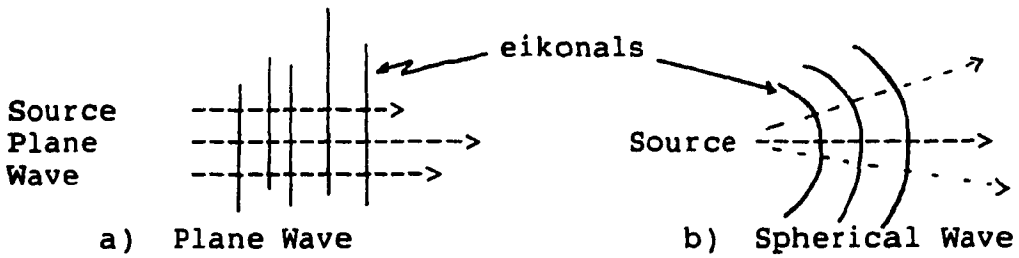


Figure 2.1 The Eikonal of a Ray System

According to GTD [8], a high frequency EM wave incident on a curved surface with a curved edge gives rise to:

a) a reflected wave

b) an edge diffracted wave

c) an edge excited wave which propagates along a surface ray

According to Keller's generalized Fermat principle, the ray incident on the edge QE of Figure 2.2 produces edge diffracted rays ed and surface diffracted rays Sr.

In the case of convex surfaces the surface rays shed a surface diffracted ray Sd from each point "Q" on its path.

ES is the boundary between the edge diffracted rays and the surface diffracted rays (Tangent to surface at $Q_E$). SB is the shadow boundary of the incident field and RB is the shadow boundary of the reflected field.

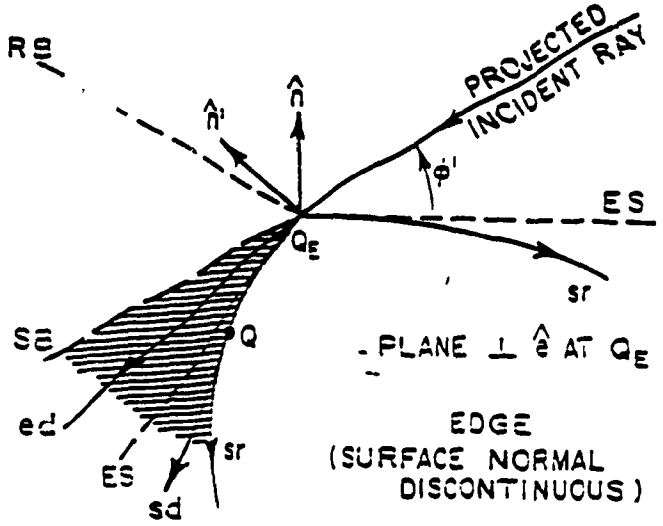


**Figure 2.2 Incident, Reflected and Diffracted Rays**

Since the behaviour of the ray optic field is different in the two regions separated by a boundary, there is a transition region adjacent to each boundary within which there is a rapid variation of the field between the two regions.

Neglecting the surface ray field, the total electric field may be represented as:

$$\vec{E} = \vec{E}^i + \vec{E}^r + \vec{E}^d \qquad (2.1)$$

where

$\vec{E}^i$ = E-field of source in absence of surface

$\vec{E}^r$ = E-field reflected from surface ignoring the edge

$\vec{E}^d$ = edge diffracted E-field

The diffracted field penetrates the shadow region which

according to geometrical optic has a zero field. However the correct high frequency field has to be continuous at the shadow and reflection boundaries, therefore the diffracted field must ensure continuity to provide the correct transition between the illuminated and shadow regions.

It is in the vicinity of the shadow and reflection boundaries that Keller's theory [5], which is where the predecessor to Kouyoumjian's, failed.

In order to find a solution which would satisfy all aspects of the geometry including the shadow region, the leading term in the asymptotic high frequency solution which originated from the eigen function method or the method of Rayleigh, will be investigated.

The diffraction coefficient which was discussed earlier is an asymptotic solution to Maxwell's equations.

## 2.3 Asymptotic Solution of Maxwell's Equations

One must begin by looking for an asymptotic high frequency solution to Maxwell's equations. The approach used follow that introduced by Luneberg and Kline [6].

Maxwell's equations in an isotropic, homogeneous linear medium are:

$$\nabla \times \vec{E} = -Z\vec{H} \quad (Z = j\omega\mu) \qquad \nabla \cdot \vec{E} = 0$$
$$\nabla \times \vec{H} = Y\vec{E} \quad (Y = j\omega\varepsilon) \qquad \nabla \cdot \vec{H} = 0 \tag{2.2}$$

Thus the Helmholtz equation is derived, using potential vectors to obtain:

$$\nabla^2\vec{E} + K^2\vec{E} = 0 \tag{2.3}$$

and

$$\nabla^2\vec{H} + K^2\vec{H} = 0 \tag{2.4}$$

Where the wave number $K = 2\Pi/\lambda$ in the medium of propagation.

Now, rewriting $K_o = 2\Pi/\lambda_o$ as the wave number in free space,

$$K = \frac{K_o\lambda_o}{\lambda} = \frac{K_o C_o f}{f V} = \frac{K_o C_o}{V} = K_o\eta \tag{2.5}$$

where f is the frequency, $\lambda_o$ the wavelength in free space, $C_o$ the speed of light in free space, V velocity in the medium and $\eta$ the refractive index of the medium.

The divergenceless of $\vec{E}$ & $\vec{H}$ fields allows one to use two vector potentials $\vec{A}$ and $\vec{F}$ to make the following assumption where either vector potentials may be used and where the scalar portion of these vectors have been factored

$$\begin{bmatrix} \vec{A} \\ \vec{F} \end{bmatrix} = \vec{C} \begin{bmatrix} \mu^a \\ \mu^f \end{bmatrix} \qquad (2.6)$$

One can obtain, by substituting in 2.3 & 2.4 the scalar wave equation ;

$$\nabla^2\mu + \left( K_o^2\eta^2 \right)\mu = 0 \qquad (2.7)$$

A solution for the above has the form $\mu = A\, e^{-jk_o\psi}$

Note that both A and $\psi$ are differentiable functions in (x,y,z).

Then the results of this substitution will be:

$$\left( \frac{\partial^2 A}{\partial x^2} + \frac{\partial^2 A}{\partial y^2} + \frac{\partial^2 A}{\partial z^2} \right) e^{-jK_o\psi} - 2jK \left( \frac{\partial A \partial \psi}{\partial x \partial x} + \frac{\partial A \partial \psi}{\partial y \partial y} + \frac{\partial A \partial \psi}{\partial z \partial z} \right)$$

$$e^{-jK_o\psi} - K_o^2 A e^{-jK_o\psi} \left( \left[ \frac{\partial \psi}{\partial x} \right]^2 + \left[ \frac{\partial \psi}{\partial y} \right]^2 + \left[ \frac{\partial \psi}{\partial z} \right]^2 \right) - jK_o A e^{-jK_o\psi} \qquad (2.8)$$

$$\left( \frac{\partial^2 \psi}{\partial x^2} + \frac{\partial^2 \psi}{\partial y^2} + \frac{\partial^2 \psi}{\partial z^2} \right) + K_o^2 \eta^2 A e^{-jK_o\psi} = 0$$

using operator rotation and manipulating it becomes:

$$AK_o^2 \left\{ |\nabla\psi|^2 - \eta^2 \right\} + jK_o \left\{ 2\nabla A \nabla\psi + A\nabla^2\psi \right\} - \nabla^2 A = 0 \qquad (2.9)$$

Now the Lunenberg-Kline expansion of the $\vec{E}$-field is of the form ;

$$A = e^{-jK_o\psi} \sum_{m=0}^{\infty} \frac{A_m}{(jK_o)^m} \tag{2.10}$$

Using the identity, $\nabla A \cdot \nabla \psi = \nabla \psi \cdot \nabla A = (\nabla \psi \cdot \nabla) A$ equation 2.9 becomes ;

$$K_o^2(|\nabla \psi|^2 - \eta^2) + jK_o(\nabla^2\psi + 2(\nabla \psi \cdot \nabla) - \nabla^2) A = 0 \tag{2.11}$$

and using a term by term analysis one can note that the first term in brackets must be a separate case and must be zero since the difference of two positive quantities are considered. Therefore rewriting the following equations which will be called the "eikonal" equations:

$$|\nabla \psi|^2 - \eta^2 = 0 \tag{2.12}$$

$$|\nabla \psi|^2 = \eta^2$$

Now considering the remaining terms and rearranging it becomes:

$$\left\{ 2 (\nabla \psi \cdot \nabla) + \nabla^2\psi \right\} A = \frac{\nabla^2 A}{jK_o} \tag{2.13}$$

expanding $\nabla^2 A$ and simplifying the right hand side

expansion the following equation is obtained :

$$\frac{\nabla^2 A}{jK_o} = \nabla^2 \left( \frac{A_{1-1}}{jK_o} + \frac{A_{2-1}}{(jK_o)^2} + \cdots\cdots + \frac{A_{m-1}}{(jK_o)^m} \right) \tag{2.14}$$

and for the left hand side

$$\left\{ 2(\nabla \psi \cdot \nabla) + \nabla^2 \psi \right\} \left\{ A_o + \frac{A_1}{jK_o} + \frac{A_2}{(jK_o)^2} + \cdots\cdots + \frac{A_m}{(jK_o)^m} \right\} \tag{2.15}$$

and now equating the associated terms in the two equations above

$$\begin{aligned} \left[ 2(\nabla \psi \cdot \nabla) + \nabla^2 \psi \right] A_o &= 0 \\ \left[ 2(\nabla \psi \cdot \nabla) + \nabla^2 \psi \right] A_1 &= \nabla^2 A_o \\ &\vdots \\ \left[ 2(\nabla \psi \cdot \nabla) + \nabla^2 \psi \right] A_m &= \nabla^2 A_{m-1} \end{aligned} \tag{2.16}$$

Three equations are obtained from the development above:

- eikonal equation $$|\nabla \psi|^2 = \eta^2 \tag{2.17}$$

- 1st order transport equation $$\left[ 2(\nabla \psi \cdot \nabla) + \nabla^2 \psi \right] A_o = 0 \tag{2.18}$$

- higher order transport equation $$\left[ 2(\nabla \psi \cdot \nabla) + \nabla^2 \psi \right] A_m = \nabla^2 A_{m-1} \tag{2.19}$$

A solution to the above three equations completely

determines the Luneberg-Kline series of the form.

$$A = e^{-jK_o\psi} \sum_{m=0}^{\infty} \frac{A_m}{(jK_o)^m} \tag{2.20}$$

where A is a function of x, y and z.

Now in this case, using the eikonal along with the first order transport and the conditional equations below,

$$|\nabla \psi|^2 = \eta^2 \tag{2.21}$$

$$\frac{\partial \vec{E}_o}{\partial \hat{S}} + \frac{\nabla^2 \psi}{2n} \vec{E}_o = 0 \tag{2.22}$$

$$\hat{S} \cdot \vec{E}_o = 0 \tag{2.23}$$

where $\hat{S} = \frac{\nabla \psi}{n}$ is a unit vector in the direction of the ray path and S the distance along the ray path.

The interest here is in the solution at the high frequency limit so the asymptotic approximation for $\vec{E}$ reduces to

$$E(S) \approx e^{-jK_o\psi(S)} E_o(S) \tag{2.24}$$

After integrating Equation 2.24, it becomes

$$E(S) \cong E_o(o)\, e^{-jK_o\psi(0)} \sqrt{\frac{Q_1Q_2}{(Q_1+S)(Q_2+S)}}\, e^{-jKS} \qquad (2.25)$$

$Q_1$ and $Q_2$ are the principal radii of curvature at S=0. This equation is referred to as the geometrical-optics field where the quantity in the square root is the divergence factor.

This equation could have been determined by using classical geometry, however classical geometrical optics ignores the polarization and wave nature of the electromagnetic fields and this is why the leading term in the Luneberg-Kline asymptotic expansion contains this missing information.

It is apparent that when Q1 = -S or Q2 = -S equation 2.25 becomes infinite and the asymptotic approximation is no longer valid. This region where -S = Q (1 or 2) is called the caustic region and the field at the caustic must be found from separate considerations. However equation 2.25 is valid near the caustic zone at high frequencies.

Furthermore, using Maxwell's curl equation $\nabla \times \vec{E} = -j\omega\mu \vec{H}$ the leading term in the asymptotic approximation for the magnetic field is

$$\vec{H} = \hat{S} \times \vec{E} / Z \qquad (2.26)$$

where $Z = \mu / \epsilon$ is the characteristic impedance of the medium and E is given by Equation 2.25.

## 2.4 Reflection

Geometrical optics provides a high frequency approximation for the incident, reflected and refracted fields.

First the geometrical optics field reflected from the point Qr on a perfectly conducting smooth surface S is found.

The geometrical optics is:

$$E^r(S) = E^i(Q_r) \overline{\overline{R}} \sqrt{\frac{Q_1 Q_2}{(Q_1+S)(Q_2+S)}}\, e^{-jKS} \qquad (2.27)$$

in which Q1, Q2 are the principal radii of curvature of the reflected wavefront at Qr, in Figure 2.3 and R the dyadic reflection coefficient.

Using the lens and mirror formulas of elementary pnysics it can be shown that:

$$\frac{1}{Q_1} = \frac{1}{2} \cdot \left( \frac{1}{Q_1} + \frac{1}{Q_2} \right) + \frac{1}{f_1} \qquad (2.28)$$

$$\frac{1}{Q_2} = \frac{1}{2}\cdot\left(\frac{1}{Q_1} + \frac{1}{Q_2}\right) + \frac{1}{f_2} \qquad (2.29)$$

where,

$$\frac{1}{f_1} = \frac{1}{\text{Cos }\theta}\cdot\left(\frac{\text{Sin}^2\theta_2}{a_1} + \frac{\text{Sin}^2\theta_1}{a_2}\right)\cdot\sqrt{\frac{1}{\text{Cos}^2\theta_1}\left(\frac{\text{Sin}^2\theta_2}{a_1} + \frac{\text{Sin}^2\theta_1}{a_2}\right) - \frac{4}{a_1 a_2}} \qquad (2.30)$$

If a1 or a2 become infinite, as in the case of a flat plane or cylindrical scatterers, geometrical optics fails.

The Luneberg-Kline expansions for reflected fields tend to become singular as the specular point approaches close to an edge or a reflection shadow boundary on the surface. Futherermore, these terms do not describe the diffracted field which penetrates into the shadow region, nor do they insure continuity at the shadow-reflection boundary. It is evident that the Luneberg-Kline series cannot be used to treat diffraction.

## 2.5 Diffraction

In order to overcome the limitation of the geometrical optics field, it is necessary to introduce the diffracted field.

The postulates of Keller's theory called GTD, are as

follows [5]:

1. The diffracted field propagates along rays which are determined by a generalization of Fermat's principle to include points on the boundary surface in the trajectory.

2. Diffraction like reflection and transmission is a local phenomenon at high frequencies.

3. The diffracted wave propagates along its ray so that:
   a) power is conserved in a strip or tube of rays.
   b) the phase delay along the ray path equals the product of the wave number of the medium and the distance.

Diffracted rays are initiated at points on the boundary surface where the incident geometrical optics field is discontinuous, i.e. at the incident field. The diffracted rays like the geometrical optics rays follow paths which make the optical distance between the source point and the

field point a minimum or maximum. Thus the portion of the ray path which traverses a homogeneous medium is a straight line, and if a segment of the ray path lies on a smooth surface, it is a surface extremal or geodesic.

For the points away from the diffracting surface, a normal congruence of rays emanating from a point of diffraction on the radiating surface will be considered normal. The high frequency diffracted field at P in Figure 2.2 may be found by asymptotically approximating its integral representation

$$E^d(S) = \int F e^{-JK} \, \partial a \tag{2.31}$$

where

$$F = \frac{JKZ_c}{4\pi r}\left[ \hat{r} \times (\hat{r} \times ( \hat{n} \times H^d)) - \frac{1}{Z_c} \hat{r} \times (E^d \times \hat{n}) \right] \tag{2.32}$$

And a solution is obtained which has the same form as 2.27 which is not an unexpected result.

$$E^d(S) \cong E^d(0) \sqrt{\frac{Q_1 Q_2}{(Q_1+S)(Q_2+S)}} \cdot e^{-JKS} \tag{2.33}$$

Choosing the point of diffraction on the boundary surface as the reference point 0, it is clear that it must be independent of the location of 0, hence

$$\lim_{Q' \to 0} E^d(0)\sqrt{Q'} \quad \text{exists}$$

and furthermore the diffracted E field is proportional to the incident E field at $Q_E$, in Figure 2.2, thus

$$\lim_{Q' \to 0} E^d(0)\sqrt{Q'} = E^i(Q_E)\cdot\overline{\overline{D}} \tag{2.34}$$

where $\overline{\overline{D}}$ is the dyadic edge diffraction coefficient.

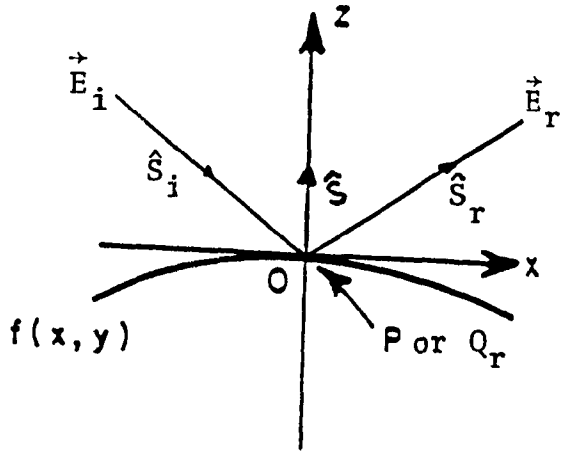


**Figure 2.3 A Smooth Curved Surface Near the Point P.**

Therefore, the edge diffracted electric field must be proportional to the incident field at the point of diffraction.

The constant of proportionality is referred to as a diffraction coefficient and for electromagnetic fields it is a dyadic.

$$E^d(S) \cong E^i \cdot \bar{\bar{D}} \sqrt{\frac{Q'}{S(Q+S)}} \qquad (2.35)$$

in which Q is the distance between the caustic on the boundary surface (the point of diffraction) and the second caustic of the diffracted ray, which is away from the surface.

That distance Q' between the caustics is derived in Reference [7], Volume 1, Appendix II as being:

$$\frac{1}{Q'} = \frac{1}{Q_e'} + \frac{1}{f} \qquad (2.36)$$

$$\frac{1}{Q'} = \frac{1}{Q_e'} + \frac{\hat{\eta}_e \cdot (\hat{S}' - S)}{a \, \mathrm{Sin}^2 \beta_o} \qquad (2.37)$$

where,

$Q'$ = radius of curvature of incident wavefront at Qe taken in the plane containing the incident ray and the unit vector tangent to the edge at $Q_e$.

$\hat{\eta}_e$ = unit normal vector associated with the edge, directed away from the centre of curvature.

a = positive value, radius of curvature of the edge at $Q_e$

$\beta_o$ = angle between the incident ray and tangent to the edge.

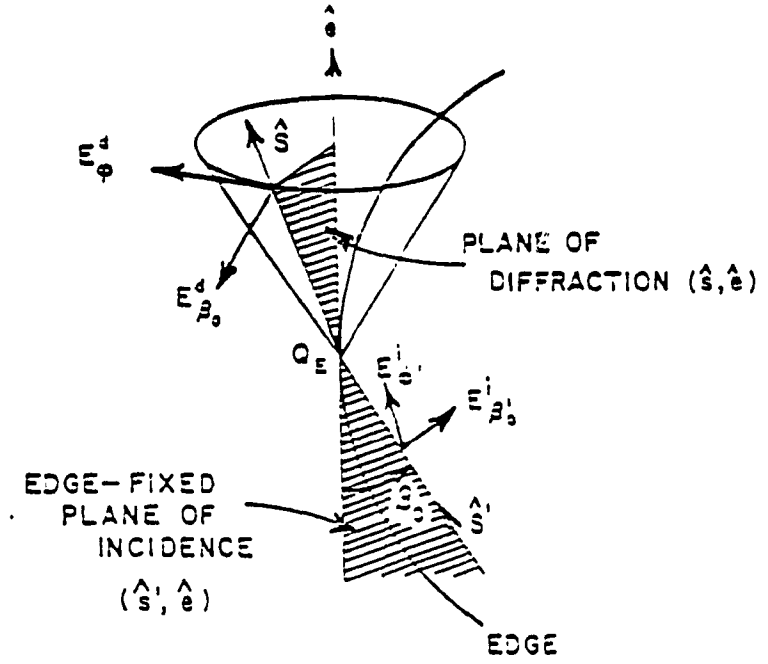


**Figure 2.4 Locus of the Rays Diffracted by a Wedge**

## 2.6 Edge Diffraction

The edge diffraction is of particular interest to us because the wing of an aircraft can be treated as edges to calculate the diffracted electromagnetic field.

The locus of the rays diffracted by a wedge is shown in Figure 2.4.

For each type of edge illumination, it is shown [8] that the Dyadic diffraction coefficient can be represented as the sum of two dyadic. In our case using the spherical coordinates $(S,\beta_o,\phi)$ for the diffracted ray and $(S',\beta'_o,\phi')$

for the incident ray:

$$D(\phi,\phi',\beta_o'') = -\hat{\beta}_o'\hat{\beta}_o D_s(\phi,\phi',\beta_o') - \hat{\phi}'\hat{\phi} D_n(\phi,\phi',\beta_o) \tag{2.38}$$

where,

$D_s$ = scalar diffraction coefficient for the acoustically soft (Dirichlet) boundary at the surface of the wedge.

$D_n$ = scalar coefficient for the acoustically hard (Neumann)boundary.

If the field point <u>is not close</u> to a shadow or reflection boundary and $\phi' = 0$ or $n\pi$, the scalar diffraction coefficient is

$$D_{\substack{s\\n}}(\phi,\phi',\beta_o) = \frac{e^{-\pi/4}\,\mathrm{Sin}\,\pi/n}{n\sqrt{2\pi K}\,\mathrm{Sin}\,\beta_o} + \left\{ \frac{1}{\mathrm{Cos}\,\frac{\pi}{4} - \mathrm{Cos}\,\frac{(\phi-\phi')}{n}} \pm \frac{1}{\mathrm{Cos}\,\frac{\pi}{4} - \mathrm{Cos}\,\frac{(\phi+\phi')}{n}} \right\} \tag{2.39}$$

The wedge angle is $(2-n)\pi$ where the plane surfaces forming the wedge are $\phi = 0$ and $\phi = n\pi$, where $n = 1,2,\ldots$

The above formulation, which was presented by Keller, becomes singular as a shadow boundary or reflected boundary is approached, resulting in a discontinuity in the incident and reflected fields.

In order to compensate for the discontinuity problem in

Keller's diffraction coefficient, Kouyoumjian introduced a function which will provide the field calculation at those regions of rapid field change adjacent to the shadow and reflection boundaries commonly called transition regions.

The new expression is,

$$D_{\substack{s\\h}}(\phi,\phi',\beta_o) = \frac{-e^{-j\pi/4}}{2n\sqrt{2\pi K\,\mathrm{Sin}\beta_o}}\cdot\left[\mathrm{Cot}\left[\frac{\pi+(\phi-\phi')}{2n}\right]\cdot F\left\{KLa^{+}(\phi-\phi')\right\}+\right. \tag{2.40}$$

$$\mathrm{Cot}\left[\frac{\pi-(\phi-\phi')}{2n}\right]F\cdot KLa^{-}(\phi-\phi')\Big\} \pm \left\{\mathrm{Cot}\left[\frac{\pi+(\phi+\phi')}{2n}\right]\right.$$

$$\left.\left.F\left\{KLa^{+}(\phi+\phi')\right\}\mathrm{Cot}\left[\frac{\pi-(\phi+\phi')}{2n}\right]F\left\{KLa^{-}(\phi+\phi')\right\}\right\}\right]$$

where,

$$F(X) = 2j\sqrt{X}\,e^{-jX}\int_{\sqrt{x}}^{\infty} e^{-j\tau^2}\partial\tau \tag{2.41}$$

when X is small we have the approximation

$$F(X) = e^{-j((\pi/4)+X)}\cdot\left(\sqrt{\pi X}-2Xe^{j\pi/4}-\frac{2X^2}{3}e^{-j\pi/4}\right) \tag{2.42}$$

when X is large then,

$$F(X) = 1 + \frac{j}{2X} - \frac{3}{4X^2} - \frac{j15}{8X^3} + \frac{75}{16X^4} \qquad (2.43)$$

Note that if the argument in the four transition functions in the Kouyoumjian diffraction coefficient is large, one can obtain Keller's formulation.

In the Kouyoumjian transition function F,

$$a^{\pm}(\phi \mp \phi') = 2\cos^2\left(\frac{2n\pi N^{\pm} - (\phi - \phi')}{2}\right) \qquad (2.44)$$

where $N^+$ are integers such that,

$$2\pi N^+ - (\phi \mp \phi') = \pi \qquad (2.45)$$

$$2\pi N^- - (\phi \mp \phi') = -\pi \qquad (2.46)$$

and if X is greater than 10, the function F(X) is approximately equal to 1, which can be visualized when analyzing equation 2.43, L is defined as:

$$L = \begin{cases} S \sin^2\beta_o \ldots\ldots\ldots\ldots\ldots\ldots \text{plane wave} \\ \dfrac{rr'}{r + r'} \ldots\ldots\ldots\ldots\ldots\ldots \text{cylindrical wave} \\ \dfrac{SS'}{S + S'} \sin^2\beta_o \ldots\ldots\ldots\ldots \text{conical and spherical wave} \end{cases}$$

The transition function is expressed as a Fresnel integral, and can be visualized in Figure 2.4. Usually no more than one of the four transition functions is significantly different from one. Using equation 2.38, the value of the diffracted field can be obtained. Now an investigation of surface shading must be done.

| | The cotangent is singular when | value of N at the boundary |
|---|---|---|
| $\cot\left(\frac{\pi+(\phi-\phi')}{2n}\right)$ | $\phi = \phi' - \pi$, a SB surface $\phi=0$ is shadowed | $N^+ = 0$ |
| $\cot\left(\frac{\pi-(\phi-\phi')}{2n}\right)$ | $\phi = \phi' + \pi$, a SB surface $\phi=n\pi$ is shadowed | $N^- = 0$ |
| $\cot\left(\frac{\pi+(\phi+\phi')}{2n}\right)$ | $\phi = (2n-1)\pi-\phi'$, a RB reflection from surface $\phi=n\pi$ | $N^+ = 1$ |
| $\cot\left(\frac{\pi-(\phi+\phi')}{2n}\right)$ | $\phi=\pi - \phi'$, a RB reflection from surface $\phi=0$ | $N^- = 0$ |

**Table 2.1 Behaviour of the Terms in $D_{s,h}$, Equation 2.38.**

As discussed before, at a shadow or reflection boundary one of the cotangent functions in equation 2.38 becomes singular and the other three remain bounded. Table 2.1 shows the location of the boundary at which each cotangent becomes singular. Discontinuity in the geometrical optics field at a shadow or reflection boundary is compensated

separately by one of the four terms in the diffraction coefficient.

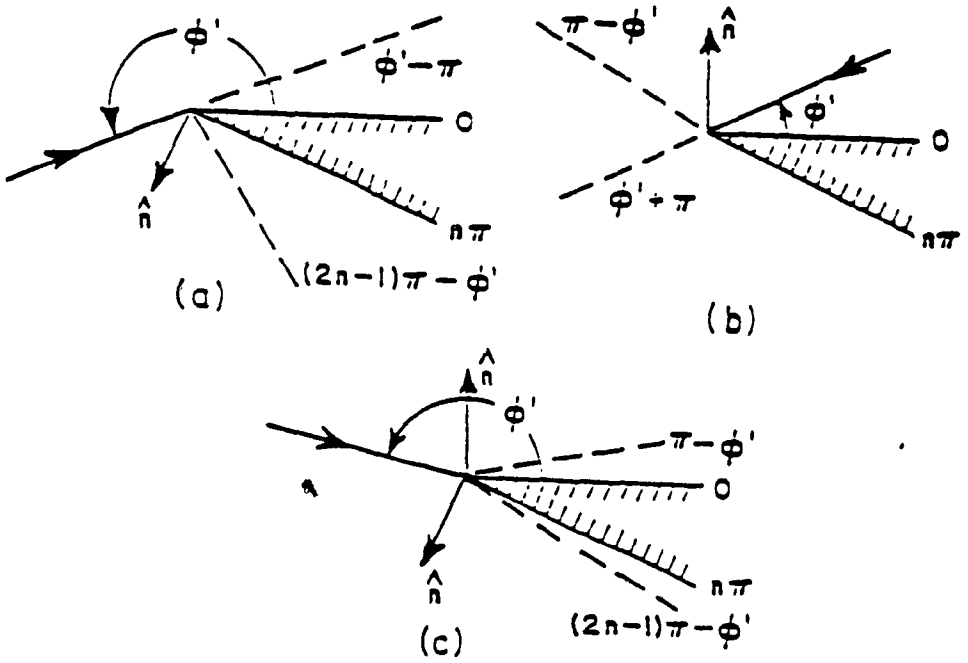


**Figure 2.5 Edge Diffraction Angles**

## 2.7 Surface Shading

What is of interest to us in the surface diffraction is the diffraction phenomena on a convex surface as shown in Figure 2.6

So far the field behaviour in the regions shown was reviewed except for the region between the convex surface and the boundary ES.

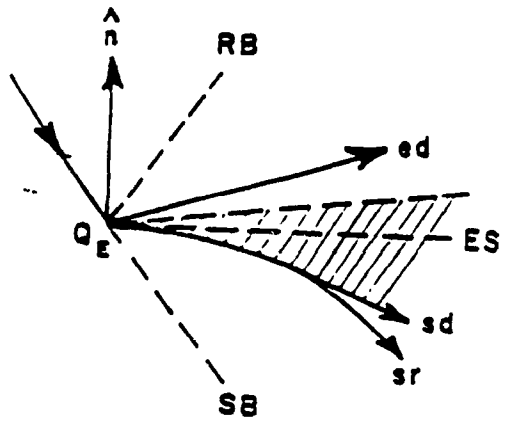


**Figure 2.6 Surface Shading**

When an incident ray strikes a smooth curved perfectly conducting surface at the shadow boundary, a part of its energy is diffracted into the shadow region.

This means that a ray incident on the shadow boundary at Qe divides: one part of the incident energy continuing straight on as predicted in geometrical optics and a second part following the surface S into the shadow region as a surface ray which sheds diffracted rays tangentially as it propagates.

The law of surface diffraction states that the incident and diffracted rays are tangent to S and to the surface ray Q1 and Q2 respectively, and that the surface ray is the shortest distance between Q1 and Q2 on S, ie: the surface ray is a geodesic curve.

The diffraction by a curved edge in a curved screen

(n=2) on the convex side is of prime importance when analyzing aircraft geometry.

On the convex side of a curved screen there are surface ray modes known as creeping waves, which shed energy tangentially as they propagate along the surface.

A scalar diffraction coefficient must be found for a curved edge. Again, that coefficient must describe the field in the transition regions.

Three possibilities exist when considering surface shading:

1. Both source and observation points off the surface (scattering problem)

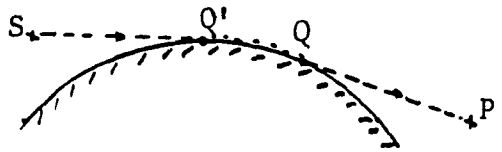


2. Source on the surface and observation point off the surface (radiation problem)

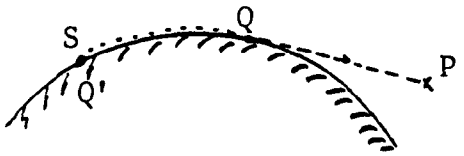


3. Both source and observation points on the surface (coupling problem)


**Figure 2.7 Surface Shading Source Location**

It is observed that the field at point P in the shadow region is associated entirely with the surface diffracted rays, because Geometrical Optic rays do not penetrate into the shadow zone.

Keller introduced the surface diffracted rays via a generalization of Fermat's principle. Two consequences of Fermat's principle are that:

a) the portion of the ray path on the surface must be a surface geodesic.

b) the surface ray field decays due to a continual leakage of energy via the surface diffracted rays which are shed along the forward tangents to the surface ray paths.

The field behaviour going from the illuminated region to the shadow region is complicated since it has to change rapidly and continuously. The ray optical GTD field representation fails within the transition regions [9].

Therefore the GTD solution had to be modified in order to extend its validity in the transition region.

Such modification was done employing uniform procedures for constructing asymptotic high frequency solutions:

- Fock's method of parabolic equations;

- Method of boundary layers;

- Uniform asymptotic evaluation of the integral representations for the solutions to canonical problems. The shaded region adjacent to ES in Figure 2.6 is referred to as a transition region and is defined in reference [10] as:

$$m(Q') = \left( \frac{2}{K\rho_g(Q')} \right)^{\frac{1}{3}} \tag{2.47}$$

where k = wavenumber of surrounding medium

$\rho_g$ = surface radius of curvature in the direction of the surface ray at Q1 or Q'.

Within this shaded region the field must change rapidly and continuously. This is where the GTD field representation fails as stated above.

Fock's method of parabolic equations in general does not reduce exactly to the corresponding solutions when the field point moves outside the transition region. Thus Fock's solutions are only partially uniform.

The boundary layer technique appears to provide a systematic procedure for generating an asymptotic expansion for the diffraction problem. However this procedure does

not appear to be convenient for engineering application. R.H. Pathak [10] developed a uniform solution from Keller's method of canonical problems. The present UTD solutions for the diffraction by convex surfaces have been developed heuristically considering the principle of locality of wave propagation, radiation and diffraction, which is valid at high frequencies.

The only other solution for a convex surface is presented by James [11] but seems to be only partially uniform at the transition regions.

Pathack's solution, which is described in detail in [7] and [8], will be reviewed in order to understand his approach.

## 2.8 UTD Convex Surface Diffraction

Assuming a 2D field varying in the transverse plane, then E(z) and H(z) must be characterized by the following EM boundary conditions on the convex cylinder (perfectly conducting):

$E(Z) = 0$ for TM(Z) case

$\hat{\eta}\, V(t)\, H(Z) = 0$ for TE(Z) case

where $\hat{\eta}$ is a unit vector

and V(t) the transverse gradient operator

Pathak presents the field $\mu$ at an observation point as a problem to determine the field as a boundary value problem.

First $\mu$ must satisfy the wave equation:

$$\mu(\nabla_c^2+K^2) = f\delta(X-X')\delta(Y-Y') \qquad (2.48)$$

f represents the strength of the line source and is the Dirac delta function.

Now $\mu$ can be represented, depending on the case observed as:

$$\mu = \begin{cases} \mu^i+\mu^r & \text{.....in the lit region} \\ \mu^d & \text{.....in the shadow region} \end{cases}$$

where $\mu^i$, $\mu^r$ and $\mu^d$ are incident, reflected and diffracted fields.

Figure 2.8 shows the three types of fields one must consider.

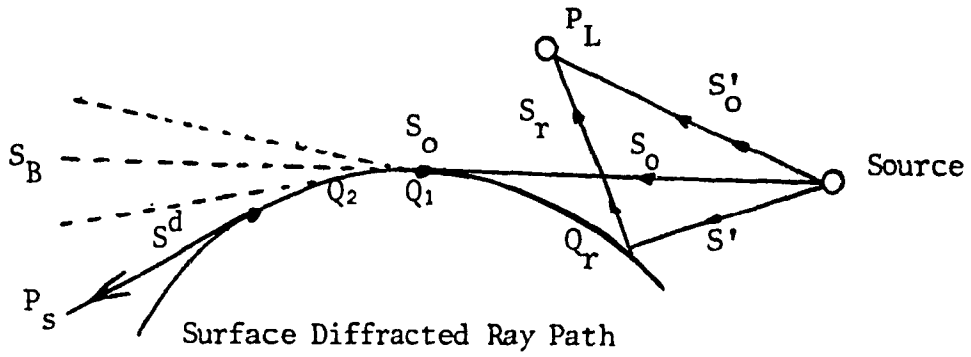


**Figure 2.8 Incident, Reflected and Diffracted Field.**

Now the formula for the incident field is:

$$\mu^i(P) \cong A \frac{e^{-jK|Q'P|}}{|Q'P|} = A \frac{e^{-jKS'_o}}{S'_o} \qquad (2.49)$$

where A is the strength of the incident ray. The formula for the reflected field is:

$$\mu^r(P_L)=\mu^i(Q_r)\left[-\sqrt{\frac{-4}{\varepsilon^L}}\cdot e^{-j(\varepsilon^L)^{3/12}}\left\{\frac{e^{-j\pi/4}}{2\varepsilon^L\sqrt{\pi}}\left[1-F(X^d)\right]+\hat{P}_h^s(\varepsilon)\right\}\right]\cdot \qquad (2.50)$$

$$\sqrt{\frac{\rho^r}{\rho^r+S^r}}$$

and for the diffracted field is:

$$\mu^d(P_s) = \mu^i(Q_1)\cdot\left[-\sqrt{m(Q_1)m(Q_2)}\cdot e^{-jt}\cdot\sqrt{2/K}\right]\cdot \left\{\frac{e^{-j\pi/4}}{2\varepsilon\sqrt{\pi}}\cdot\left[1-F(X^d)\right]+\hat{P}_{\underset{h}{s}}(\varepsilon)\right\}\cdot\frac{e^{-jKS^d}}{\sqrt{S^d}} \tag{2.51}$$

Now the various parameters contained in the equations above are defined as follows:

$$F(X) = 2j\sqrt{X}\, e^{jX}\int_X^\infty e^{-j\tau^2}\partial\tau \tag{2.52}$$

and,

$$\hat{P}_{\underset{h}{s}}(\partial)=\begin{pmatrix}P^*(\delta)\\ q^*(\delta)\end{pmatrix}\cdot e^{-j\pi/4}-\frac{e^{-j/4}}{2\delta(\sqrt{\pi})} \quad \text{for} \begin{pmatrix}TM_z\\ TE_z\end{pmatrix} \tag{2.53}$$

The transition function F(X) involves a Fresnel integral whereas the transition function $P_S(S)$ which is referred to as the Pekeris Caret function, contains the Fock integral where:

$$P^*(\delta)=\frac{1}{\sqrt{\pi}}\int_{-\infty}^{\infty}\frac{V(\tau)\cdot e^{-j\partial\tau}}{\omega_z(\tau)}\,\partial\tau \tag{2.54}$$

and

$$q^{*}(\partial)= \frac{1}{\sqrt{\pi}} \int_{\infty}^{\infty} \frac{V'(\tau)\cdot e^{-j\partial\tau}}{\omega_z'(\tau)}\, \partial\tau \qquad (2.55)$$

in which $V(\tau)$ and $\omega_z(\tau)$ are the Fock-type Airy functions given by:

$$2jV(\tau)=\omega_1(\tau)-\omega_2(\tau) \qquad (2.56)$$

where,

$$\omega_{1,2}(\tau)= \frac{1}{\sqrt{\pi}} \cdot \int_{\infty, e^{j2\pi/3}}^{\infty, -j\varepsilon} e^{-\tau t - t^3/3}\, dt \qquad (2.57)$$

with $\varepsilon$ being a small positive number, and

(2.58)

and,

$$V(\tau) = \frac{\partial V(\tau)}{\partial \tau}$$

$$\omega_z'(\tau)= \frac{\partial \omega_z(\tau)}{\partial \tau} \qquad (2.59)$$

Plots of the transition functions F(X), are shown in Figure 2.9.

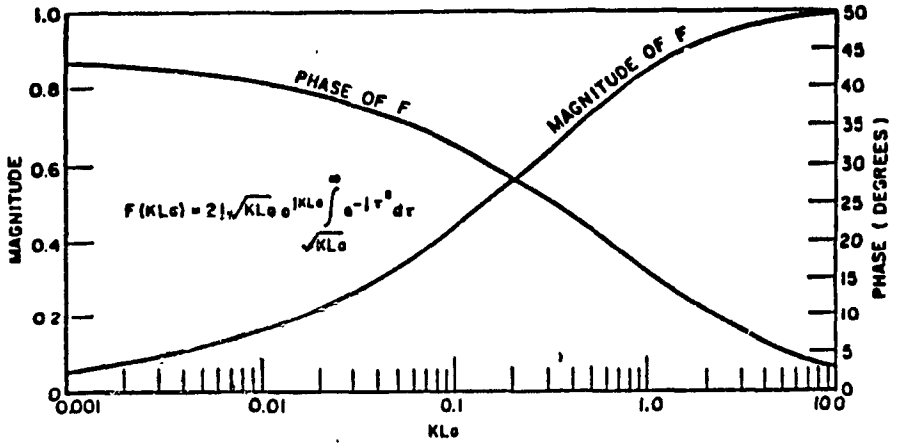


Transition function.

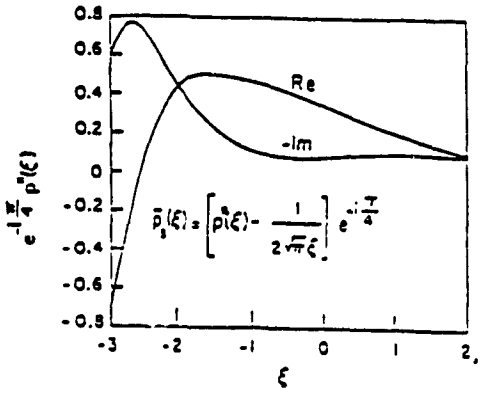


Plot of $e^{-i\frac{\pi}{4}} p^*(\xi)$ versus $\xi$ based on tabulated data for $p(\xi)$ by Logan (1959).

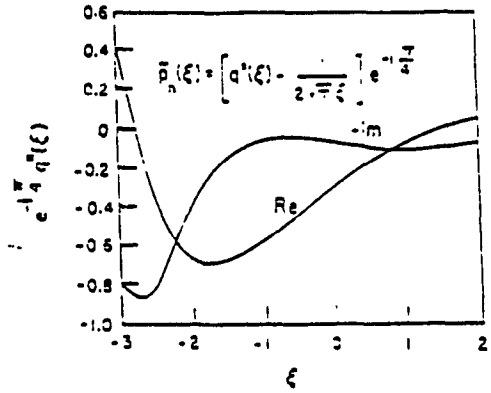


Plot of $e^{-i\frac{\pi}{4}} q^*(\xi)$ versus $\xi$ based on tabulated data for $q(\xi)$ by Logan (1959).

**Figure 2.9 Plots of Transition Functions**

Now, lets define the parameters appearing in the three main field determination formulas.

The Miller type Airy function $A_i(\tau)=V(\tau)/\sqrt{\pi}$

and $$A_i'(\tau)=\frac{\partial}{\partial\tau} A_i(\tau)$$

The parameters $q_n$ and $\bar{q}_n'$ are defined by $A_i(-q_n)=0$ and Ai $A_i'(-q_n)=0$ respectively.

Explicit values are provided in the table shown above. It must be noted also that:

$$\hat{P}_{\substack{s \\ h}}(\delta)_{\delta>>0} \cong \frac{+}{-}\sqrt{\frac{-\delta}{4}}\, e^{j\delta^3/12} \tag{2.60}$$

$$\varepsilon^L = -2m(Q_r)\mathrm{Cos}\Theta^i \tag{2.61}$$

$$m(Q) = \left(\frac{K\rho_g(Q)}{2}\right)$$

$$\rho^r = \frac{\rho_g(Q_r)\mathrm{Cos}\Theta^i}{2} \tag{2.62}$$

where $\Theta^i$ is formed by the incident (or reflected) ray and the normal $(\hat{\eta})$ to the surface, thus

$$\mathrm{Cos}\Theta^i = \hat{\eta}\cdot\hat{S}^r = -\hat{\eta}\cdot\hat{S}^i \tag{2.63}$$

$$X^L = \frac{2KS^iS^r}{S^i+S^r}\,\mathrm{Cos}^2\Theta^i \tag{2.64}$$

$$X^d = K\,\frac{S_oS^d}{S_o+S^d}\cdot\frac{\varepsilon^2}{2m(Q_1)m(Q_2)} \tag{2.65}$$

$$\varepsilon = \int_{Q_1}^{Q_2}\frac{m(t')}{\rho_g(t')}\,dt^2 \tag{2.66}$$

$q_g(Q_o)$ = the surface radius of curvature at point Qo on the surface.

The transition function F $(X^{h,d})$ enforces the continuity and boundedness of the total field at the SB (Shadow Boundary).

The transition function Ps dominates the exterior to the SB transition region wherein it allows the above solution to reduce properly to the GTD solution.

Close to the SB as SB is approached from the shadow side.

The arguments $X^{h,d}$ of the function F $(X^{h,d})$ approach zero near the SB.

It can be shown that $\mu$ is not only continuous at the SB, but it is also smooth at the SB.

It must also be noted that $\varepsilon^L$ tends toward zero and is largely negative in the deep lit region where X becomes a large positive number.

The expressions can be reduced as follows:

<u>in deep lit region</u>:

$$\mu(P_L)|_{\varepsilon_L<<0} = \mu^i(P_L)+\mu^i(Q_r)\cdot R_h\sqrt{\frac{\rho^r}{\rho^r+S^r}}\cdot e^{-jKS^r} \qquad (2.67)$$

where

$$R_{s,h} = \pm 1 \quad \text{for} \quad \begin{pmatrix} TM_z \\ TE_z \end{pmatrix} \tag{2.68}$$

and in deep shadow region:

$$\mu(P_s)\big|_{\varepsilon>>0} = \mu^d(P_s) \cong \mu^i(Q_1)\left[\sum_{n=1}^{N} {}^{n}(Q_1)\, e^{-\int_{Q1}^{Q2}\alpha_n^{Sn}(t')dt'}\right. \tag{2.69}$$

$$\left. e^{-jKt} \cdot D_n^{Sn}(Q_2)\right] \cdot \frac{e^{-jKS^d}}{\sqrt{S^d}}$$

where $D_n^{s,h}$ and $\alpha_n^{Sn}$ represent Keller's diffraction and attenuation coefficients defined as:

$$\left[D_n^s\right]^2 = \frac{1}{\sqrt{2\pi K}} \cdot \frac{me^{-j\pi/12}}{(A_i'(-q_n))^2} \tag{2.70}$$

$$\left[D_n^h\right]^2 = \frac{1}{\sqrt{2\pi K}} \cdot \frac{me^{-j\pi/12}}{\bar{q}_n (A_i(-\bar{q}_n))^2} \tag{2.71}$$

$$\alpha_n^s = \frac{q_n}{\rho_g} \cdot me^{j\pi/6} \tag{2.72}$$

$$\alpha_n^h = \frac{\bar{q}_n}{\rho_g} \cdot me^{j\pi/6} \tag{2.73}$$

Finally, the field value at the SB region is seen to be:

$$\mu(P_{SB})=\left\{\frac{\mu^i(P_{SB})}{2}-\mu^i(Q_1)m(Q_1)\sqrt{\frac{2}{K}}e^{-j\pi/4}\begin{bmatrix}P^*(0)\\q^*(0)\end{bmatrix}\frac{e^{-jK\rho_{SB}}}{\sqrt{l_{SB}}}\right\} \qquad (2.74)$$

where $l_{SB}=S^d$ for $TM_z$ and $TE_z$

Now these above 3 equations are those used in the GTD AIR code, from the University of Ohio USA, to define the field diffracted by a smooth convex surface.

Within AAPG the above mathematical expressions have been expressed as free space wave spreading loss, curved surface "shading" loss and edge diffraction loss. The formulation has been simplified somewhat, as will be seen in the following chapter, in order to adapt the equations to the practical approach of aircraft antenna analysis.

A full appreciation of the mathematical approach could not be possible without the fundamental view of the geometrical theory of diffraction.

# CHAPTER 3

# ANTENNA-TO-ANTENNA PROPAGATION WITH GRAPHICS-COMPUTER CODE DESCRIPTION

## 3.1 Introduction

The complexity of modern aircraft has increased the requirement to design and test for electromagnetic compatibility. On the other hand, industry and test establishments have limitations on resources and test frequencies. It is therefore vital to have instruments which will help to pre-determine possible system interactions on a given platform and to provide details of each interaction with regard to frequency coincidence and interference path [12]. AAPG may be considered as such a tool.

This chapter discusses the structure and usage of the AAPG program. Using state-of-the-art analytic geometry algorithms, AAPG computes the ray optical coupling paths between antennas and uses the Geometrical Theory of Diffraction (GTD) formulation to calculate the propagation loss along these paths. For each of the interactions between a transmitter and receiver via their respective antennas, AAPG computes the electromagnetic interference

(EMI) margin and presents the results in a graphical format which make visible, the constituent components of the EMI margin. Results for typical aircraft systems are used to illustrate the methodology [13].

## 3.2 Structure of AAPG

The Antenna-to-Antenna Propagation with Graphics (AAPG) code is a computer program originally developed in 1978 at Concordia University in Montreal under the sponsorship of the Canadian Department of Defence. Since 1980, the Defence Research Establishment Ottawa (DREO), USAF Rome Air Development Centre (RADC), the US Department of Defence Electromagnetic Compatibility Analysis Centre (ECAC) and Concordia University have pursued AAPG developments on a joint basis.

The AAPG code, written in Fortran 77, occupies approximately 200k words of 16-bit memory. Using overlay techniques the programme can be run on small minicomputers. A PC version is also available.

AAPG fulfills two fundamental objectives: to accurately compute EMI margins and to present the results of these computations in a concise, visual manner.

Consequently, the AAPG program consists of two

principal modules:

a) The Electromagnetic Compatibility Computation System (EMCCS); and
b) The Graphical Data Management System (GDMS).

The EMCCS, which uses analytic geometry and the Geometrical Theory of Diffraction (GTD), determines geodesic coupling paths and their losses and fills a mass-storage data file (MSDF) with the results of its calculations.

Subsequently, the GDMS accesses portions of the MSDF to display those particular aspects of the analysis with which the user may be concerned. Figure 3.1 shows the structure of the major components of AAPG.

The EMC problem can be viewed as a total set of interactions, $T_{ij}$ between emitters and receptors as shown in Figure 3.2. By analysis, the more meaningful interactions are reduced to a smaller set and then the more critical ones can be identified for evaluation by ground and flight tests. The examples that follow illustrate this process.

AAPG also allows the relocation of antenna systems so the re-evaluation of the interference margin on a real-time basis can be accomplished. This provides the user with a dynamic approach to EMC analysis.

## 3.3 Input Data File

The input data file contains a geometrical description of the aircraft and the specifications of the On-Board transmitting and receiving equipment.

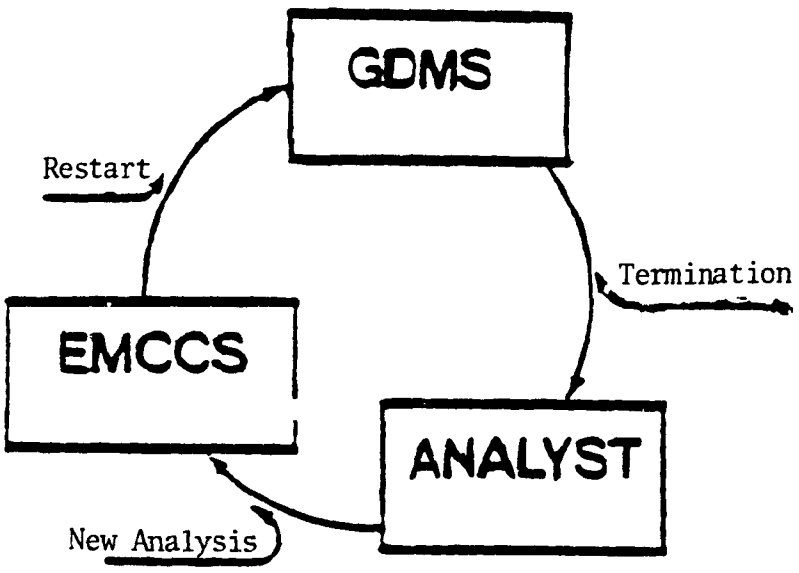


**Figure 3.1 Structure of AAPG**

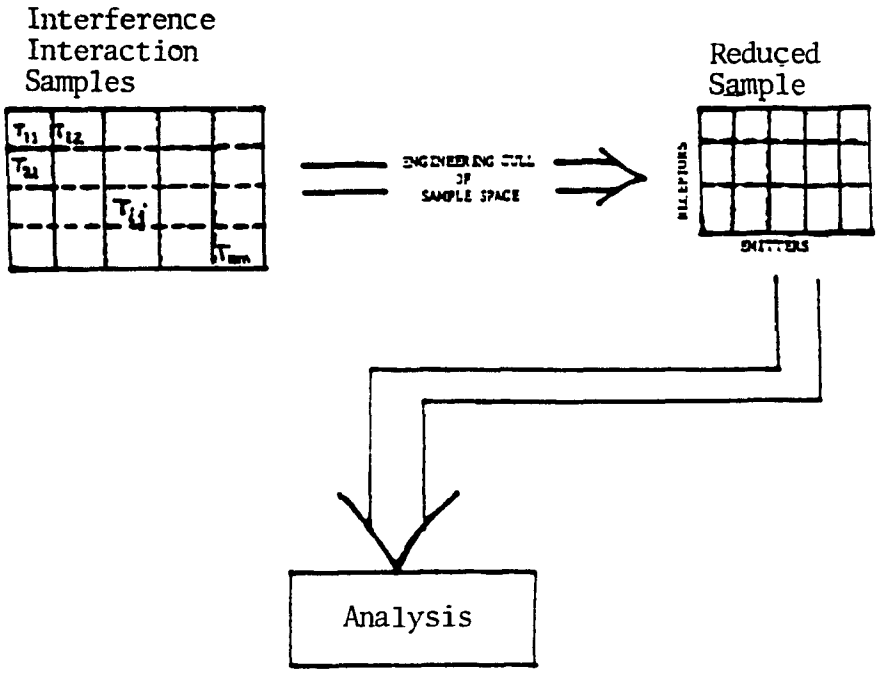


**Figure 3.2 Interference Interaction Reduction**

The aircraft model as shown in Figure 3.3, consists of a cylinder representing the fuselage with a cone at one end. The conical portion may be truncated with a flat bottom below. Planar segments are utilized to model the wings and stabilizers. The coordinate system for the description of the aircraft uses butt line, water line and fuselage station as indicated in Figure 3.3.

Immediately following the aircraft geometrical data in the input file, AAPG expects to read the electronic equipment data. The user must group the electronic equipment in transmitting/receiving subsystems called "TRS".

Each TRS is assigned a name, a security classification and will contain technical information on each subsystem such as:

a) Power output for fundamental and up to five higher order harmonics and receiver sensitivity threshold
b) Tuning range
c) Upper/lower frequency "roll-off" rates
d) Identification of the antenna(s) which are used
e) Antenna gain and pattern.

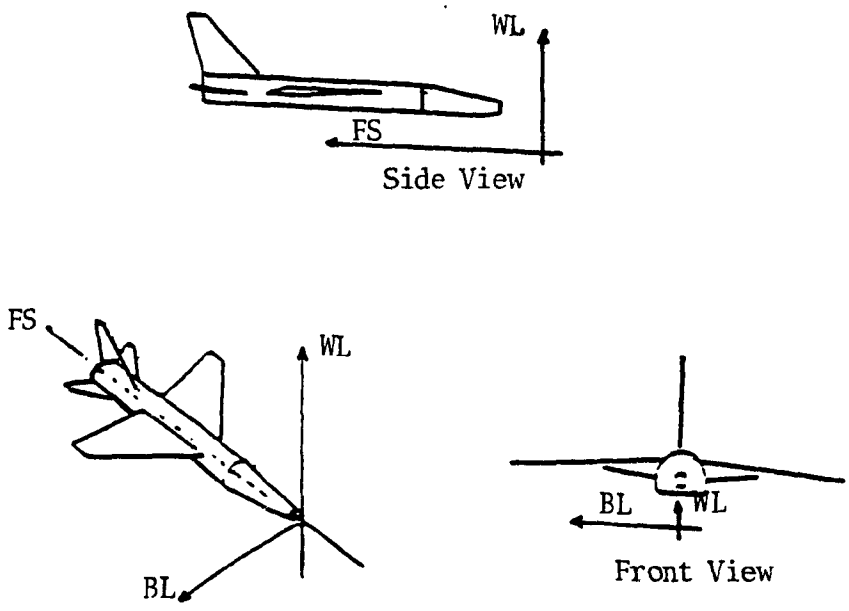


Figure 3.3 AAPG Coordinate System

## 3.4 The Computation Parameters

One of the main design objectives for obtaining a complete software package is to accurately evaluate the magnitude of potential antenna-to-antenna coupled interference and compute the EMI margin. This margin is defined as the ratio of the transmitted signal level, once it reaches a receiver's front end, to the sensitivity of the receiver.

Thus the EMI Margin (in decibels) is the single numerical value which describes the magnitude of the potential antenna-to-antenna coupled electromagnetic interference.

The following equation shows the factors which are computed in evaluating this EMI margin.

$$M = [P_t - L_{Ct} + G^T] - TL + [G_R - L_{CR} - S_R] \qquad (3.1)$$

where $M$ = The EMI Margin, in dB

$P_T$ = Transmitter power, in dBm

$L_{CT}$ = Transmitter-to-antenna cabling loss, in dB

$G_T$ = Transmitter antenna gain in the coupling path direction, in dBi

$TL$ = Transmission loss, in dB

$G_R$ = Receiver antenna gain in the coupling path direction, in dBi

$L_{CR}$ = Receiver-to-antenna coupling loss, in dB

$S_R$ = Receiver sensitivity, in dBm

These EMI margin components, computed at the frequency of the greatest interference (FGI), can be viewed as three distinct blocks. The first and third blocks of data concern the emitter and receptor information which is entered as part of the TRS data in the input file.

The second block or Transmission Loss information, represent the data computed by the AAPG code. The TL factor contains the loss incurred along the coupling path between the two antennas and may be composed of any one or a combination of :

a) Free space loss,

b) Surface Shading loss, and

c) Edge shading loss.

The free space loss ($L_{FS}$) is calculated using the Friis [14] formula for point to point spreading loss:

$$L_{FS} = -20 \text{ Log}_{10} (\lambda/4 \pi D)$$

where $\lambda$ is the wavelength of the interference frequency in meters and D the distance of the path in meters.

The surface shading loss ($L_{CS}$), representing the loss incurred in wave propagation over a curved-surface "creeping wave" loss, is evaluated using the work of Hasserjian and Ishimaru [7]:

$$L_{CS} = A/(\eta A+\xi) \qquad (3.2)$$

where

$$A = \rho_S \cdot \theta_S \sqrt{2\pi/\lambda D}$$

$\rho_S$ = geometric mean of the radii of the spiral and points in meters

$\theta_S$ = angle spannd by the coupling path spiral

D = spiral distance in meters

$$\eta = \begin{cases} .005478 & \text{for } A < 26 \\ .003340 & \text{for } A \geq 26 \end{cases}$$

$$\xi = \begin{cases} .5083 & \text{for } A < 26 \\ .5621 & \text{for } A \geq 26 \end{cases}$$

Finally the edge shading loss ($L_{KE}$) is evaluated using the formulation for edge diffraction presented by Kouyoumjian and Pathak [8]:

$$L_{KE} = 20 \log_{10}\left\{\left((D_1+D_2)\pm(D_3+D_4)\right)\sqrt{\frac{R+S}{RS}}\cdot e^{-j2\pi(R+S)}\right\} \qquad (3.3)$$

where R and S are distances to/from the source/receiver to the diffraction point, and the $D_i$'s are the complex diffraction coefficients, described at length in [8].

## 3.5 Using AAPG

Once the EMCCS has read the input file and completed its calculations to store the pertinent information in the

MSDF, the control is given to the GDMS.

From this point on, the user is guided by a series of menu-driven displays. The GDMS is controlled by a Display Manager shown in Figure 3.4(a) which can call up each sub-package shown in Figures 3.4(b) through 3.4(e).

Within the Display Manager, Figure 3.4(a), the first three options, "Frequency Coincidence Display", "Antenna Location Display", and "EMI Margin Display" will provide various information to the user while the fourth option, "Antenna Positioning Input", will permit the user to move antennas in an attempt to reduce EMI margins.

The Frequency Coincidence Display Package can be used to generate five types of information all of which pertain to a specific frequency-coincident receiver/transmitter pair or $T_{ij}$ as identified before. The summary of coincidence data (Figure 3.5) lists the code numbers of each frequency-coincident receiver/transmitter pair. This code serves as an index to the other packages of AAPG. The frequency-coincidence plot shows the frequency overlap of a receiver with each coincident transmitter operating frequency and its harmonic. (Figure 3.6a). A power-versus-frequency plot is also available to compare the transmitter emission spectrum to the receiver sensitivity threshold for a particular receiver/transmitter pair. (Figure 3.6b).

```
*** DISPLAY MANAGER ***
COMMAND CODES
"F"- FREQUENCY COINCIDENCE DISPLAY
"A"- ANTENNA LOCATION DISPLAY
"M"- EMI MARGIN DISPLAY
"I"- ANTENNA POSITIONING INPUT
"E"- EXIT FROM THE GDMS
```

(a) Display Manager

```
ANTENNA LOCATION DISPLAY PACKAGE
COMMAND CODES
"D"- DISPLAY SUBSYSTEM ANTENNAS
"A"- DISPLAY INFORMATION AGAIN
"N"- DISPLAY NEXT SUBSYSTEM
"E"- EXIT
```

(b) Antenna Location Display

```
FREQUENCY COINCIDENCE DISPLAY PACKAGE
COMMAND CODES
"S"- SUMMARY OF COINCIDENCE DATA
"P"- PLOT OF COINCIDENCE DATA
"N"- DISPLAY NEXT PAGE
"E"- EXIT
```

(c) Frequency Coincidence Display

```
PROPAGATION PATH DISPLAY PACKAGE
COMMAND CODES
"S"- SELECT INFORMATION
"D"- DISPLAY PROPAGATION PATH
"A"- DISPLAY INFORMATION AGAIN
"N"- DISPLAY NEXT EMI DATA SET
"E"- EXIT
```

(d) Propagation Path Display

```
ANTENNA POSITIONING PACKAGE
COMMAND CODES
"P"- ENTER NEW ANTENNA POSITION
"R"- RETURN TO COMMAND MODE
"C"- MODIFY ANTENNA DATA FILE
"E"- EXIT
```

(e) Antenna Positioning package

Figure 3.4 AAPG Menus

The Antenna Location Display package provides a means to view the location and pattern for each antenna relative to the aircraft model. This data comprises a useful tool to validate the antenna information as to the antenna location as in Butt line, water line, and fuselage station on the model and the modelled antenna patterns, as shown in Figure 3.7a.

The antenna pattern can also be verified by accessing the antenna pattern diagram, Figure 3.7b, where all pertinent information on each antenna may be examined.

AAPG also provides the capability to view the platform using full graphic options i.e., side, front, top views individually or on a single display, which permits viewing the aircraft from any elevation or azimuth angle. A close-up view option is also available.

The Propagation Path Display Package for which the sub-menu is presented in Figure 3.4(d), provides a means to analyze each interaction $T_{ij}$ calculated in the EMCCS. The user may select the antenna pair for which he/she wishes to perform a detailed analysis.

The selection of a particular $T_{ij}$ produces a display as shown in Figure 3.8. This display contains the tabulation

value for the worst-case frequency of each transmitter harmonic. Also present in that display, is the aircraft model with the antenna locations and the actual coupling path between these antenna locations. The two antennas are well identified in this graph and if the users wish to have a closer look at the path, simple mnemonic commands can be entered to have a close-up view, side view, top view or front view of the platform. The model can also be displayed from any elevation and/or azimuth. The set of displays and data available in this package provides a means to obtain a detailed analysis of each $T_{ij}$ interaction value. The user obtains an appreciation of power levels, frequencies, and a view of the path of interest. Thus he validates the input information and appreciates each of the calculation elements.

The "Antenna Position Input" module permits the relocation of each antenna and also allows the user to alter its characteristics. By selecting the antenna of interest, a display similar to that of Figure 3.9 can be obtained. By utilizing the electronic cursor or by typing the coordinates or a combination of both, the antenna can be relocated on the two views of Figure 3.9, where both the old and new positions are displayed along with their coordinates.

Once the antenna relocation is implemented, the code produces a listing of the antenna characteristics which can

be modified individually. Subsequently, the user executes a recompute command which has the effect of recycling the entire set of interactions $T_{ij}$ and renders available the new set of data such that a new analysis can be done.

As shown in Figure 3.9, the DMEAN1 antenna from Figure 3.8 was repositioned in order to illustrate the dynamic process of the antenna position input module. Figure 3.10 shows the new EMI margin results and path which clearly illustrates the new coupling path loss with a shift in the predominant loss from edge shading to surface shading. In this case, the antenna relocation analysis shows an improvement in the interference margin between the two systems.

This process can be accomplished as often as necessary to analyze or optimize the relocation of an antenna.

## 3.6 Validation

The numerical accuracy of AAPG is difficult to evaluate due to the lack of good measurement data. The AAPG predictions of EMI margins, however, were compared with measurements taken on a KC-135B aircraft while in flight. The comparisons for the 63 line-of-flight couplets and another 60 couplets which involved fuselage curvature have been done (15)]. The results appear in Figure 3.11 where

one can note that most interactions were predicted using AAPG, within a few decibels. Qualitative validation was also accomplished using the F-14 aircraft [15] where AAPG correctly predicted 131 of 156 systems compatibility.

AAPG has proven to be thus far, a fundamentally valuable tool for EMI prediction combining both mathematical formulation and graphic representation to the users so that a better feel for numerical values can be obtained.

CE-144A FREQUENCY COINCIDENCE DATA SUMMARY CE-144A 01-AUG-89

| RCVR | XMTRS | RCVR | XMTRS | RCVR | XMTRS | RCVR | XMTRS |
|---|---|---|---|---|---|---|---|
| HF | | VHFCOM2 | | VIR-32 | | VIR-32 | |
| 1 HFRX | | 5 VC2IMR | | 9 VORRX | | 13 GSIMRX | |
| 1.01 TX1FM | | 5.01 VTX2AM | | 9.01 VTX2AM | | 13.04 VTX3FM | |
| | | 5.02 VTX4AM | | 9.02 TX1FM | | | |
| VHFCOM1 | | 5.03 TX1FM | | | | DME | |
| | | 5.04 VTX3FM | | 10 VORIMR | | | |
| 2 VC1RX | | | | 10.01 VTX2AM | | 14 DMERX | |
| 2.01 VTX2AM | | ADF-60A | | 10.02 TX1FM | | 14.01 VTX2AM | |
| 2.02 TX1FM | | | | 10.03 VTX3FM | | 14.02 VTX4AM | |
| 2.03 VTX3FM | | 6 RX1 | | | | 14.03 VTX3FM | |
| | | NO COINCIDENCE | | 11 MBRX | | 14.04 DTX | |
| 3 VC1MRX | | | | 11.01 TX1FM | | | |
| 3.01 VTX2AM | | 7 RX2 | | | | 15 DMEIMR | |
| 3.02 VTX4AM | | NO COINCIDENCE | | 12 GSRX | | 15.01 VTX2AM | |
| 3.03 TX1FM | | | | 12.01 VTX2AM | | 15.02 VTX4AM | |
| 3.04 VTX3FM | | CMA-771A | | 12.02 VTX4AM | | 15.03 VTX3FM | |
| | | | | 12.03 TX1FM | | 15.04 DTX | |
| VHFCOM2 | | 8 CMARX | | 12.04 VTX3FM | | | |
| | | NO COINCIDENCE | | | | ARN-118 | |
| 4 VC2RX | | | | 13 GSIMRX | | | |
| 4.01 VTX2AM | | | | 13.01 VTX2AM | | 16 ARNRX | |
| 4.02 TX1FM | | | | 13.02 VTX4AM | | 16.01 VTX2AM | |
| 4.03 VTX3FM | | | | 13.03 TX1FM | | 16.02 VTX4AM | |

PAGE 1 ( 0.00)

TYPE >N< TO SEE NEXT PAGE

**Figure 3.5 Frequency Coincidence Data Summary**

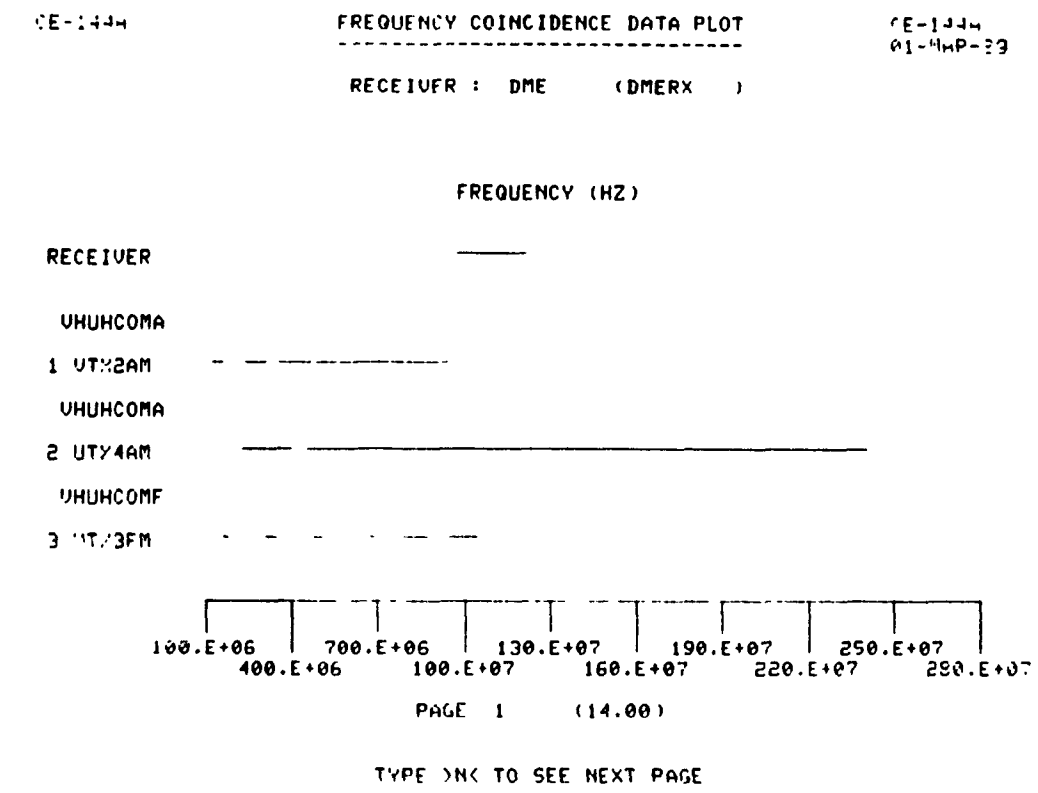


**Figure 3.6a) Frequency Coincidence Path Plot**

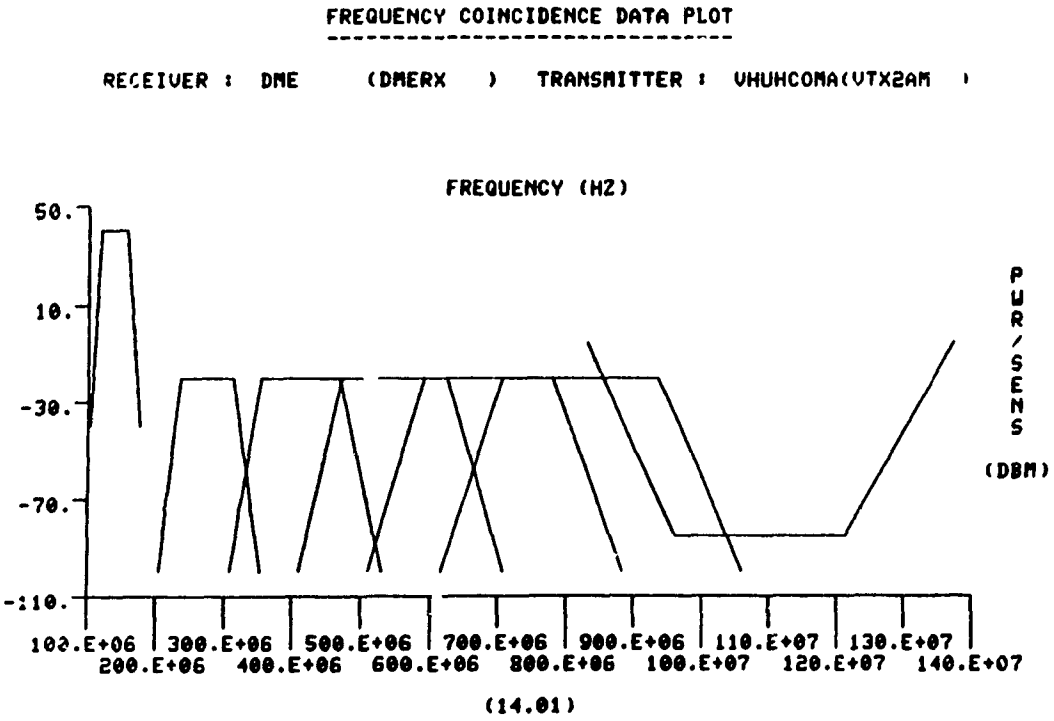


**Figure 3.6b) Data Plot Power Vs Frequency**

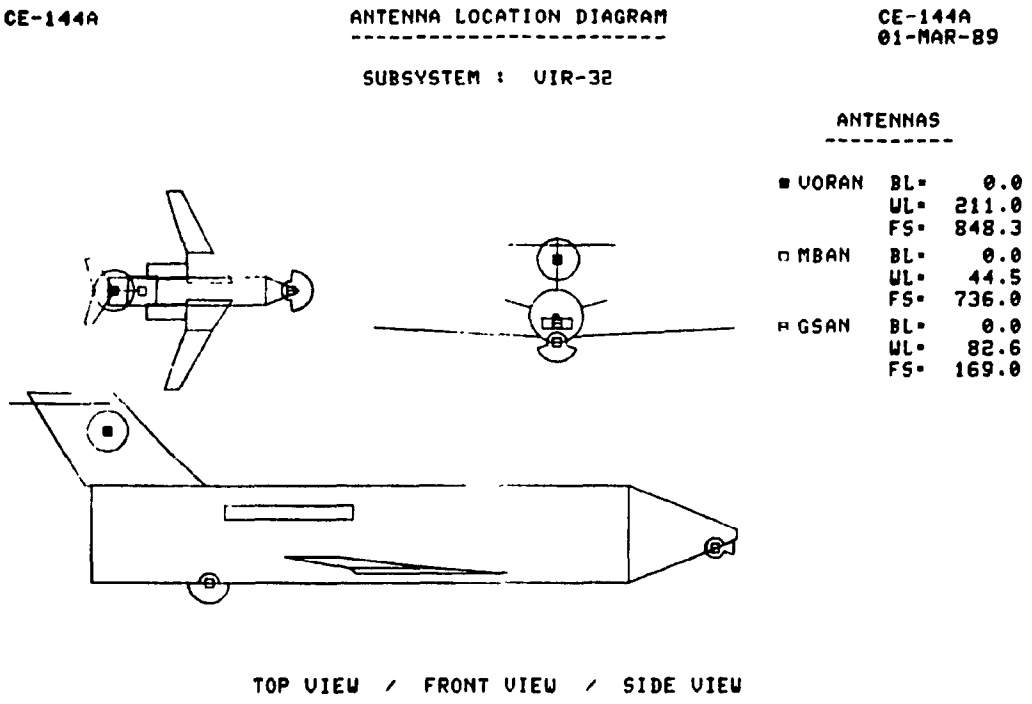


**Figure 3.7 a) Antenna Location Diagram**

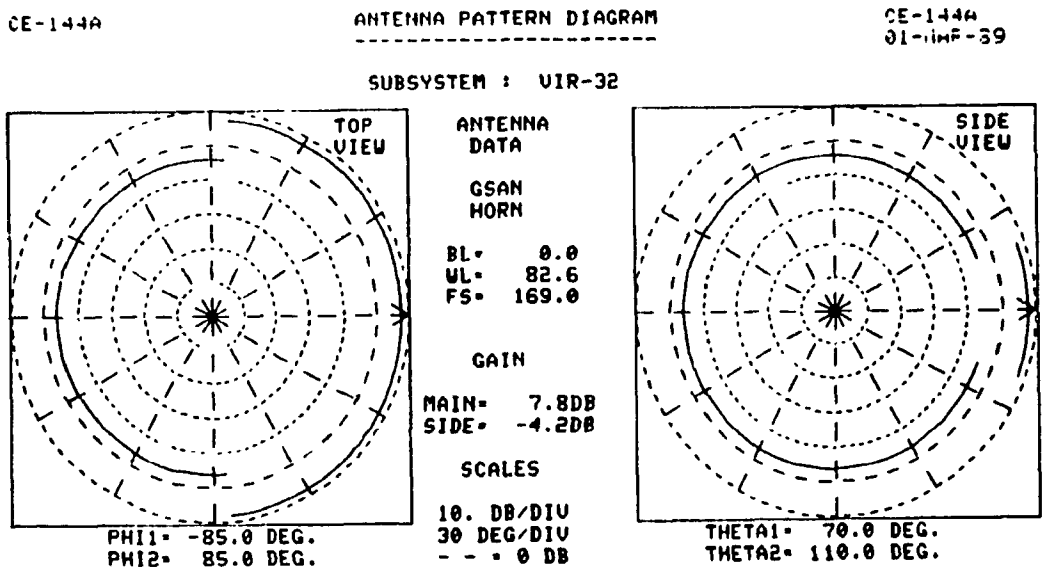


**Figure 3.7 b) Antenna Pattern Diagram**

CE 144A

ELECTROMAGNETIC INTERFERENCE MARGIN CALCULATION

TRANSMITTER : UHUNCOMA(UTX2AM ) RECEIVER : DME (DMERX )

| DESCRIPTION | HARMONIC NO 5 832.5 MHZ | HARMONIC NO 6 935.9 MHZ |
|---|---|---|
| TRANSMITTER POWER | 60 7 | -20.0 |
| XMTR CABLE LOSSES | 0 0 | 0 0 |
| XMTR ANTENNA GAIN | 2.1 | 2.1 |
| TRANSMISSION LOSS | -49 0 | -50.0 |
| SURFACE SHADING | 32 0 | -33.6 |
| EDGE SHADING | 0 0 | 0.0 |
| RCVR ANTENNA GAIN | 2 1 | 2 1 |
| RCVR CABLE LOSSES | 0 0 | 0.0 |
| RCVR SENSITIVITY | -5.0 | 69.8 |
| EMI MARGIN \ FIELD WARNING | -132 5 \ 22. | -29.6 \ 25 |

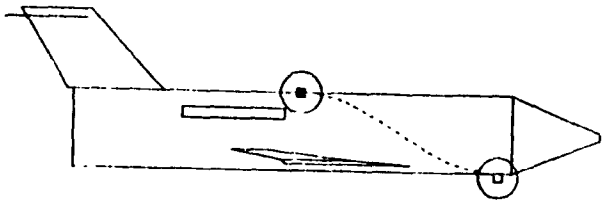

TRANSMITTER ANTENNA

■ UANTAA (MAIN) EL = 0.74 AZ = -33.44

RECEIVER ANTENNA

□ DMEAN1 (MAIN) EL = 2.05 AZ = -148.57

ELEVATION = 0. DEG.
AZIMUTH = 90. DEG.

(14.01-00)

Figure 3.8 EMI Margin

CE-144A

ANTENNA POSITION INPUT

SUBSYSTEM : DME ANTENNA : DMEAN1

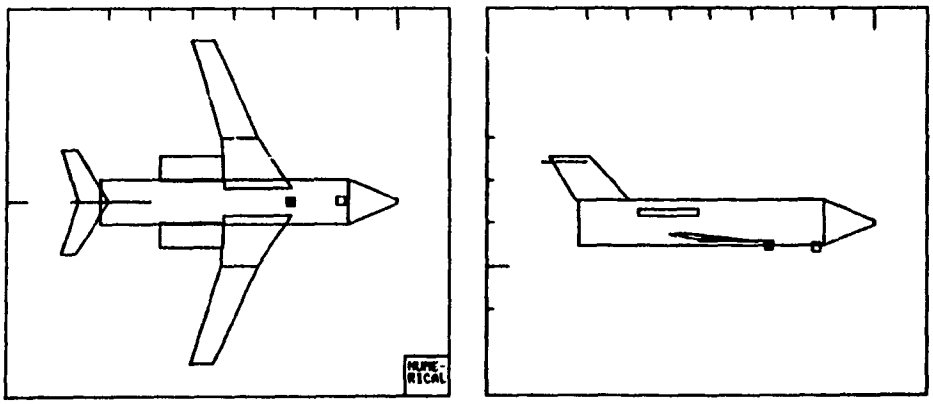


| POSITION | BUTT LINE | WATER LINE | FUSELAGE STATION |
|---|---|---|---|
| OI | 0. | 45. | 402. |
| NE | -2. | 40. | 283. |

IF POSITION IS CORRECT ENTER >OK< OK

Figure 3.9 Antenna Position Input

CE-144A ELECTROMAGNETIC INTERFERENCE MARGIN CALCULATION CE-144A 01-MAR-89

TRANSMITTER : UHUNCOMA(UTXBAM ) RECEIVER : DME (DMERX )

| DESCRIPTION | HARMONIC NO 6 838.6 MHZ | HARMONIC NO 6 935.0 MHZ |
|---|---|---|
| TRANSMITTER POWER | -60.7 | -20.0 |
| XMTR CABLE LOSSES | 0.0 | 0.0 |
| XMTR ANTENNA GAIN | 2.1 | 2.1 |
| TRANSMISSION LOSS | -46.4 | -47.4 |
| SURFACE SHADING | -36.8 | -37.8 |
| EDGE SHADING | -11.7 | -12.8 |
| RCVR ANTENNA GAIN | 2.1 | 2.1 |
| RCVR CABLE LOSSES | 0.0 | 0.0 |
| RCVR SENSITIVITY | -5.0 | -69.8 |
| EMI MARGIN \ FIELD WARNING | -145.4 \ 17. | -43.1 \ 19. |

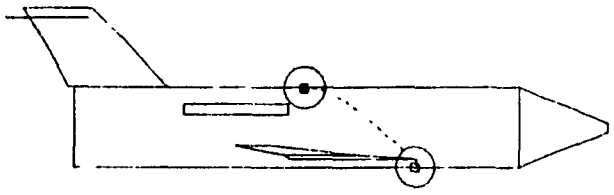

TRANSMITTER ANTENNA
■ UHNTAM (MAIN) EL : 0.00 AZ : -40.93

RECEIVER ANTENNA
□ DMEAM1 (MAIN) EL : 0.00 AZ : -85.62

ELEVATION : 0. DEG.
AZIMUTH : 90. DEG.

(14.01-00)

Figure 3.10 New EMI Margin

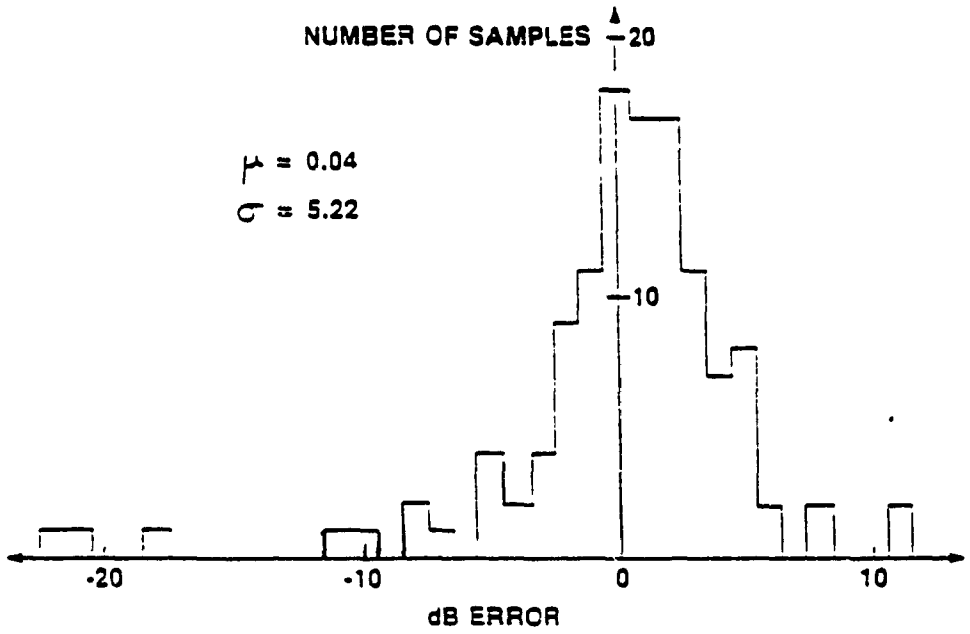


Figure 3.11 Quantitative KC-135 Aircraft Validation of the Free-Space and Curved-Surface Losses Computed by AAPG

# CHAPTER 4

# THE WING DIFFRACTION POINT IMPROVEMENT

## 4.1 Introduction

The modern times have imposed new technologies and geometry in building airplanes, especially military aircraft. There is for instance multi stabilizers, variable geometry wings and more. It is obvious that the location of systems antennas and/or critical loads like weapons, will make great use of this new geometry and give rise to various interacting phenomenon as far as the electromagnetic link between two observation points is concerned.

It is therefore expected to note an increase in edge diffraction when dealing with modern airframes which makes this variable an important one.

In AAPG it was noted that the wing diffraction point was established in an approximate way when the electromagnetic path was intercepting a wing. The edge diffraction point was determined as follows:

a) from the intercepting point the perpenticular distance was established to the front edge of the wing;

b) then the same calculation was done for the rear edge of the wing;

c) these two distances were compared and the edge closest to the piercing point was retained;

d) following this, the perpendicular distance to the tip edge was calculated;

e) then this distance was compared with the distance obtained in step a and again the closest edge was kept;

f) finally, the closest point on the closest edge was the diffraction point kept for the overall path calculation.

Intuitively the above mentioned method does not provide an optimum point at which an electromagnetic path between two locations of interest would diffract. The situation is even more ambiguous when considering fighter aircraft similar to the F15 airframe which present a pronounced angle between the wing tip and the wing root at the fuselage, as shown in Figure 4.1

In order to eliminate doubt and to improve the calculations, a modified algorithm was assembled which systematically determines the optimum diffraction point.

## 4.2 Modified Wing EDGE Diffraction Point Algorithm

One of the prime concerns when approaching a modification to the program was to keep the computing time to a strict minimum, therefore the diffraction point had to be localized without having to iterate along the entire length of the wing edges.

The objective was therefore to modify the subroutine WANGEDG to optimize the location of the diffraction point in the overall path between two antennas or points of interest.

In order to accomplish this task a study of the procedure in calling these pertinent subroutines had to be done.

Once two antenna locations are obtained, AAPG determines if a straight line between the two points of interest can be traced without intercepting the fuselage geometry. If it can, then the routine STLINE is called, and if not then the routines CYLINDR and subsequently URGENT are called.

However, in both cases the next step is to determine if the path between the two locations, whether it is a straight line or not, pierces a wing. This is accomplished by calling the routine WNGINT which determines if the path

pierces a wing and, in the affirmative, it provides the orthogonal coordinates of this intercepting point.

Following this step is the determination of the diffraction point. This point will be of great importance in the electromagnetic interference margin calculations mainly due to the angle to and from this point to/from the antennas and to the overall path distance.

Initially the subroutine WNGEDG which will determine the optimum diffraction point, establishes an approximate point on each edge which will also be the starting point for iteration. This starting point is determined as follows:

a) from the piercing point provided by the routine WINGINT a perpendicular line to each of the wing edges is traced, and then the routine makes use of the vector dot product to locate the point.

b) one first have the information shown in Figure 4.2 which provides a vector perpendicular to the front edge as (Xintr-Xedge, Yintr-Yedge, Zintr-Zedge) and another vector which follows the front edge of the wing i.e. (Xcoef, Ycoef, Zcoef) where

$$Xcoef = Ptbl - Pfbl \qquad (4.1)$$

$$Ycoef = Ptwl - Prwl \quad (4.2)$$

$$Zcoef = Wtfs - Wffs \quad (4.3)$$

these two vectors being perpendicular will present a dot product of zero or;

$$(Xintr-Xedge)Xcoef+(Yintr-Yedge)Yceo+(Zintr-Eedge)Zcoef=0 \quad (4.4)$$

c) In addition, it is known that the point of diffraction will be located on the edge or a straight line which constitutes the edge of the wing. In the case of the front edge, the parametric form of a straight line is used;

$$Xedge = Pfbl + Xcoef \cdot T \quad (4.5)$$

$$Xedge = Pfwl + Ycoef \cdot T \quad (4.6)$$

$$Xedge = Wffs + Zcoef \cdot T \quad (4.7)$$

where Pfbl, Pfwl and Wffs is a point on the line and Xcoef, Ycoef and Zcoef are the direction numbers.

Now replacing Xedge, Yedge and Zedge with their respective values in the first equation 4.4;

$$(Xintr-Pfbl-Xcoef.T)Xcoef+(Yintr-Pfwl-Ycoef.T)Ycoef + (Zintr-Wffs-Zcoef.T)\ Zcoef =0 \quad (4.8)$$

Effectuating the calculations and rearranging ;

```
T=(Xintr*Xcoef+Yintr*Ycoef+Zintr*Zcoef-(PFBL *
Xcoef+PFWL*Ycoef+WFFS*Zcoef))/(Xcoef**2+Ycoef**2+
Zcoef**2)                                          (4.9)
```

Subsequently programming the parametric form of the straight line equations 4.5 through 4.7, this point Xedge, Yedge and Zedge which represents the closest point on the edge of interest, can be obtained.

This procedure is first accomplished on the leading edge of the wing in order to find this approximate diffraction point. Once this point is located, it is necessary to iterate along the wing edge, on both sides, in order to optimize this diffraction point. This is done as follows:

a. starting with the point found previously, and the point which is the perpendicular projection of the piercing point on the front edge of the wing, one calculates the overall distance from the antenna location #1 to antenna location #2 via this diffraction point.

b. this point is then moved along the edge by .01 in the positive direction and obtain a new diffraction point on the edge.

c. subsequently, recalculation of the distance from antenna #1 to antenna #2 via this new diffraction point is done.

d. the two distances are then compared, and if the new distance is shorter than the previous one the new diffraction point is kept as the new starting point and the process is repeated. When the new distance is longer than the previous one, the previous point is the optimum point in that direction.

e. therefore when the new distance is longer than the previous one, the search is done in the other direction. At this point the algorithm goes back to the initial point which is the perpendicular projection on the front edge and start looking in the negative direction adding -.01 to the initial point and comparing the newly calculated distance with the

optimum distance found in the positive direction.

f. again if this new distance is shorter the new point on the edge is kept as the optimum diffraction point for this entire edge, if not then the previous point is kept as the optimum point.

The above procedure will provide the optimum diffraction point on the leading edge. However, this is not necessarily the overall optimum diffraction point. The search must also be done on the rear edge and the wing tip.

Thus the next step is to repeat the previous steps for the rear edge comparing the newly found distance with the optimum distance obtained on the leading edge and keeping the point which gives the shorter distance between antenna #1 and antenna #2.

Finally the wing tip is investigated for the optimum diffraction point by scanning the points on the tip and comparing once more with the optimum distance obtained before.

Once this search for the optimum wing diffraction point is finalized one can use with confidence the point obtained

as the diffracted point where the path between antennas 1 and 2 will be routed.

The calculation accomplished as per the algorithm above is done for the right and/or the left wing as required, depending on whether the path between the two antennas intercept the right, the left or both wings.

A primitive flow chart of this subroutine is in Appendix A and the listing in Appendix B.

## 4.3 Results

Figures 4.1 and 4.3 shows the difference in paths between two antennas located above and below the leading edge of the wing. It can be seen in Figure 4.1 that the primitive way of calculating the path was to trace a perpendicular line to the edge using this point as the diffraction point. Figure 4.3 illustrates that the optimum point is located further towards the wing tip.

The difference in electromagnetic interference margin is quite noticeable between the old way of calculating the diffraction point and the new way. Figures 4.4 and 4.5 show that the initial way gives an EMI margin of 117.2 dB with a distance of 5.2 wavelength at the first harmonic while the new approach shown in Figures 4.6 and 4.7, gives a margin of

116.5 dB with a distance of 4.8 wavelength.

Figures 4.4 through 4.7 illustrate the improvement obtained with the inclusion of the modification. One can note that the path in the old version was forced to the leading edge of the wing and this is because a perpendicular point could not be found on the wing tip. The transmitter antenna being in front of the forward wing tip corner, was forcing the diffraction point to be either on the leading edge or the rear edge of the wing.

In the modified version, no restriction exists where the diffraction can be located. Therefore the real optimum diffraction point can be obtained. Figures 4.8 through 4.11 show the old and new propagation path and EMI margin involved between two other systems. Again it may be observed that the proper path shown in Figures 4.10 and 4.11 is quite different than the formal one in Figures 4.8 and 4.9. The EMI margin difference between the old and new approach is .2 decibel with one wavelength difference.

Additional interesting interactions between systems are presented in Figures 4.12 through 4.15. Again the improvement in the path determination by the optimization of the diffraction point may be observed.

## 4.4 Summary

On most military fighter aircraft the wing area is a most sensitive area for ordnance and must be a source of special attention when evaluating the electromagnetic field strength. A too large field level, could have a disastrous impact on the fighter's operation.

It can be noted in all the path improvements provided by the wing diffraction modification that the electromagnetic interference margin is in most cases higher with a shorter distance between the two points of interest. This is quite significant since it is always safer to predict a higher interference margin than a lower one.

In the wing diffraction cases it is much better to ensure higher EMI figure prediction than to have a lower prediction. Thus the modifications provide a safer value in the inter-system electromagnetic interference margin .

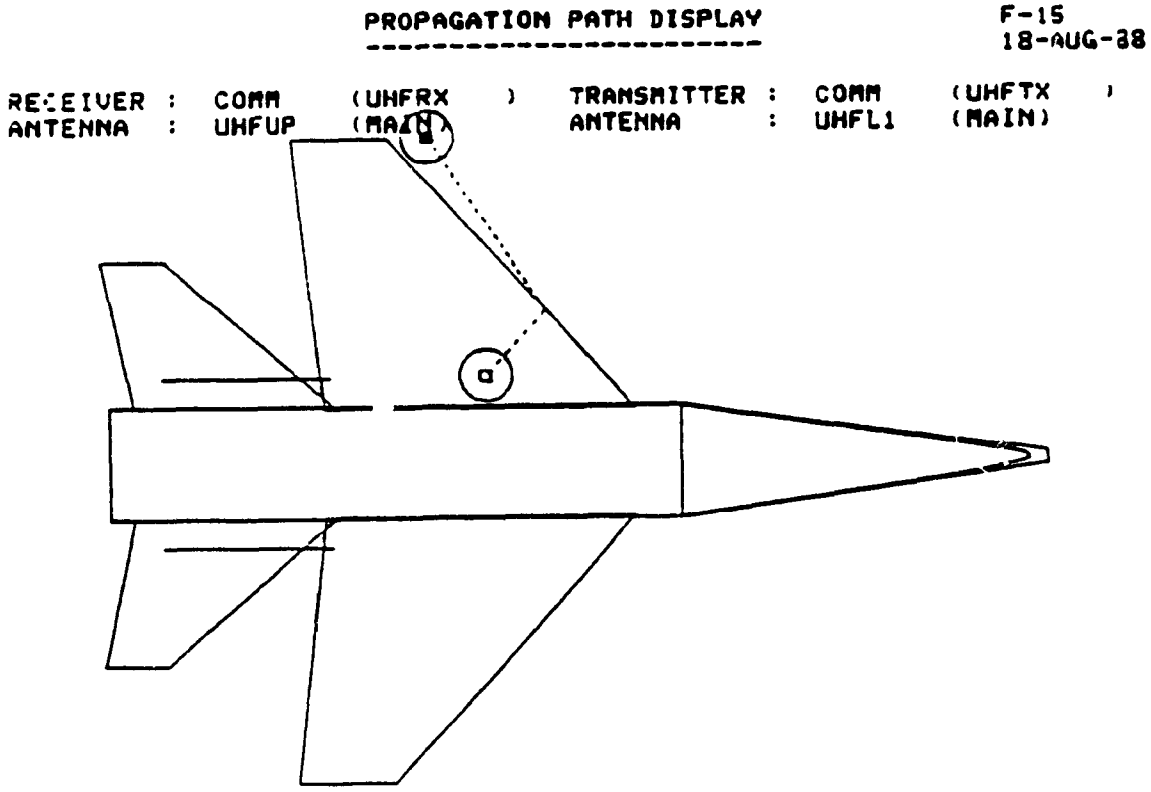


**Figure 4.1 Unmodified Path-Top View**

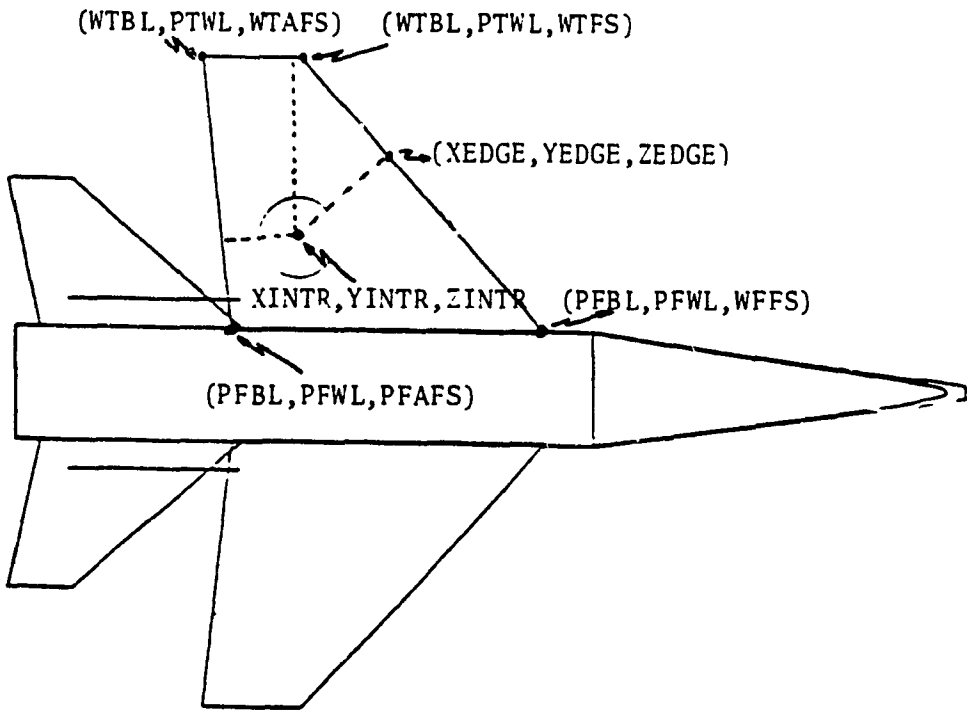


**Figure 4.2 Major Points Identification**

PROPAGATION PATH DISPLAY F-15
18-AUG-88

RECEIVER : COMM (UHFRX ) TRANSMITTER : COMM (UHFTX )
ANTENNA : UHFUP (MAIN) ANTENNA : UHFL1 (MAIN)

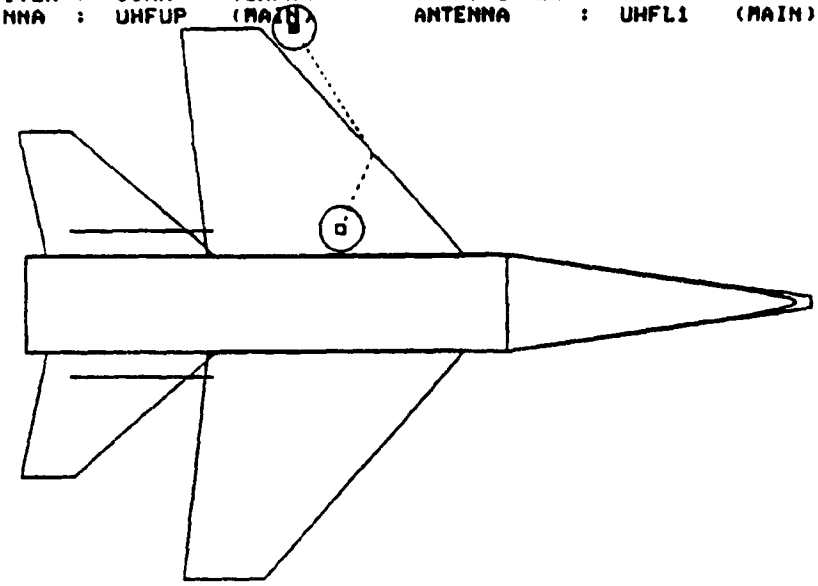

Figure 4.3 Modified Path-Top View

ELECTROMAGNETIC INTERFERENCE MARGIN CALCULATION F-15
12-OCT-88

TRANSMITTER : COMM (UHFTX ) RECEIVER : COMM (UHFRX )

| DESCRIPTION | HARMONIC NO : 225.0 MHZ | HARMONIC NO : 400.0 MHZ |
|---|---|---|
| TRANSMITTER POWER | 50.0 | -89.9 |
| XMTR CABLE LOSSES | 0.0 | 0.0 |
| XMTR ANTENNA GAIN | 2.1 | 2.1 |
| TRANSMISSION LOSS | -36.3 | -41.3 |
| SURFACE SHADING | 0.0 | 0.0 |
| EDGE SHADING | -1.7 | -2.2 |
| RCVR ANTENNA GAIN | 2.1 | 2.1 |
| RCVR CABLE LOSSES | 0.0 | 0.0 |
| RCVR SENSITIVITY | -101.0 | -101.0 |
| EMI MARGIN | 117.2 | -28.2 |
| \ FIELD WARNING | \ 5.2 | \ 9.2 |

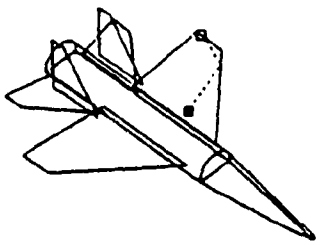

TRANSMITTER ANTENNA
UHFUP (MAIN) EL : -4.88 AZ : -111.31

RECEIVER ANTENNA
UHFL2 (MAIN) EL : 3.49 AZ : 20.76

ELEVATION : 45. DEG.
AZIMUTH : 45. DEG.

Figure 4.4 Unmodified Path-Left Wing Case

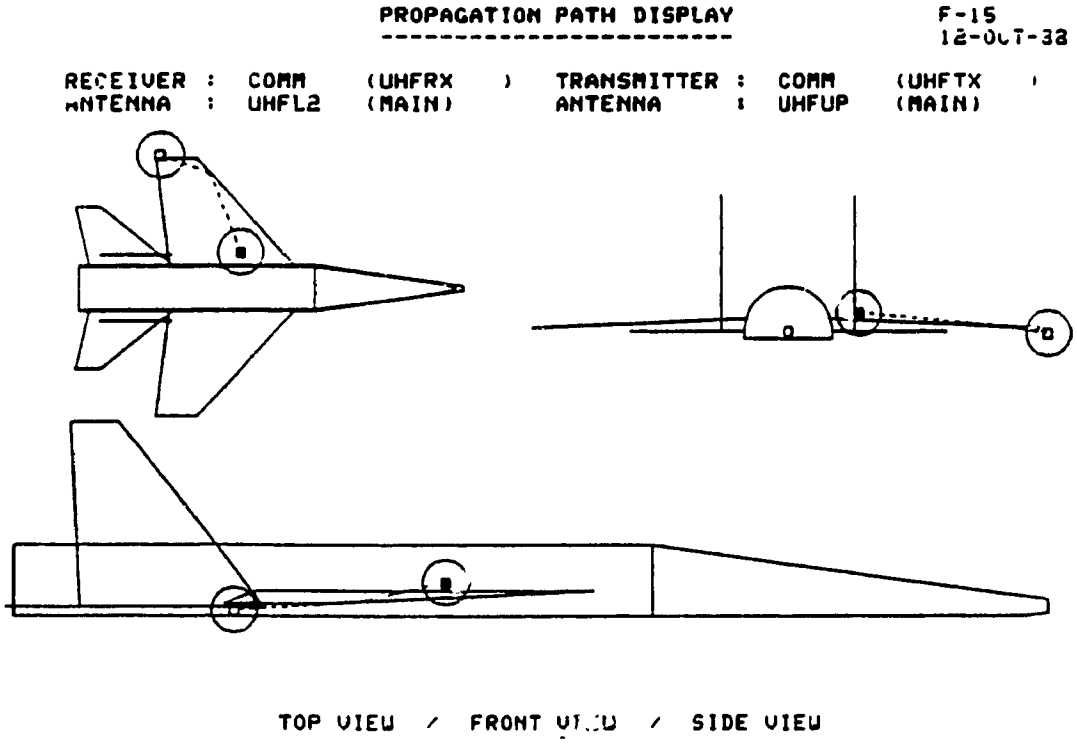


**Figure 4.5 Unmodified Path, Left Wing-All View**

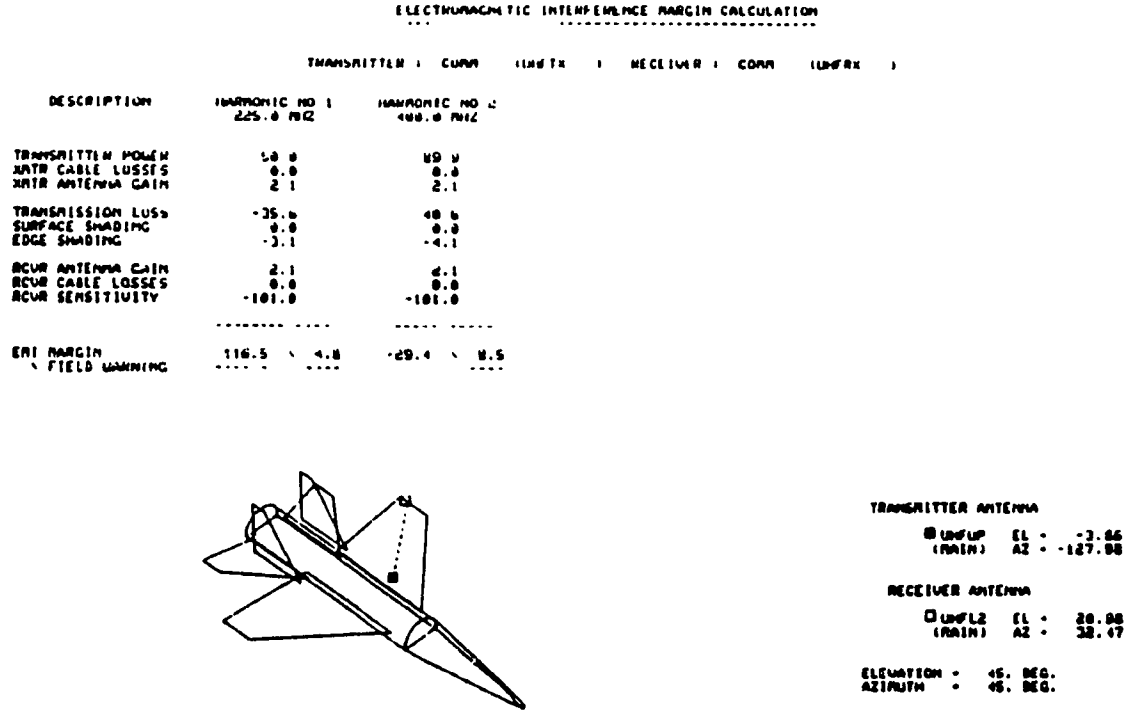


**Figure 4.6 Modified Path, Left Wing Case**

PROPAGATION PATH DISPLAY

RECEIVER : COMM (UHFRX ) TRANSMITTER : COMM (UHFTX
ANTENNA : UHFL2 (MAIN) ANTENNA : UHFUP (MAIN)

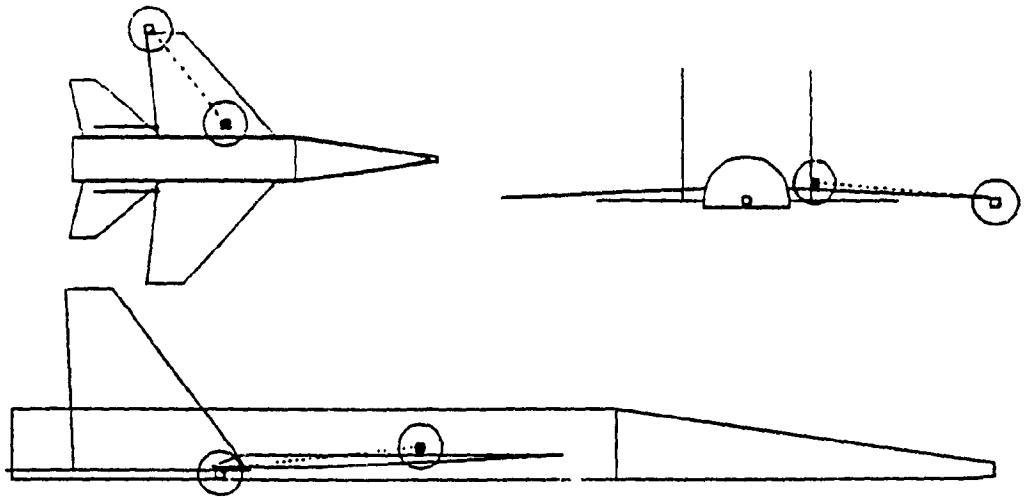

TOP VIEW / FRONT VIEW / SIDE VIEW

Figure 4.7 Modified Path, Left Wing-All View

ELECTROMAGNETIC INTERFERENCE MARGIN CALCULATION

TRANSMITTER : IDENT (IFFTX ) RECEIVER : IDENT (IFFRX )

| DESCRIPTION | HARMONIC NO : 1.030 GHZ |
|---|---|
| TRANSMITTER POWER | 26.8 |
| XMTR CABLE LOSSES | 0.0 |
| XMTR ANTENNA GAIN | 2.1 |
| TRANSMISSION LOSS | -44.3 |
| SURFACE SHADING | 0.0 |
| EDGE SHADING | -2.9 |
| RCVR ANTENNA GAIN | 2.1 |
| RCVR CABLE LOSSES | 0.0 |
| RCVR SENSITIVITY | -77.0 |
| EMI MARGIN | 60.9 > 13. |
| > FIELD WARNING | ------ |

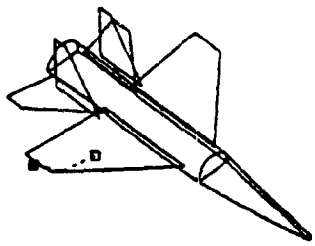

TRANSMITTER ANTENNA
■ IFFLO (MAIN) EL : 3.33 AZ : -19.33

RECEIVER ANTENNA
□ IFFUP (MAIN) EL : -4.85 AZ : 104.72

ELEVATION : 45. DEG.
AZIMUTH : 45. DEG.

Figure 4.8 Unmodified Path, Right Wing Case

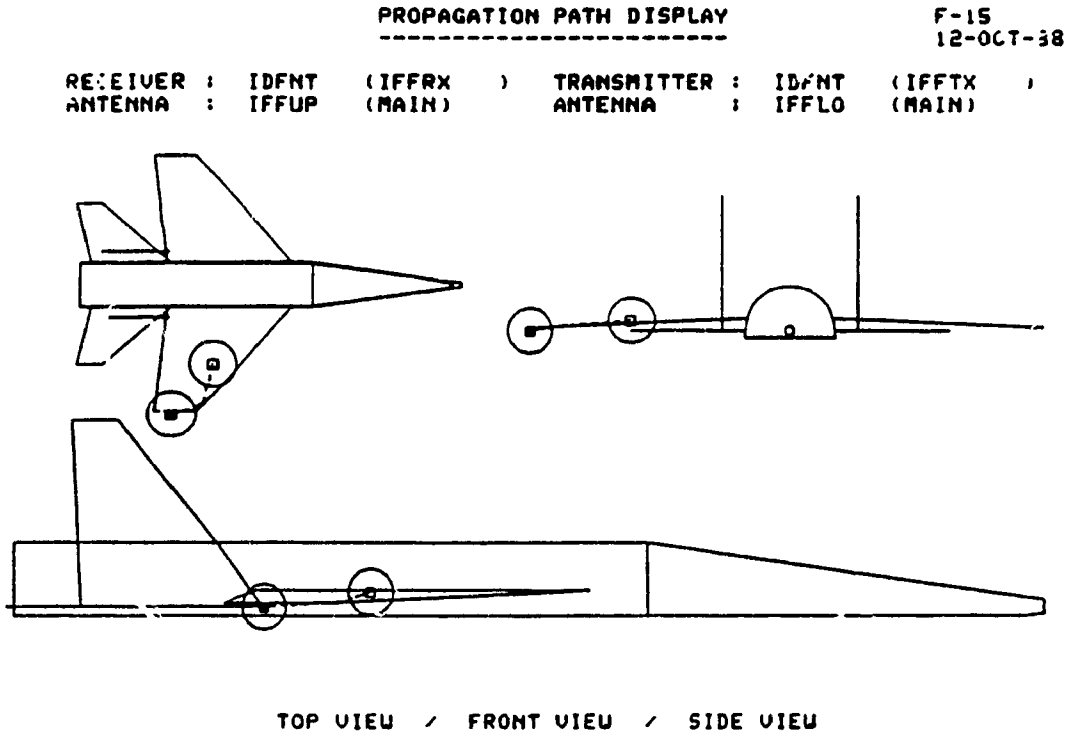


**Figure 4.9 Unmodified Path, Right Wing-All View**

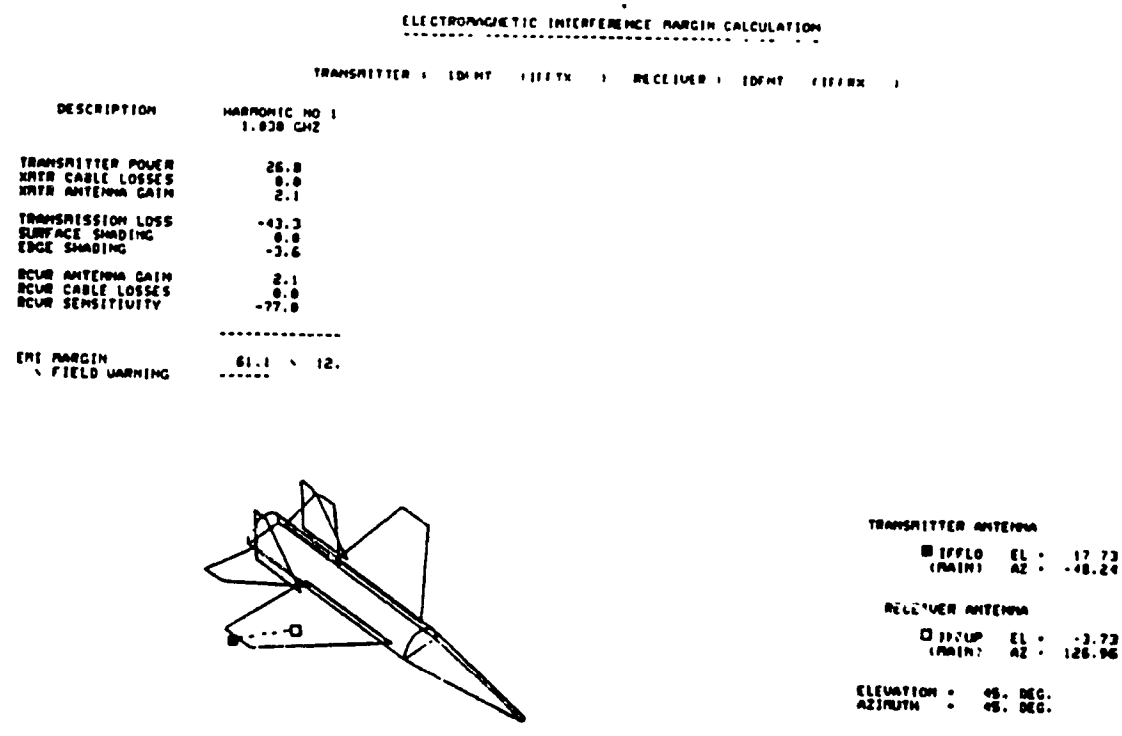


**Figure 4.10 Modified Path, Right Wing Case**

PROPAGATION PATH DISPLAY

RECEIVER : IDENT (IFFRX ) TRANSMITTER : IDENT (IFFTX )
ANTENNA : IFFUP (MAIN) ANTENNA : IFFLO (MAIN)

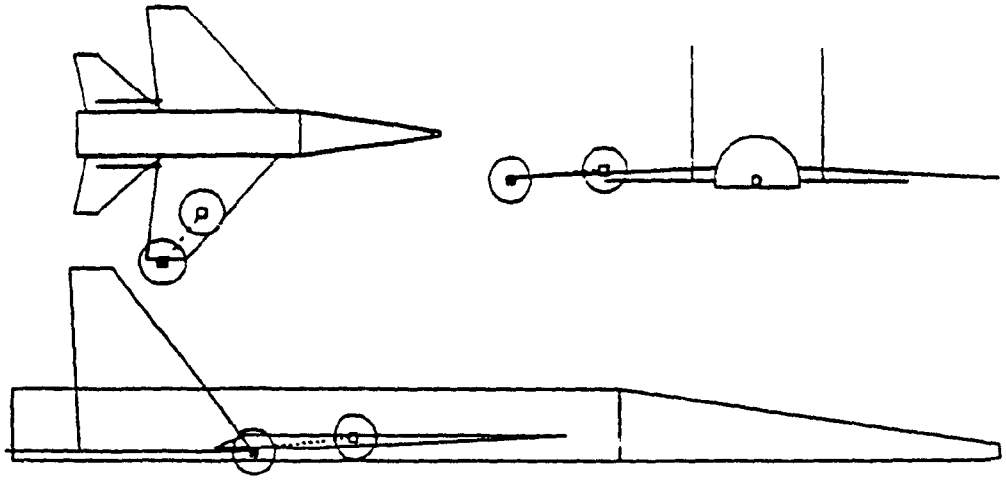

TOP VIEW / FRONT VIEW / SIDE VIEW

Figure 4.11 Modified Path, Right Wing Case-All View

ELECTROMAGNETIC INTERFERENCE MARGIN CALCULATION

TRANSMITTER : COMM (UHFTX ) RECEIVER : IDENT (IFFRX )

| DESCRIPTION | HARMONIC NO 2 893.2 MHZ | HARMONIC NO 3 1.630 GHZ |
|---|---|---|
| TRANSMITTER POWER | -93.2 | -93.0 |
| WITH CABLE LOSSES | 0.0 | 0.0 |
| WITH ANTENNA GAIN | 2.1 | 2.1 |
| TRANSMISSION LOSS | -50.1 | -51.3 |
| SURFACE SHADING | 0.0 | 0.0 |
| EDGE SHADING | -22.8 | -23.4 |
| RCVR ANTENNA GAIN | 2.1 | 2.1 |
| RCVR CABLE LOSSES | 0.0 | 0.0 |
| RCVR SENSITIVITY | 3.6 | -77.0 |
| EMI MARGIN \ FIELD WARNING | -164.8 \ 25. | -16.5 \ 29. |

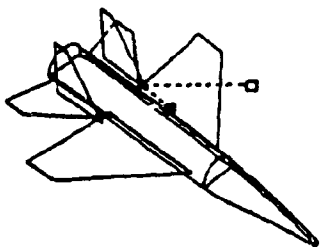

TRANSMITTER ANTENNA
■ UHFUP EL = -2.25
(MAIN) AZ = -175.82

RECEIVER ANTENNA
□ IFFUP EL = 10.25
(MAIN) AZ = 124.76

ELEVATION = 45. DEG.
AZIMUTH = 45. DEG.

Figure 4.12 Unmodified Path, Different Wing Edge Case

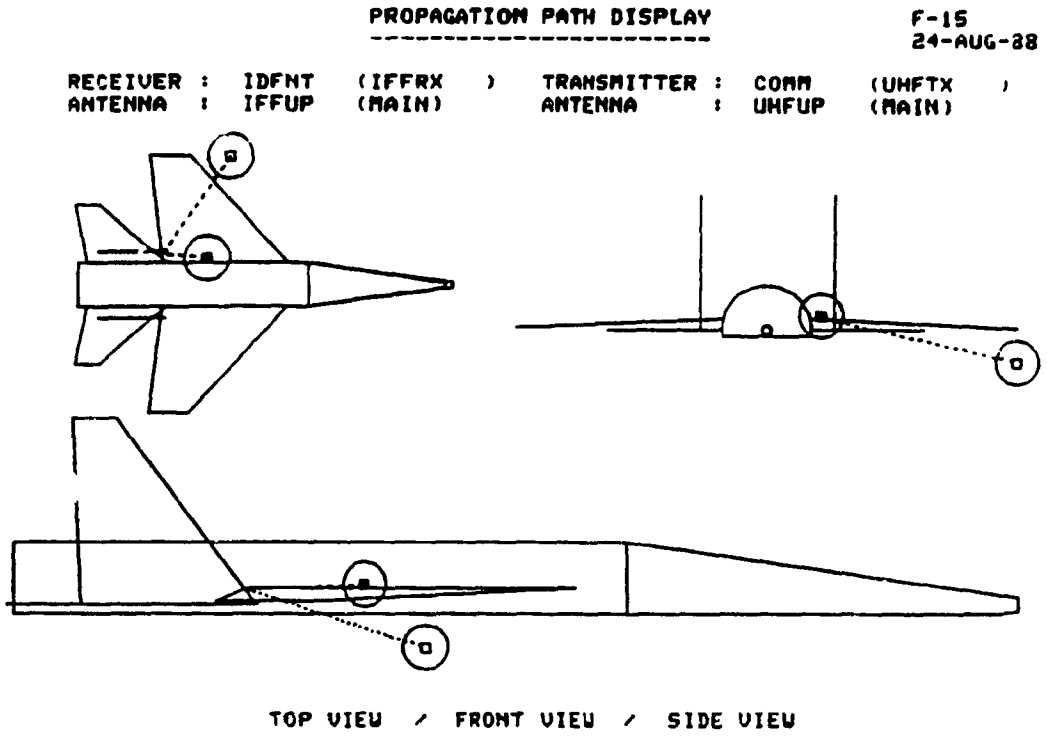


Figure 4.13 Unmodified Path, Different Wing Edge Case- All View

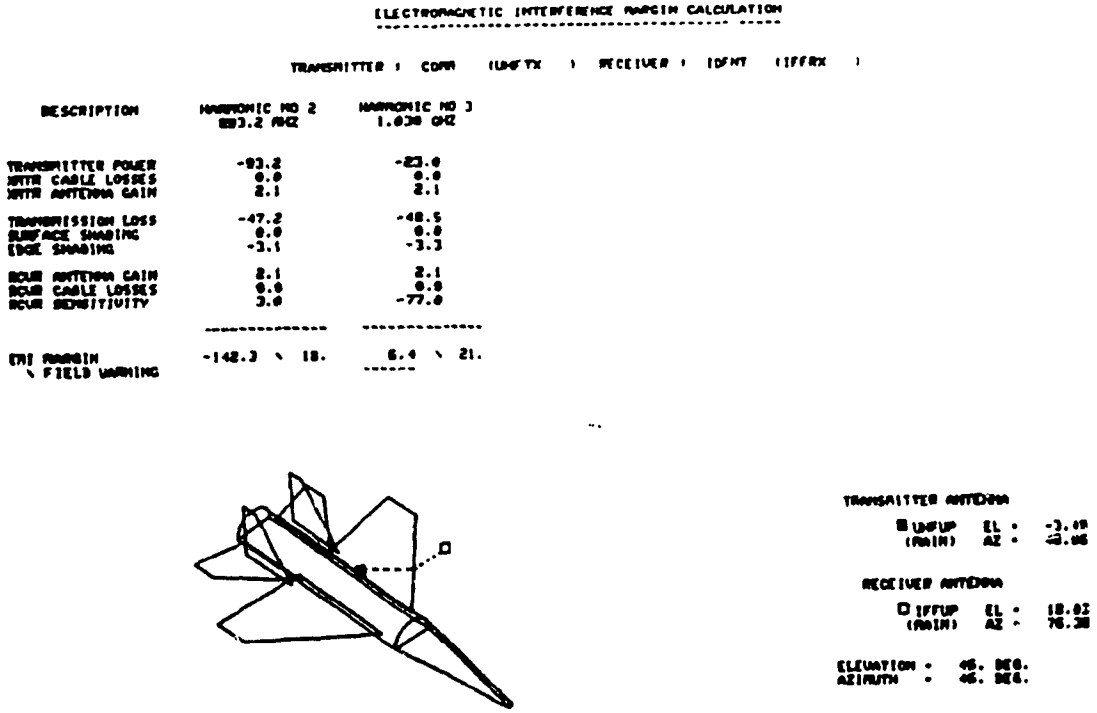


Figure 4.14 Modified Path, Different Wing Edge Case

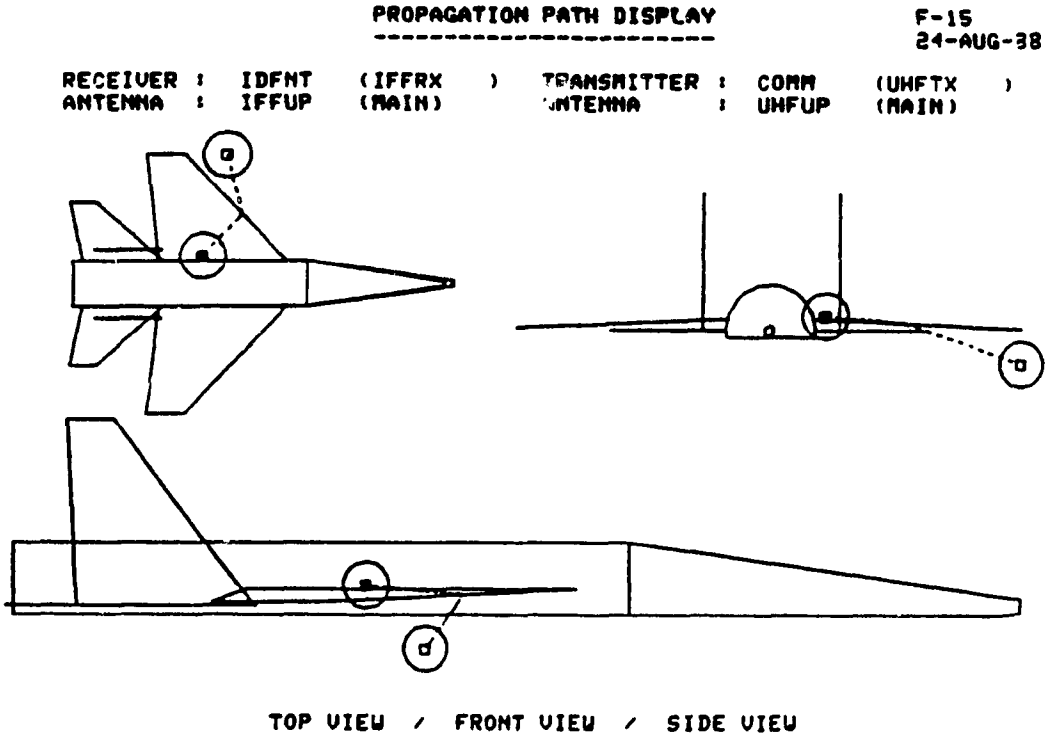


Figure 4.15 Modified Path, Different Wing Edge Case-All View

# CHAPTER 5

# CYLINDRICAL/CONICAL SPIRAL

# INTERSECTION POINT

## 5.1 Introduction

Emission and reception points on an aircraft are often located on the conical portion of the airframe which represents the nose, and on the cylindrical geometry representing the body. The intersection line between the cylindrical and conical geometry which, on a real aircraft is a change of radius of curvature, must be analyzed whenever an interaction involves two antennas located on each side of this intersection line.

The point where the propagation path will cross this intersection line must be determined in a precise manner otherwise the path distance and the shading loss calculation would be incorrect.

The approach utilized to calculate this crossover point in AAPG Version 7, assumed a constant rate of change of the angle variation versus distance. This assumption would be correct if considering a geometry with constant radius of curvature like a cylinder. However, the conical shape

presents a varying radius of curvature which renders the assumption incorrect.

A refinement of the method to search for the optimum crossover point is required.

## 5.2 Version 7 Initial Approach

As mentioned previously, the first approach used in early versions of AAPG assumed a constant rate of change in angle with distance.

The calculation to locate the crossover point was accomplished in the following manner.

With two antenna points: P1 located on the cylindrical portion of the airframe, P2 on the conical part, the geodesic path had to proceed from P1 to P2 via an intersection point.

As in Figure 5.1, the angle $\theta_\mu$ must be determined in order to locate the intersection point.

If "B" is the distance from P1 to the cone/cylinder intersection and A is the distance from P2 to this same intersection, with $\theta_1$ as the angle to P1 and $\theta_2$ the angle to P2, the following formulation is used to determine $\theta_\mu$ ;

$$\frac{A^2 + R^2}{B} = \frac{\theta_\mu - \theta_1}{\theta_2 - \theta_\mu} \qquad (5.1)$$

Where R is the radius of the cylindrical portion of the airframe.

It can be noted in Figure 5.2 that this method provides a nice smooth geodesic curve which goes from antenna 1 to antenna 2, however the curve or path is not in compliance with the Fermat principle. In short, this path does not present the shortest way to proceed from P1 to P2.

This deficiency is due to the assumption that the angle variation of the geodesic is constant with the distance. This of course would be correct if the geometry utilized would be of cylindrical form only. But in our case, using a combination of cylindrical and conical geometry, this assumption is no longer valid.

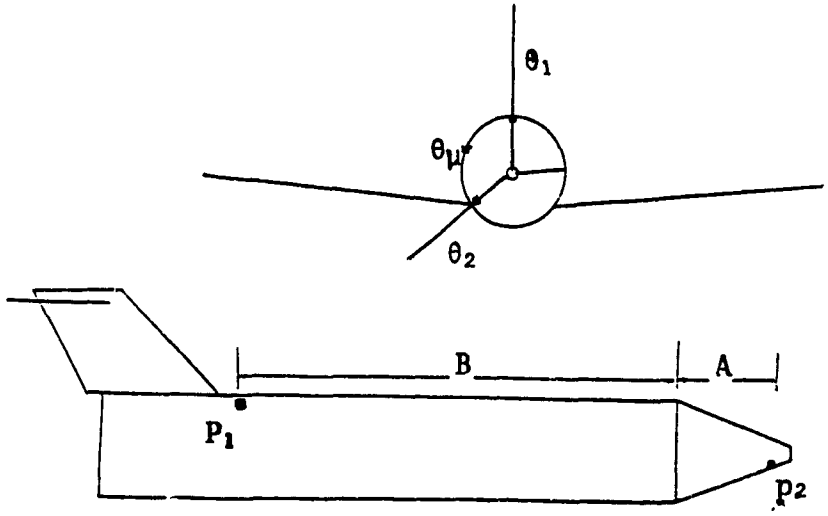


**Figure 5.1 Cross Point Approximation**

## 5.3 Optimization Technique

The crossover point, on the cylindrical/conical intersection line, not representing the optimum point that the shortest path between the two antennas should intercept, an optimization technique was needed.

The manner utilized to find the crossover point was kept, and an iterative technique approach was used to find the point which would provide the shortest path [19]. Appendix C to this document provides the flow chart of the approach and Appendix D shows the code listing.

## 5.4 Results

The AAPG code containing the modification discussed above was run using the Challenger aircraft.

Figure 5.2 illustrates two antennas with a connecting path of which the intercept point on the cylindrical/conical intersection line was found using the old method. Figure 5.3 in turn, shows a path where the iterative method was used to optimize the intercept point.

One may note that the path length was improved by one wavelength which represents an increase of 4.7 dB in the EMI

margin. Figures 5.4 and 5.5 provide a closer look at the old propagation path and the new one respectively.

Another example of the improvement provided by the iterative method is presented in Figures 5.6 and 5.7. Again a path length difference of one wavelength is observed and an EMI margin increase of 1.5 dB when using the iterative method.

Figures 5.8 and 5.9 illustrate the detailed path of the formal approach and the modified version respectively.

## 5.5 Validity

The validity of the iterative technique is supported when the distance found with the modification to the code presented a shorter path. Thus proving that the formal method does not observe the Fermat criterion.

Using the modified code provides a shorter path which in turn alters the electromagnetic interference margin in a positive manner.

Having a higher figure as the EMI margin, the engineering study of systems will be safer and will provide better information for the analysis of systems on board any airframe.

CE-144B

ELECTROMAGNETIC INTERFERENCE MARGIN CALCULATION

TRANSMITTER : HF ANTXN : RECEIVER : [illegible]

| DESCRIPTION | HARMONIC NO 1 8.000 GHZ | HARMONIC NO 2 8.000 GHZ | HARMONIC NO 3 8.000 GHZ |
|---|---|---|---|
| TRANSMITTER POWER | -10.0 | -70.0 | -70.0 |
| XMTR CABLE LOSSES | 0.0 | 0.0 | 0.0 |
| XMTR ANTENNA GAIN | 2.1 | 2.1 | 2.1 |
| TRANSMISSION LOSS | -74.3 | -74.3 | -74.3 |
| SURFACE SHADING | -27.8 | -27.8 | -27.8 |
| EDGE SHADING | 0.0 | 0.0 | 0.0 |
| RCVR ANTENNA GAIN | -12.0 | -12.0 | -12.0 |
| RCVR CABLE LOSSES | 0.0 | 0.0 | 0.0 |
| RCVR SENSITIVITY | -30.0 | -30.0 | -30.0 |
| EMI MARGIN \ FIELD WARNING | -82.0 \ 414 | -152.0 \ 414 | -152.0 \ 414 |

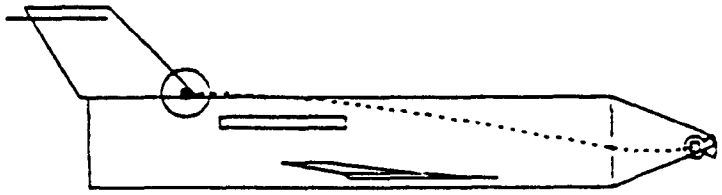

TRANSMITTER ANTENNA
HF ANT (MAIN) EL : 0.00 AZ : -11.38

RECEIVER ANTENNA
[illegible] (SIDE) EL : -1.84 AZ : -183.78

ELEVATION : 0. DEG.
AZIMUTH : 90. DEG.

Figure 5.2 Unmodified Path EMI

CE-144A

ELECTROMAGNETIC INTERFERENCE MARGIN CALCULATION

TRANSMITTER : HF ANTXN : RECEIVER : [illegible]

| DESCRIPTION | HARMONIC NO 1 8.000 GHZ | HARMONIC NO 2 8.000 GHZ | HARMONIC NO 3 8.000 GHZ |
|---|---|---|---|
| TRANSMITTER POWER | -10.0 | -70.0 | -70.0 |
| XMTR CABLE LOSSES | 0.0 | 0.0 | 0.0 |
| XMTR ANTENNA GAIN | 2.1 | 2.1 | 2.1 |
| TRANSMISSION LOSS | -74.3 | -74.3 | -74.3 |
| SURFACE SHADING | -23.1 | -23.1 | -23.1 |
| EDGE SHADING | 0.0 | 0.0 | 0.0 |
| RCVR ANTENNA GAIN | -12.0 | -12.0 | -12.0 |
| RCVR CABLE LOSSES | 0.0 | 0.0 | 0.0 |
| RCVR SENSITIVITY | -30.0 | -30.0 | -30.0 |
| EMI MARGIN \ FIELD WARNING | -87.3 \ 413 | -147.3 \ 413 | -147.3 \ 413 |

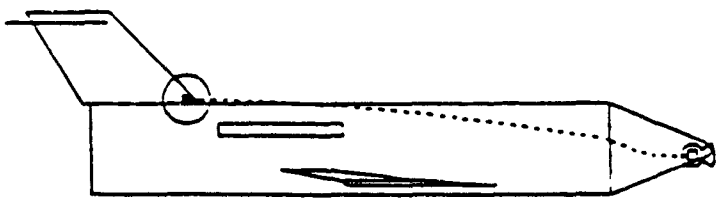

TRANSMITTER ANTENNA
HF ANT (MAIN) EL : 0.00 AZ : -0.00

RECEIVER ANTENNA
[illegible] (SIDE) EL : 7.04 AZ : -148.35

ELEVATION : 0. DEG.
AZIMUTH : 90. DEG.

Figure 5.3 Modified Path EMI

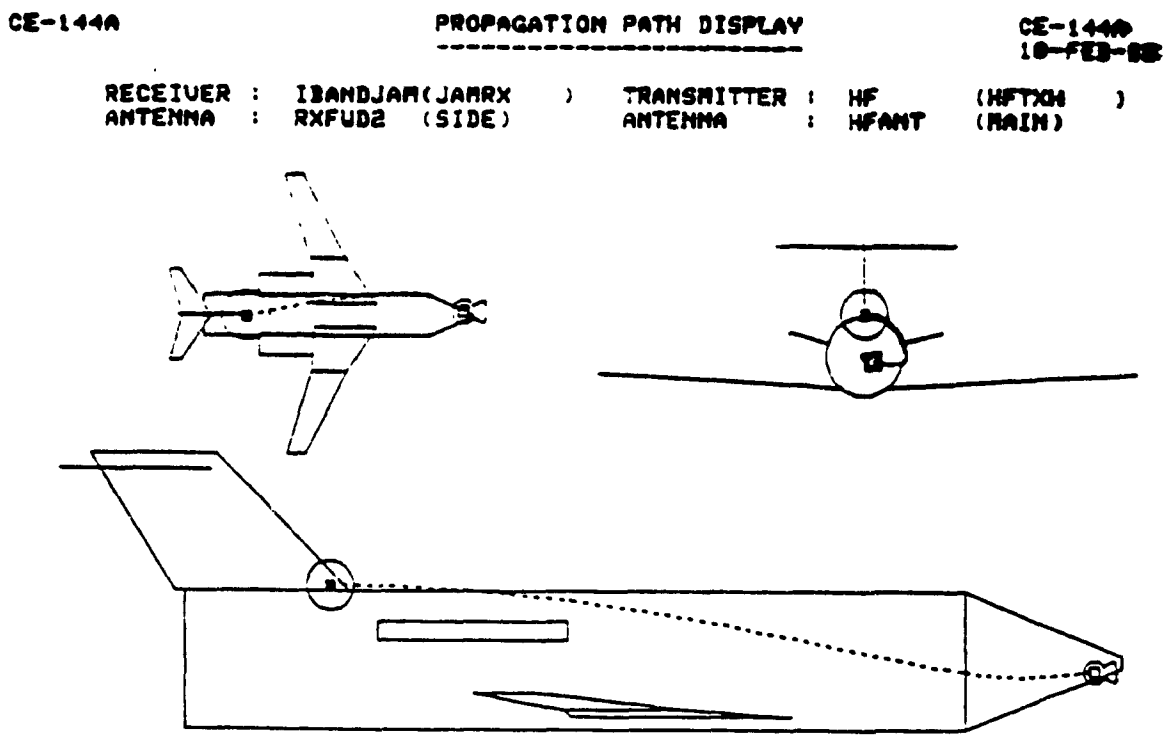


Figure 5.4 Unmodified Path-All View

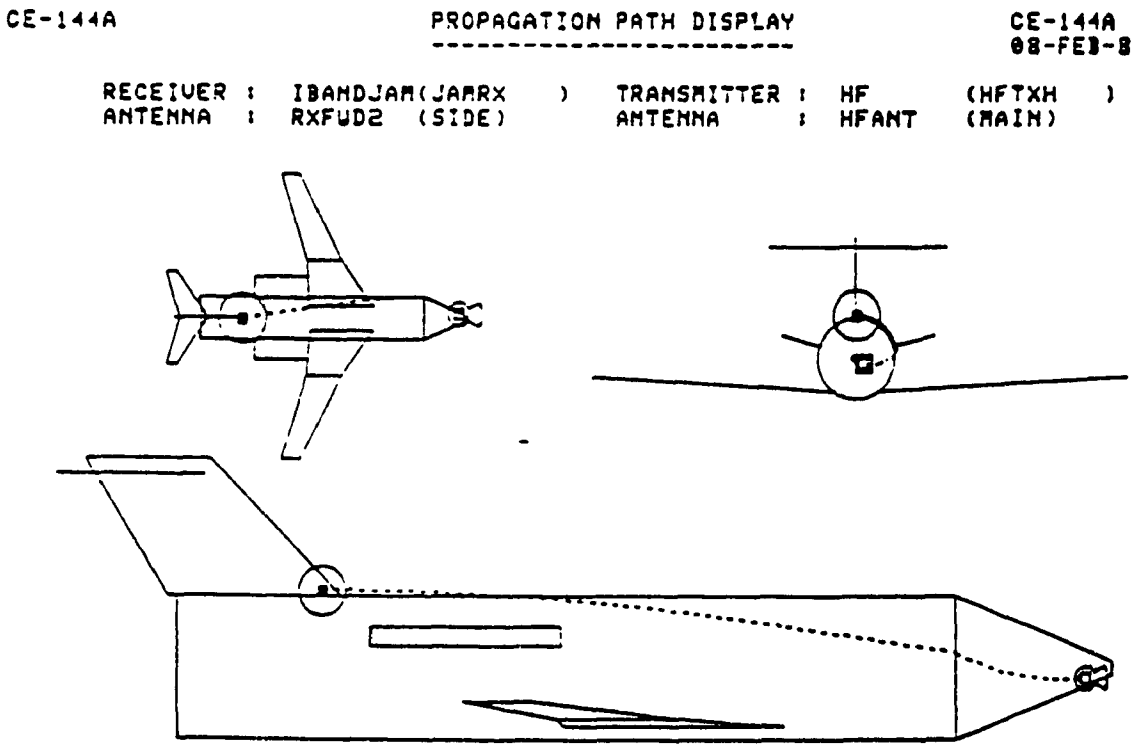


Figure 5.5 Modified Path-All View

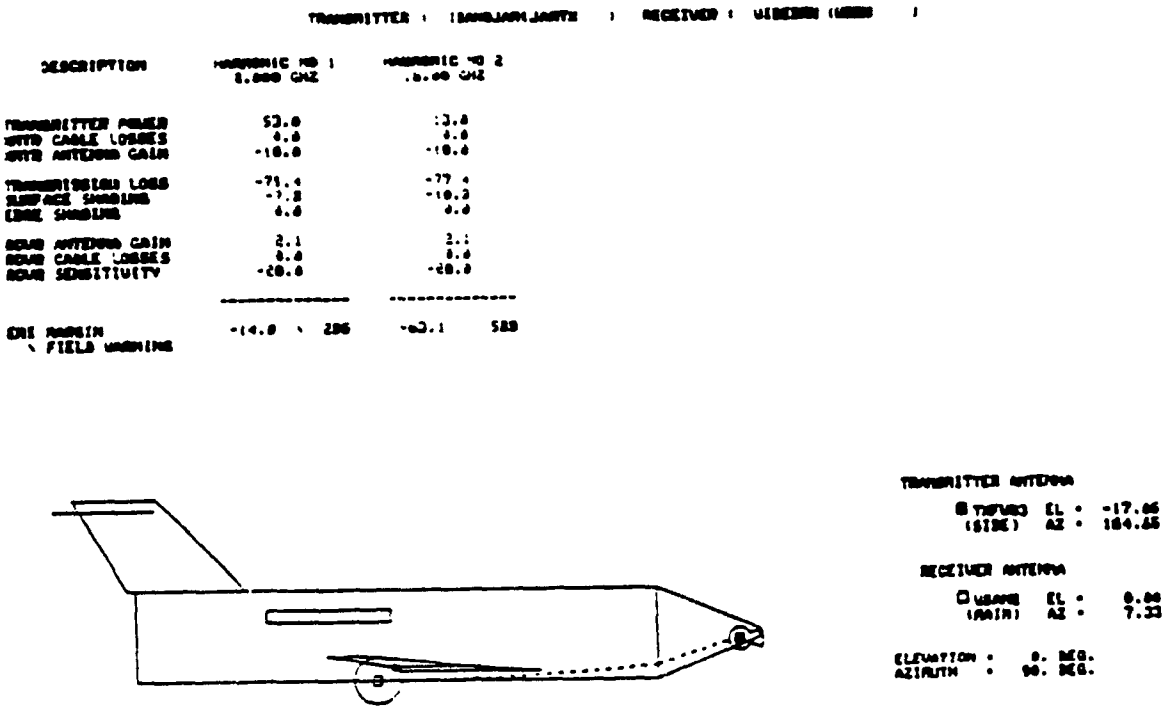


Figure 5.6 Unmodified Path EMI

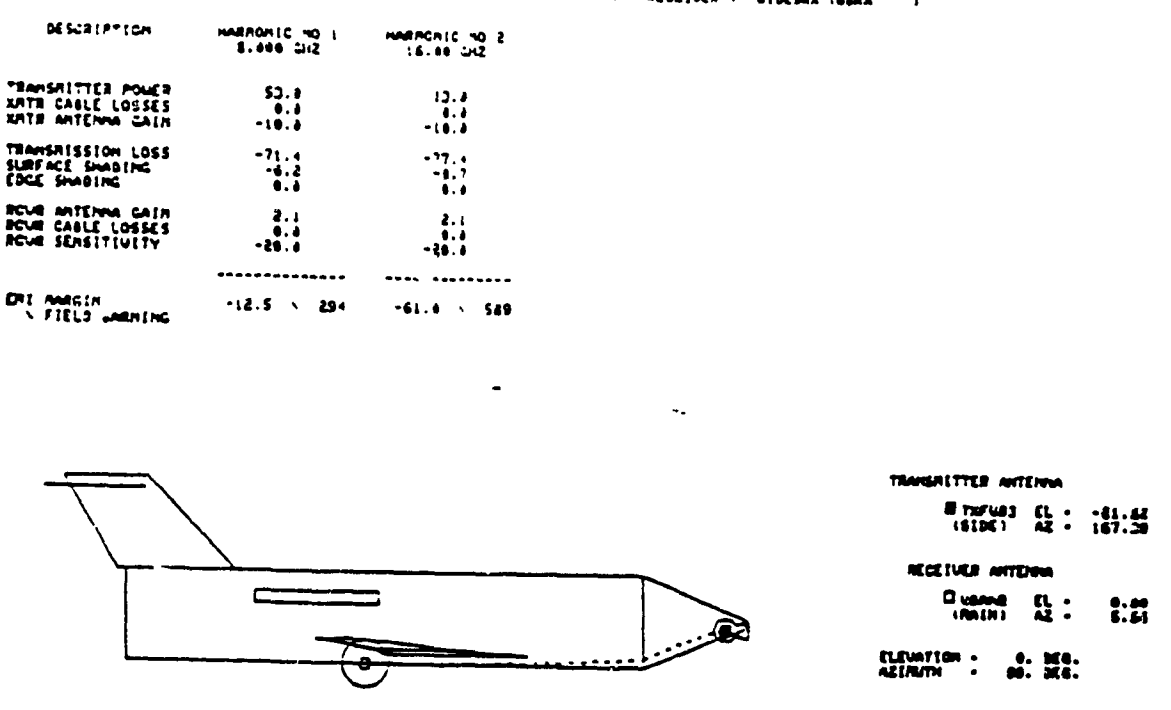


Figure 5.7 Modified Path EMI

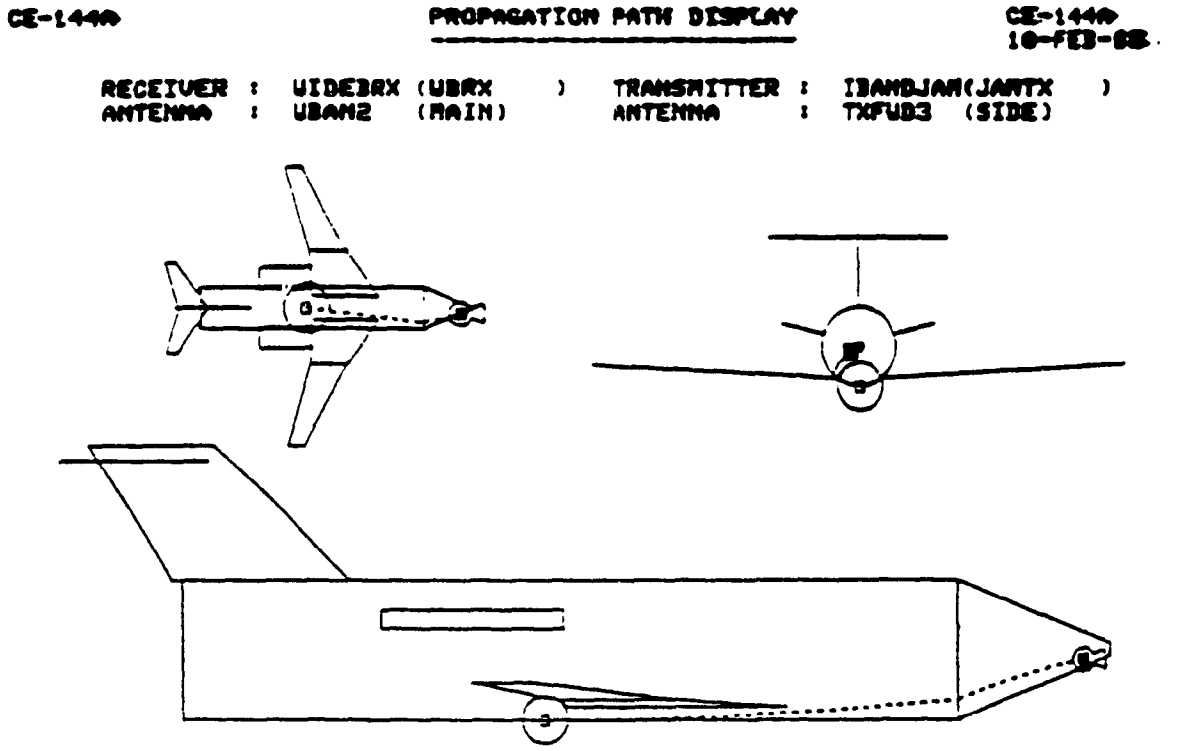


Figure 5.8 Unmodified Path-All View

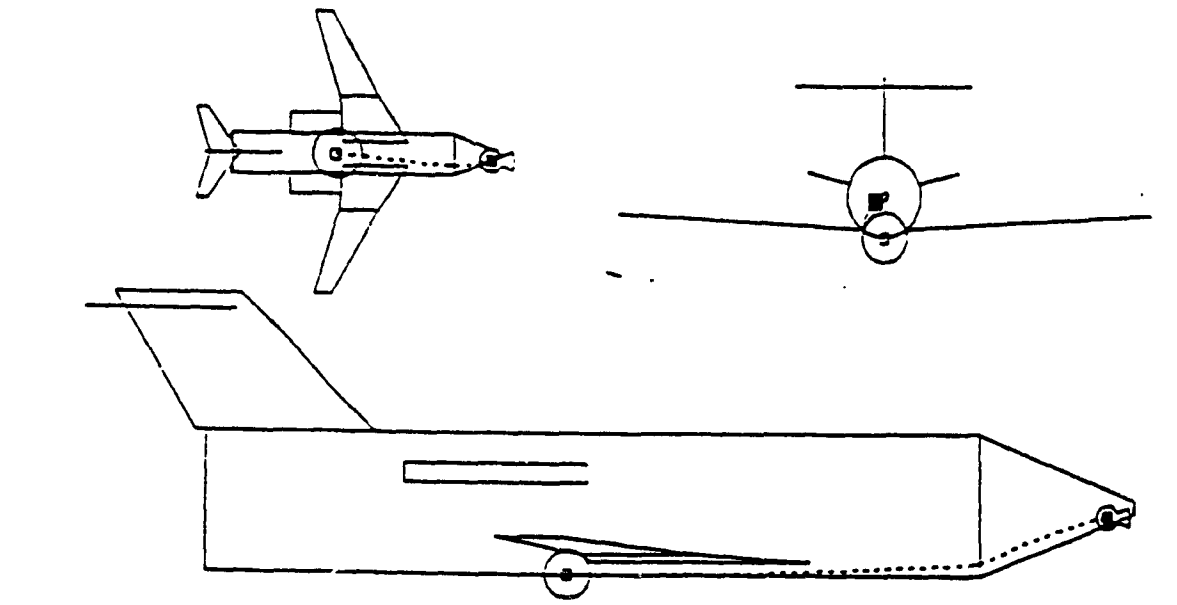


Figure 5.9 Modified Path-All View

# CHAPTER 6

# CONE REGION PATH IMPROVEMENT

## 6.1 Introduction

Within AAPG, when the emitting and the receiving points are located ahead of the cylinder/cone interface line, the code presents certain difficulties in handling the propagation path between the two points of interest, thus giving incorrect EMI figures.

This situation could occurr during close formation flying, during refueling operations or while carrying special equipment or ordnance on an airframe. It is therefore important to have the tools to predict the interference margin when the electromagnetic field strength could have a disastrous effect on critical payloads.

In its original version, AAPG did not verify if the emitting and receiving points were in line of sight but immediately assumed a combination of cylindrical spiral, conical spiral and straight lines. As can be seen in Figures 6.1 and 6.2, the path is incorrect which in turn provides an erroneous EMI margin calculated from the wrong path. A modification is therefore needed.

The approach here has been done in two steps: 1) verification as to whether two antennas, located ahead of the cylinder/cone intercept lines are in line of sight, 2) determination of the appropriate geodesic when the airframe geometry is intercepted.

ELECTROMAGNETIC INTERFERENCE MARGIN CALCULATION

F-15
23-AUG 88

TRANSMITTER : COMM (UHFTX ) RECEIVER : COMM (UHFRX )

| DESCRIPTION | HARMONIC NO 1 225.0 MHZ | HARMONIC NO 2 450.0 MHZ |
|---|---|---|
| TRANSMITTER POWER | 50.0 | -89.9 |
| XMTR CABLE LOSSES | 0.0 | 0.0 |
| XMTR ANTENNA GAIN | 2.1 | 2.1 |
| TRANSMISSION LOSS | -32.6 | -37.6 |
| SURFACE SHADING | -6.8 | -8.9 |
| EDGE SHADING | 0.0 | 0.0 |
| RCVR ANTENNA GAIN | 2.1 | 2.1 |
| RCVR CABLE LOSSES | 0.0 | 0.0 |
| RCVR SENSITIVITY | -101.0 | -101.0 |
| EMI MARGIN | 115.9 | -31.2 |
| \ FIELD WARNING | \ 3.4 | \ 6.0 |

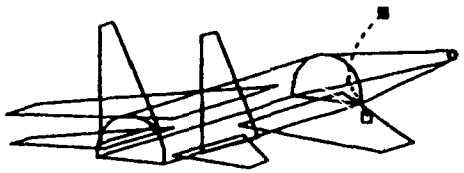

TRANSMITTER ANTENNA
UHFLP (MAIN) EL = -32.31 AZ = 133.86

RECEIVER ANTENNA
UHFL2 (MAIN) EL = 21.40 AZ = 48.73

ELEVATION = -10. DEG.
AZIMUTH = 30. DEG.

Figure 6.1 Demonstration of Incorrect Algorithm

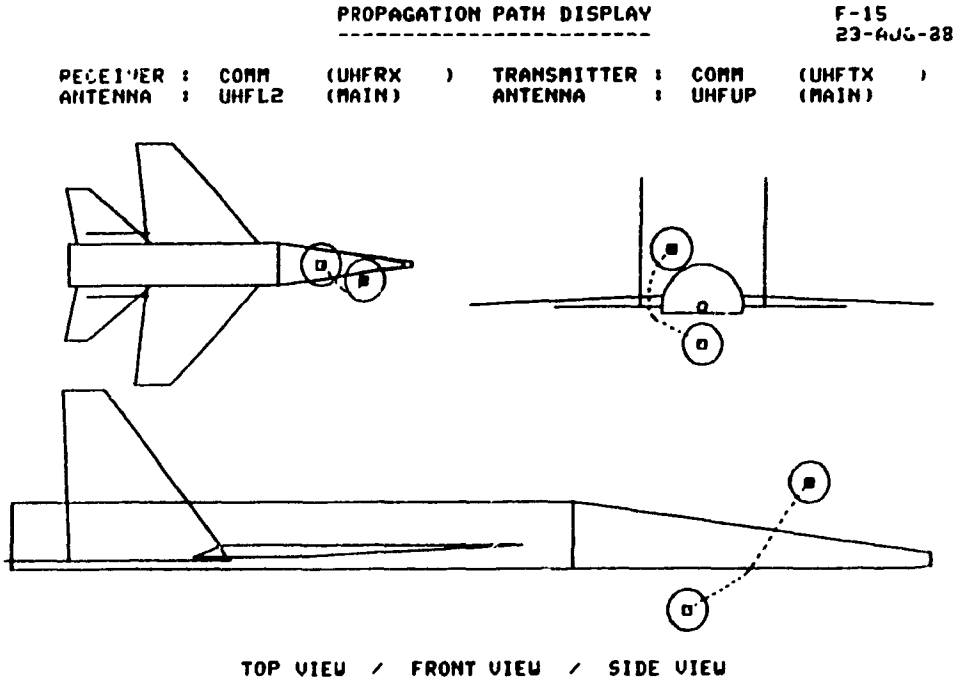


Figure 6.2 Incorrect Algorithm-All View

## 6.2 Line of Sight Verification

A new approach had to be considered when evaluating the propagation path between two antennas located forward of the cylinder/cone intersection line. A verification is accomplished in the subroutine PATHS which branch the software to the subroutine CONE when the two antennas are forward of this cylinder/cone intersection line. Once in the subroutine CONE where the path was assumed to be a conical spiral in the original version, a new subroutine called CONINT was added. A flowchart of this subroutine in shown in Appendix E and listing at Appendix F. In this new

subroutine a straight line between the emitter and receptor points is traced and verification is made to test if this line intercepts the conical geometry of the airframe.

This is done by first setting a logical variable to false assuming that the straight line will not intercept the conical geometry. Following this step, the slope of this straight line is calculated as follows using A1X, A1Y, A2X, and A2Y as the coordinates for the receiving and transmitting antennas respectively;

$$\text{Slope} = \text{Tan}\,\theta = (A2Y-A1Y)/(A2X - A1X) \qquad (6.1)$$

and the Y axis intercept would be as shown on Figure 6.5;

$$YINTC = (A1Y-A1X)*\text{Slope} \qquad (6.2)$$

which provides the equation of the line intercepting the two antenna points.

In order to obtain the equation of the circle which is formed on the cone geometry where a line potentially intercepts the cone, the origin of our coordinate system must be redefined as being the centre of the aircraft as shown in Figure 6.3. Because the conical portion of the airframe is significantly smaller than the overall length of the aircraft the circle approximation is quite valid.

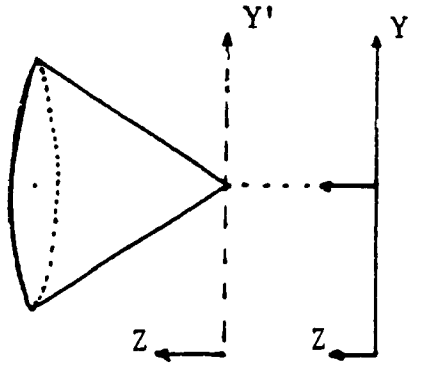


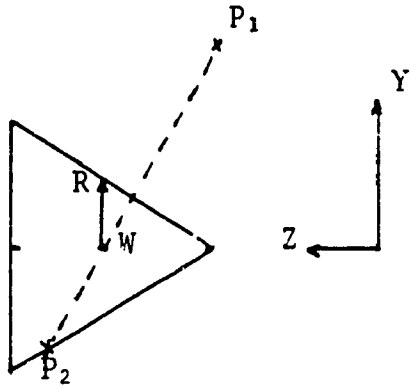


**Figure 6.3 Cone Coordinates** **Figure 6.4 Intercept Line**

The equation of the circle is:

$$(X-X_O)^2 + (Y-Y_O)^2 = R^2 \qquad (6.3)$$

and, forcing the aircraft geometry to be symmetrically located on the X axis, then:

$$X^2 + (Y-Y_O)^2 = R^2 \qquad (6.4)$$

where R is the radius of the cone at the geometrical mean distance between the two antennas as shown in Figure 4. This point is calculated using the cylindrical coordinates P1R, P1A, P1Z, P2R, P2A and P2Z for each respective point as;

$$\text{if} \qquad \Delta Z = |P2Z - P1Z| \tag{6.5}$$

$$\text{and if} \quad P1Z < P2Z$$

$$\text{then} \qquad \omega = P1Z + \frac{P1R}{P1R+P2R} \cdot AZ \tag{6.6}$$

$$\text{and if} \quad P1Z < P2Z$$

$$\text{then} \qquad \omega = P2Z + \frac{P2R}{P1R+P2R} \cdot AZ \tag{6.7}$$

On the straight line joining the two antennas, any point 'y' can be found using the straight line formula as shown in Figure 6.5 $Y = YINTC + slope\ (X-X_O)$ and $X_O$ being the WLC (water line centroid). Therefore the equation of the circle which represents the fuselage station at the point where the straight line linking the two antennas would meet the conical geometry becomes:

$$(X-X_O)^2 + Y^2 = R^2 \tag{6.8}$$

Replacing Y by the value above and with $X_O$ = WLC :

$$(X-WLC)^2 + (YINTC + slope(-WLC))^2 = R^2 \tag{6.9}$$

$$(X-WLC)^2+YINTC^2+2\ YINTC\ Slope(X-WLC)+slope^2(X-WLC)^2=R^2 \tag{6.10}$$

Rearranging :

$$(X-WLC)^2+slope^2\ (X-WLC)^2+(1+slope^2)(X-WLC)^2+2\ YINTC-slope(X-WLC)\ +\ YINTC^2-R^2)\ =\ 0 \qquad (6.11)$$

obtaining a quadratic equation of the form

$$AX^2 + BX + C = 0 \qquad (6.12)$$

where

$$A = (1 + Slope)^2 \qquad (6.13)$$

$$B = 2\ .\ YINTC\ .\ Slope \qquad (6.14)$$

$$C = YINTC^2 - R^2 \qquad (6.15)$$

and where X is the variable (X-WLC).

Subsequentially, using the solution for the quadratic equation , verification whether we can obtain real values must take place. If real values are obtained then the straight line between the two antennas intercepts the conical structure; but if no real values are found then that straight line does not intercept the conical geometry.

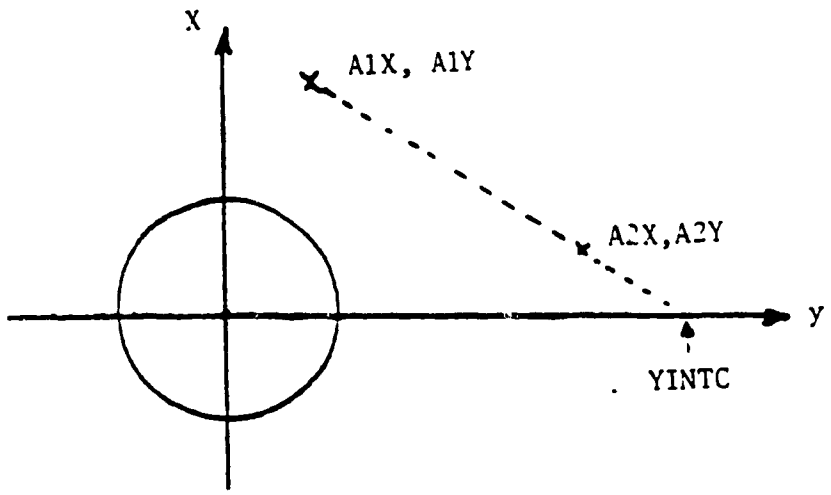


**Figure 6.5 The Intercept Line on the Y Axis**

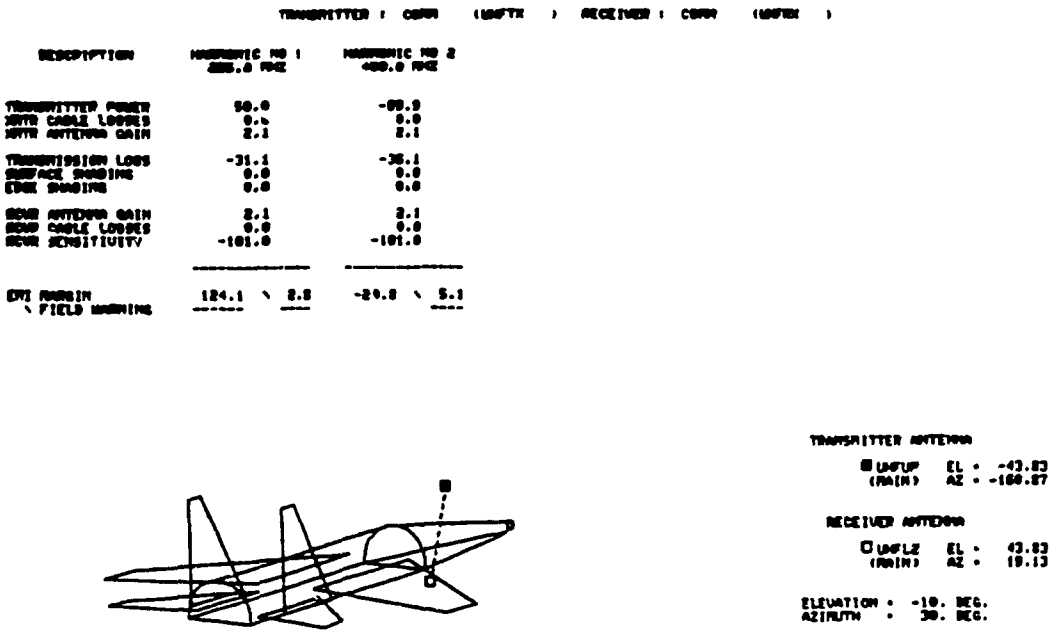


Figure 6.6 Line of Sight Modified Path

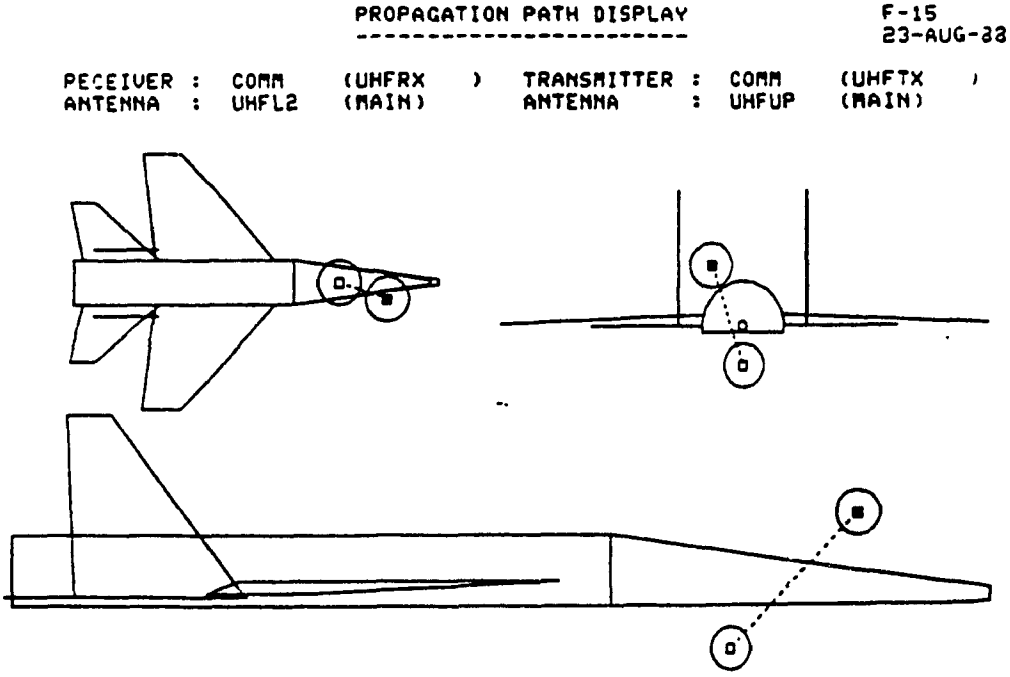


Figure 6.7 Line of Sight Modified Path-All View

TRANSMITTER : COMM (UHFTX ) RECEIVER : COMM (UHFRX )

| DESCRIPTION | HARMONIC NO 1 225.0 MHZ | HARMONIC NO 2 400.0 MHZ |
|---|---|---|
| TRANSMITTER POWER | 50.0 | -89.9 |
| XMTR CABLE LOSSES | 0.0 | 0.0 |
| XMTR ANTENNA GAIN | 2.1 | 2.1 |
| TRANSMISSION LOSS | -46.0 | -51.9 |
| SURFACE SHADING | -16.0 | -21.0 |
| EDGE SHADING | 0.0 | 0.0 |
| RCVR ANTENNA GAIN | 2.1 | 2.1 |
| RCVR CABLE LOSSES | 0.0 | 0.0 |
| RCVR SENSITIVITY | -101.0 | -101.0 |
| EMI MARGIN | 91.4 \ 18. | -58.5 \ 31. |
| \ FIELD WARNING | ------ | |

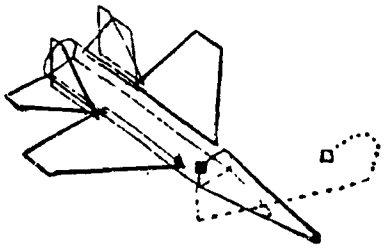

TRANSMITTER ANTENNA

■ UHFL1 (MAIN) EL = -18.40 AZ = 64.30

RECEIVER ANTENNA

□ UHFUP (MAIN) EL = -8.21 AZ = -104.78

ELEVATION = 45. DEG.
AZIMUTH = 45. DEG.

Figure 6.8 Unmodified Path

TRANSMITTER : COMM (UHFTX ) RECEIVER : COMM (UHFRX )

| DESCRIPTION | HARMONIC NO 1 225.0 MHZ | HARMONIC NO 2 400.0 MHZ |
|---|---|---|
| TRANSMITTER POWER | 50.0 | -89.9 |
| XMTR CABLE LOSSES | 0.0 | 0.0 |
| XMTR ANTENNA GAIN | 2.1 | 2.1 |
| TRANSMISSION LOSS | -39.5 | -44.5 |
| SURFACE SHADING | 0.0 | 0.0 |
| EDGE SHADING | 0.0 | 0.0 |
| RCVR ANTENNA GAIN | 2.1 | 2.1 |
| RCVR CABLE LOSSES | 0.0 | 0.0 |
| RCVR SENSITIVITY | -101.0 | -101.0 |
| EMI MARGIN | 115.7 \ 7.5 | -29.2 \ 13. |
| \ FIELD WARNING | ------ ---- | |

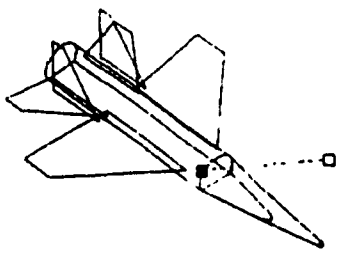

TRANSMITTER ANTENNA

■ UHFL1 (MAIN) EL = 36.04 AZ = -8.21

RECEIVER ANTENNA

□ UHFUP (MAIN) EL = -36.04 AZ = 171.79

ELEVATION = 45. DEG.
AZIMUTH = 45. DEG.

Figure 6.9 Modified Path

The above mathematical procedure has been translated into a software code using the flowchart procedure included in Appendix E.

## 6.3 Results

Comparing the results of Figures 6.1 and 6.6, which have been calculated using the original and modified versions of the code respectively, it can be noted that the EMI margin is higher at 124.1 dB, with the modified code compared to 115.9 dB, that the path distance is shorter at 2.8 wavelengths with the modified version, versus 3.4 wavelengths, and that graphically, the path within the modified version obeys the Fermat principal, while the path in the original version is obviously incorrect. Figures 6.8 and 6.9 shows a more dramatic improvement of the modified version over the original code. These latter figures illustrate a possible refueling situation where the original code predicted an EMI margin of 91.4 dB at 225 MHz with a distance of 18 wavelengths, while the modified version shows a more logical path with 115.7 dB and a distance of 7.5 wavelengths.

## 6.4 PATH Intercepting the Fuselage Geometry

Once a straight line has been traced between the two

antennas of interest, two possible cases can occur: 1) the line intercepts the conical geometry and 2) the straight line does not intercept the cone portion of the airframe. The latter case has been treated previously, therefore let us have a closer evaluation of the first case.

If the straight line intercepts the cone geometry, then it may be assumed that the path between the two antennas will be a combination of:

a) straight line - conical spiral, or

b) conical spiral - straight line.

In either case, the main task is to locate the two tangent points where a straight line from the antenna, away from the airframe, would touch on the conical portion. The antenna point $P_1$ shown in Figure 6.10, may be linked to antenna point $P_2$ using a straight line from $P_1$ to A or B, and a conical spiral from A or B to $P_2$.

Therefore, the task here is to locate the two points A and B, and to determine which path , $P^1$-A-$P_2$ or $P_1$-B-$P_2$, is the shortest, in order to satiafy Fermat's principle.

Assuming the antenna is located off the airframe at P1, Figure 6.10 shows that the tangent points A and B may be calculated using cylindrical coordinates. Knowing that $P_1$

is located at a radius P1R, angle P1A, and fuselage station P1Z and r also being known as the total distance of the point P1 from the centroid , the angle θ may be calculated as being

$$\theta = \text{Cos}^{-1}\frac{r}{P1R} \tag{6.16}$$

and once the angle θ is calculated, the angle coordinates of points A and B can found from :

$$B_\theta = P1A + \theta \tag{6.17}$$

$$A_\theta = P1A - \theta \tag{6.18}$$

which correspond to the clockwise and the counter-clockwise touch down paths respectively.

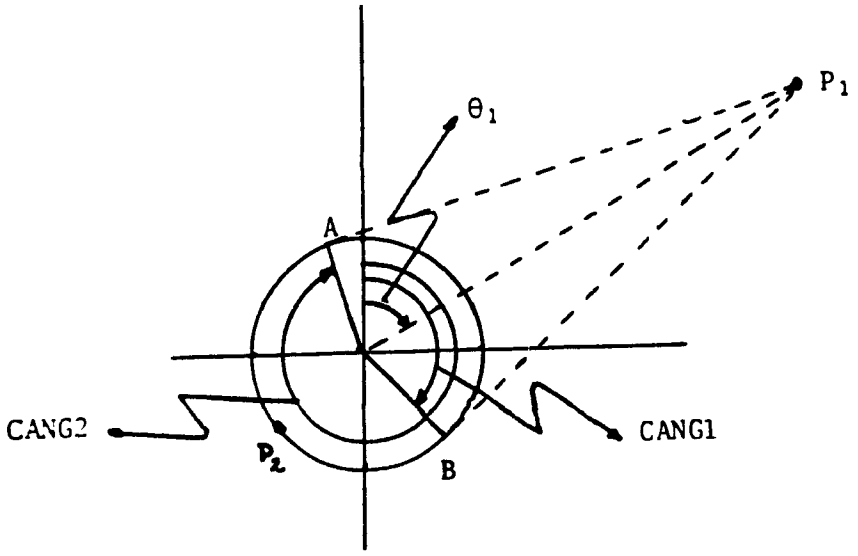


**Figure 6.10 Tangent Points Angle Definitions**

This is accomplished with a subroutine called TNGANG which returns the two angles as CANG1 (the smallest angle) and CANG2.

Having the cylindrical coordinates of the touch down point it is necessary to move this point along the Z axis if the two antennas are not located at the same fuselage station.

Due to the relatively small size of the conical geometry compared to the overall length of the airframe, an approximation can be made for the Z-axis coordinate of the tangent touch down points on the cone. This approximation is taking into account the ratio of the fuselage station of the two antennas.

Depending on whether P1Z or P2Z is the proper fuselage station at which the tangents will touch, the other coordinate will be modified, thus,

$$\text{if } P1Z < P2Z \text{ then } ZI1 = P1Z + \Delta Z \cdot \frac{P1R}{P1R+P2R} \tag{6.19}$$

$$\text{if } P1Z > P2Z \text{ then } ZI1 = P2Z + \Delta Z \cdot \frac{P2R}{P1R+P2R} \tag{6.20}$$

At this point, the two angles to the tangent points CANG1 and CANG2 (CANG1 being the smallest angle) and the fuselage station at which the touch down point occurs are known.

The radius to these tangent points from the centroid of the airframe must now be determined. This is accomplished by using ;

$$TP1R = (P1Z * TANOS) + RHOC \tag{6.21}$$

where

$$TANOS = (RHOF-RHOC)/FSN \tag{6.22}$$

With this last variable, the three coordinates of the two tangent points are obtained.

In order to compare the clockwise and counterclockwise path to determine which of the two represents the shortest length, AAPG first traces the clockwise path from P1 to P2, then by interchanging P1 and P2, the counterclockwise path is computed.

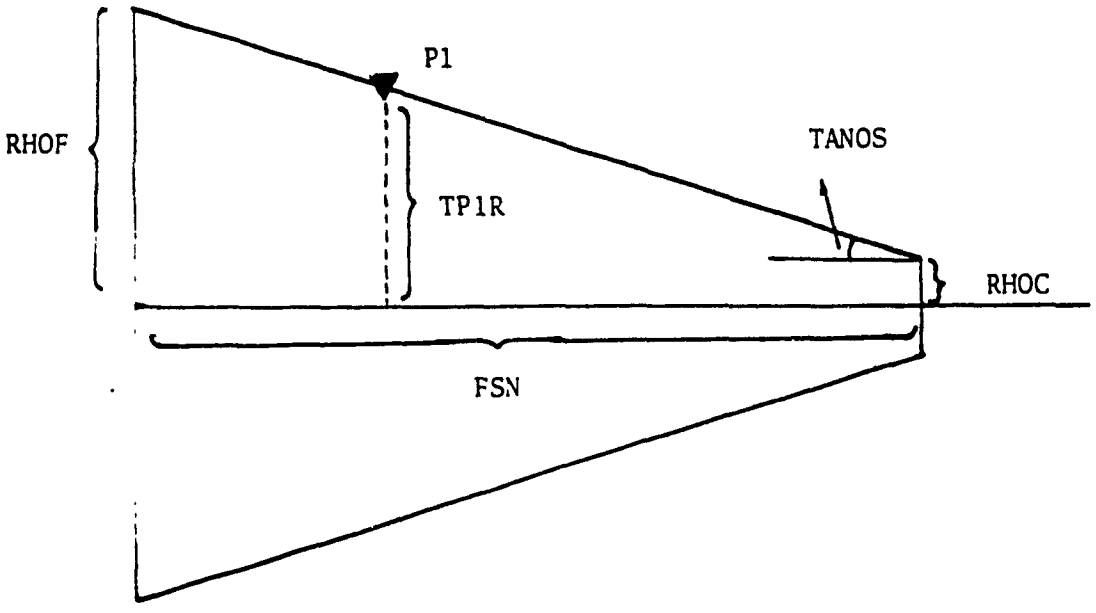


**Figure 6.11 Cone Radius Calculation Side View**

It is therefore necessary at this stage to determine which of the two tangent angles must be utilized for the proper ray tracing.

Starting with the knowledge that CANG1 is smaller than CANG2 and knowing that the path is always traced from P1 to P2 then to ensure a clockwise direction, the proper angle, explained in the following text, is choosen.

If P1A < CANG1 then CANG1 is the angle which will provide a clockwise path. Otherwise CANG2 will be the angle to choose and will be interchanged with CANG1, ensuring that CANG1 will always be the proper angle. Performing this step, the geodesic between the two antennas may now be traced.

If P1 is off the surface, the path will be a straight line from P1R, P1A, P1Z to TP1R, CANG1 and a conical spiral from that last point to P2R, P2A and P2Z.

However, if P1R is on the surface then a conical spiral is traced from P1R, P1A, P1Z to TP1R, CANG1, ZI1 and a straight line from that last point to P2R, P2A and P2Z.

The points and the appropriate codes are entered in the two arrays, PATH and ISHADE, to save these geodesics for further use in the code.

## 6.5 PATH Improvement

Upon the implementation of the above modification, one will notice a definite improvement.

Figures 6.12 and 6.13 show two antennas on the conical structure of the challenger aircraft. The path shown between the two systems is obviously not the shortest path when calculated using the unmodified version of AAPG.

Figures 6.14 and 6.15 illustrate the improved path using the modification described above. It can be seen that graphically, the path appears to follow the shortest route and that the path length has been improved in addition to the EMI margin. Figures 6.12 and 6.14, illustrate a substantial difference in the EMI field strength which goes from -85.8 dB to -17.8 dB, while the path distance is improved by 74 wavelengths.

Another example shown in Figures 6.16 and 6.17, indicate the level of difficulty experienced when using the unmodified version of AAPG. If the two antennas were located on the vertical line at the centre of the airframe, the code became confused providing erratic touch down location on the cone.

Figures 6.18 and 6.19 show the improved version of the

code where a combination of a straight line and a conical spiral may be observed.

The modification greatly improve the EMI prediction between antennas located in the conical region of the airframe. Due to the number of systems normally found in the conical area, coupled with the fact that flight formation and refuelling involve systems in the cone portion of the airframe, this modification is a significant improvement.

CONCVLTST1 ELECTROMAGNETIC INTERFERENCE MARGIN CALCULATION CONCVLTST1
18-APR-89

TRANSMITTER : RT-4 (RT-4TX ) RECEIVER : IB (JAMRX )

| DESCRIPTION | HARMONIC NO 1 9.315 GHZ |
|---|---|
| TRANSMITTER POWER | 60.8 |
| XMTR CABLE LOSSES | 0.0 |
| XMTR ANTENNA GAIN | 7.0 |
| TRANSMISSION LOSS | -70.1 |
| SURFACE SHADING | -101.6 |
| EDGE SHADING | 0.0 |
| RCVR ANTENNA GAIN | -12.0 |
| RCVR CABLE LOSSES | 0.0 |
| RCVR SENSITIVITY | -30.0 |
| EMI MARGIN \ FIELD WARNING | -85.8 \ 253 |

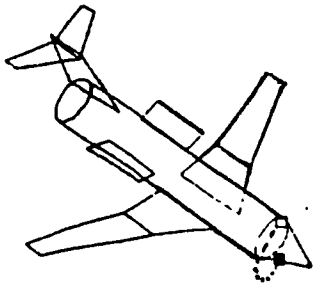

TRANSMITTER ANTENNA
■ RT (SIDE) EL = -15.07 AZ = 88.30

RECEIVER ANTENNA
□ RX (SIDE) EL = -53.85 AZ = 183.65

ELEVATION = 45. DEG.
AZIMUTH = 45. DEG.

**Figure 6.12 Unmodified Path-Case 1**

CONCYLTST1 PROPAGATION PATH DISPLAY CONCYLTST1
18-APR-89

RECEIVER : IB (JAMRX ) TRANSMITTER : RT-4 (RT-4TX )
ANTENNA : RX (SIDE) ANTENNA : RT (SIDE)

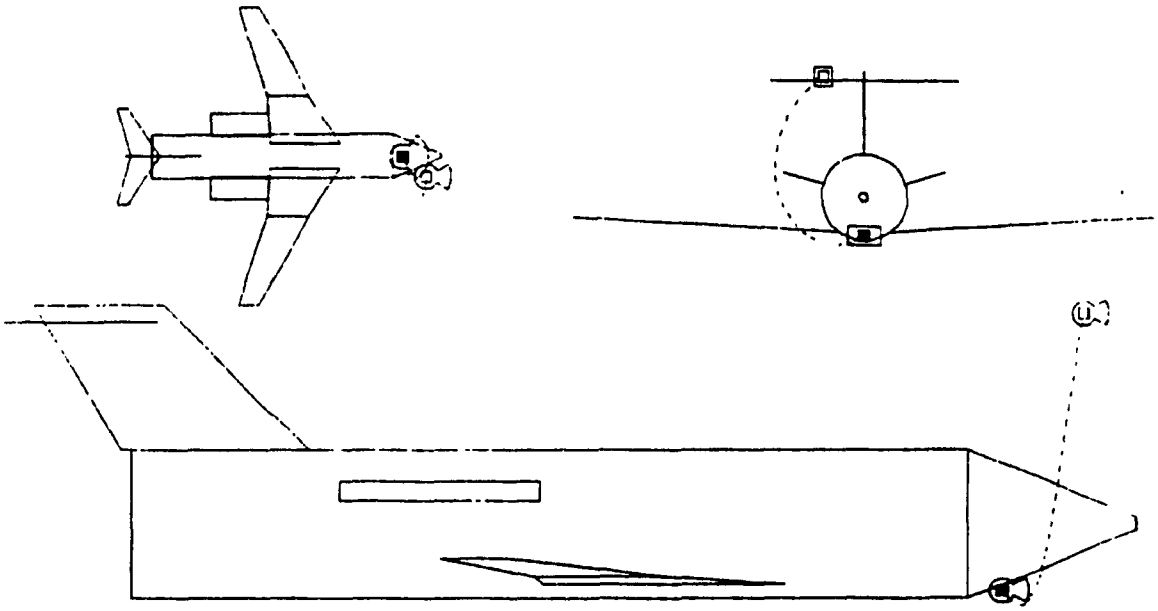

Figure 6.13 Unmodified Path, Case 1-All View

TRANSMITTER : RT-4 (RT-4TX ) RECEIVER : IB (JAMRX )

| DESCRIPTION | HARMONIC NO 1 9.316 GHZ |
|---|---|
| TRANSMITTER POWER | 60.8 |
| XMTR CABLE LOSSES | 0.0 |
| XMTR ANTENNA GAIN | 7.0 |
| TRANSMISSION LOSS | -67.0 |
| SURFACE SHADING | -36.5 |
| EDGE SHADING | 0.0 |
| RCVR ANTENNA GAIN | -12.0 |
| RCVR CABLE LOSSES | 0.0 |
| RCVR SENSITIVITY | -30.0 |
| EMI MARGIN | -17.8 \ 179 |
| \ FIELD WARNING | |

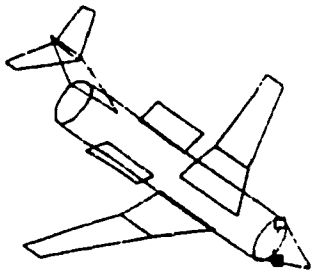

TRANSMITTER ANTENNA
RT EL = 8.04
(SIDE) AZ = 75.54

RECEIVER ANTENNA
RX EL = -73.65
(SIDE) AZ = -164.29

ELEVATION = 45. DEG.
AZIMUTH = 45. DEG.

Figure 6.14 Modified Path, Case 1

CONCYLTST1 PROPAGATION PATH DISPLAY CONCYLTST1
18-APR-89

RECEIVER : IB (JAMRX ) TRANSMITTER : RT-4 (RT-4TX )
ANTENNA : RX (SIDE) ANTENNA : RT (SIDE)

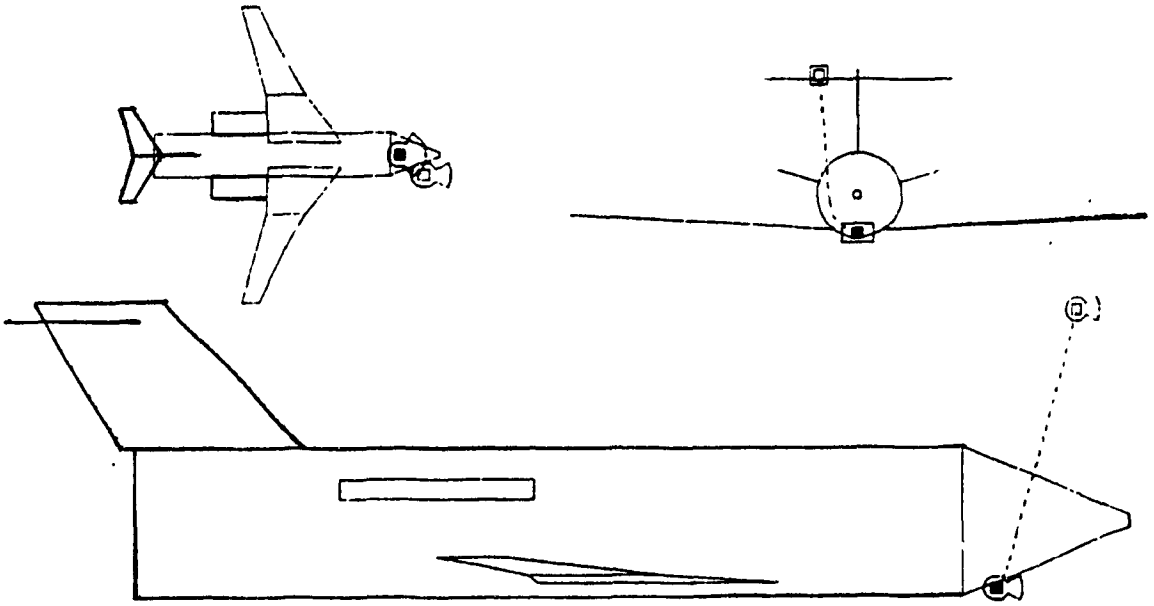

Figure 6.15 Modified Path, Case 1-All View

TRANSMITTER : RT-4 (RT-4TX ) RECEIVER : IB (JAMRX )

| DESCRIPTION | HARMONIC NO 1 9.315 GHZ |
|---|---|
| TRANSMITTER POWER | 60.8 |
| XMTR CABLE LOSSES | 0.0 |
| XMTR ANTENNA GAIN | 7.0 |
| TRANSMISSION LOSS | -76.1 |
| SURFACE SHADING | 0.0 |
| EDGE SHADING | 0.0 |
| RCVR ANTENNA GAIN | -12.0 |
| RCVR CABLE LOSSES | 0.0 |
| RCVR SENSITIVITY | -30.0 |
| EMI MARGIN | 9.7 |
| FIELD WARNING | --- |

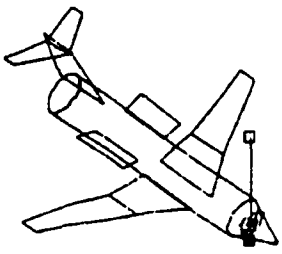

TRANSMITTER ANTENNA
RT (SIDE) EL = -22.70 AZ = -90.00

RECEIVER ANTENNA
RX (SIDE) EL = -56.85 AZ = -90.00

ELEVATION = 45. DEG.
AZIMUTH = 45. DEG.

Figure 6.16 Unmodified Path, Case 2

CONCYLTST1 PROPAGATION PATH DISPLAY CONCYLTST1
18-APR-89

RECEIVER : IB (JAMRX ) TRANSMITTER : RT-4 (RT-4TX )
ANTENNA : RX (SIDE) ANTENNA : RT (SIDE)

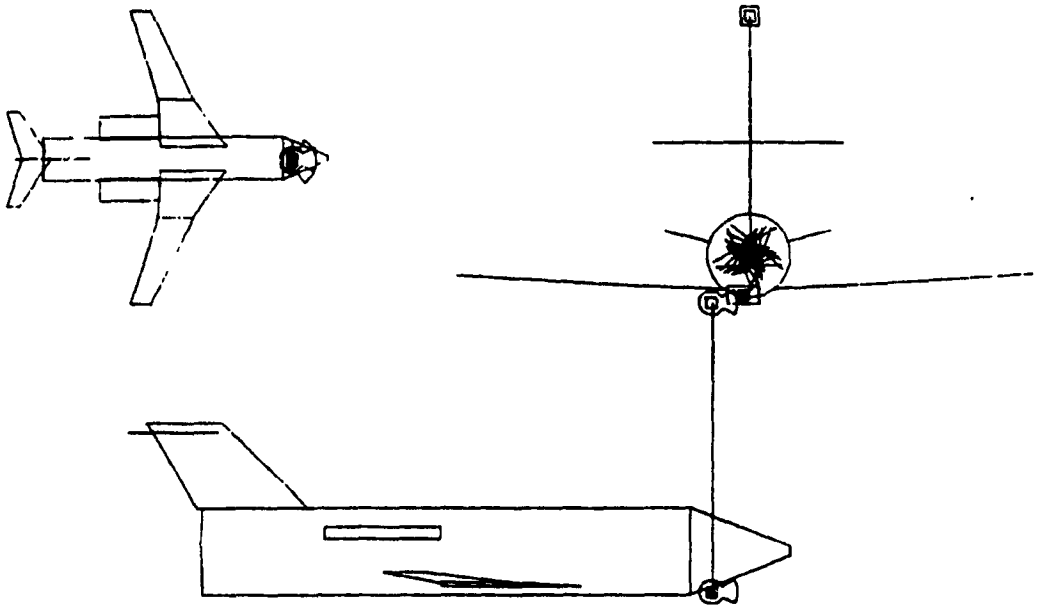

Figure 6.17 Unmodified Path, Case 2-All View

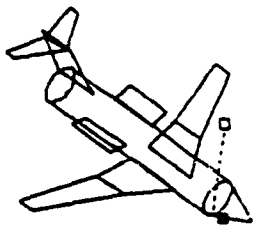

Figure 6.18 Modified Path, Case 2

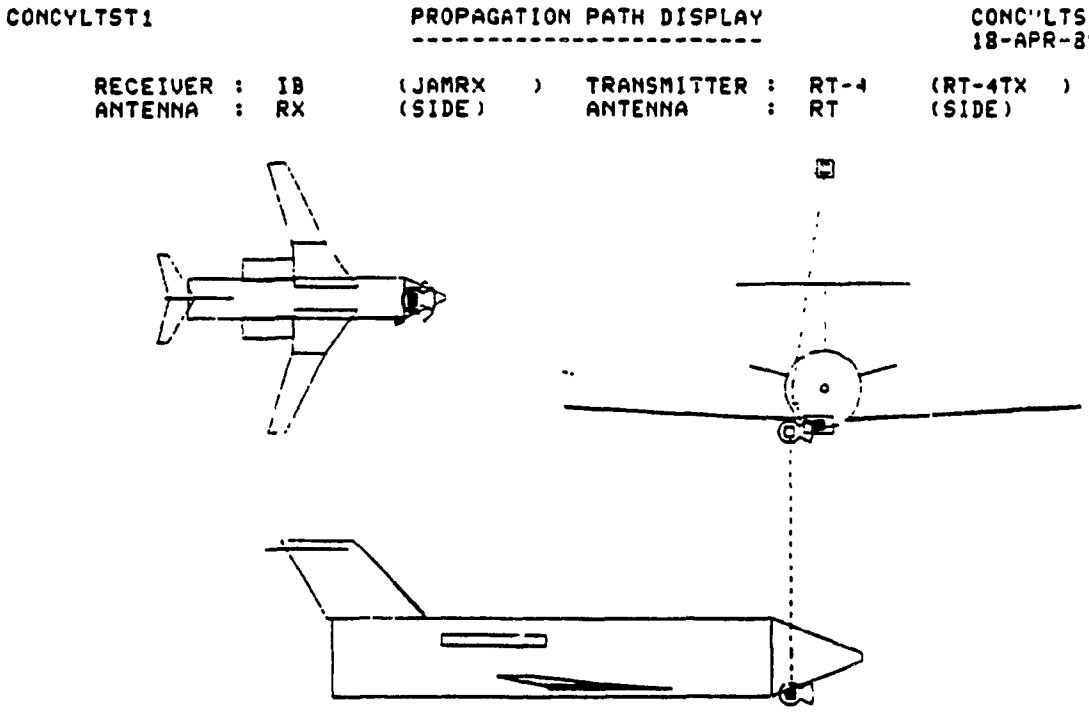


**Figure 6.19 Modified Path, Case 2–All View**

# CHAPTER 7

# CONICAL PATH DISTANCE CALCULATION IMPROVEMENT

## 7.1 Introduction

When calculating the electromagnetic field shading loss on any surface, it is vital to perform the calculation using the shortest distance between the two points of concern, otherwise the EMI margin would be incorrect.

The length of the coupling path must therefore be accurate. In AAPG, the coupling path segments between two antennas may be; straight lines, cylindrical spirals and/or conical spirals.

The determination of the straight lines and cylindrical spirals is done accurately within AAPG, however the conical spiral calculation is approximate [15].

The approximation utilized in AAPG to calculate the geodesic of a cone, expanded in Reference [28], makes use of the calculus of variations to calculate the path length, called $D_{CON}$ for distance on a cone, as follows:

$$D_{CON} = \left| \frac{1+B^2}{2A} \left( \mathrm{Tan}\gamma_2 \mathrm{Sec}\gamma_2 - \mathrm{Tan}\gamma_1 \mathrm{Sec}\gamma_1 + \ln \frac{\mathrm{Sec}\gamma_2 - \mathrm{Tan}\gamma_2}{\mathrm{Sec}\gamma_1 - \mathrm{Tan}\gamma_1} \right) \right| \qquad (7.1)$$

where, $A = \dfrac{|\theta_2-\theta_1|}{\rho_2-\rho_1}$ $\qquad$ $B = \dfrac{Z_2-Z_1}{\rho_2-\rho_1}$

$$\gamma_1 = \frac{\rho_1 A}{\sqrt{1+B^2}} \qquad \gamma_2 = \frac{\rho_2 A}{\sqrt{1+B^2}}$$

The above conical path distance is an approximation and is only utilized if $\rho_1 \neq \rho_2$ and $Z_1 \neq Z_2$. When the range and angles of radii spanned by a conical spiral is negligible, AAPG uses a straight line computation or a cylindrical spiral computation, as in equation 7.2, to determine the path length.

$$D_{CYL} = \sqrt{\rho^2 \cdot |\theta_2-\theta_1| + (Z_2-Z_1)^2} \qquad (7.2)$$

Using a cylindrical spiral computation to determine the path length between two points, at the same fuselage station, on a conical geometry, is also improper. The shortest path will intuitively move forward, towards the apex of the cone between the two points, therefore the cylindrical spiral also represents an approximation.

## 7.2 Geodesic Calculation Using 2-D Mapping

For two given points P and Q on a surface S, a cylinder unrolled in a plane, the shortest path is the straight line segment joining P and Q, as shown in Figure 6.1. For a

general surface, the shortest arc, if it exists, must be a geodesic [6].

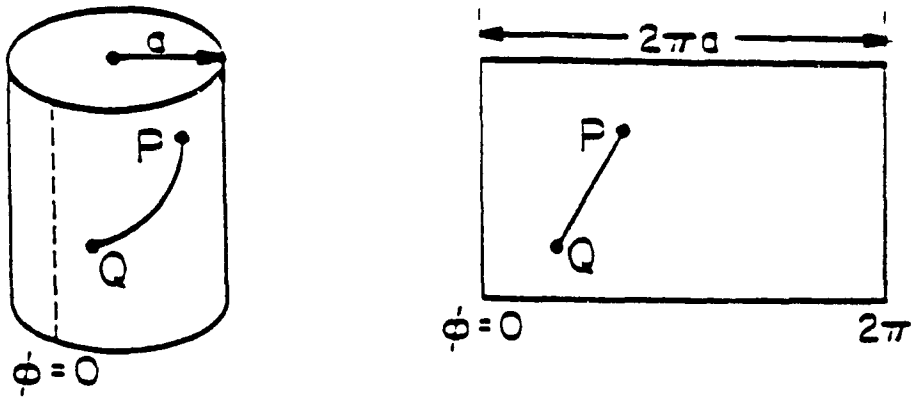


**Figure 7.1 Cylinder Developed Into a Rectangular Plane**

It is a relatively simple algorithm to determine the shortest path between the two points on a plane. The difficulty here resides in the transformation of a conical surface, which may be called a developable surface, [29] to a plane.

A developed surface is the one which [6];

a) may be generated by a continuous motion of a straight line (the straight lines on the surface are called generators), and

b) has the same tangent plane at all points

on any given generator.

Examples of developable surfaces are cylinders and cones, which when cut along a generator may be opened up to become a plane, without stretching or shrinking [29].

Figure 7.2 shows a cone and the plane into which it is developed.

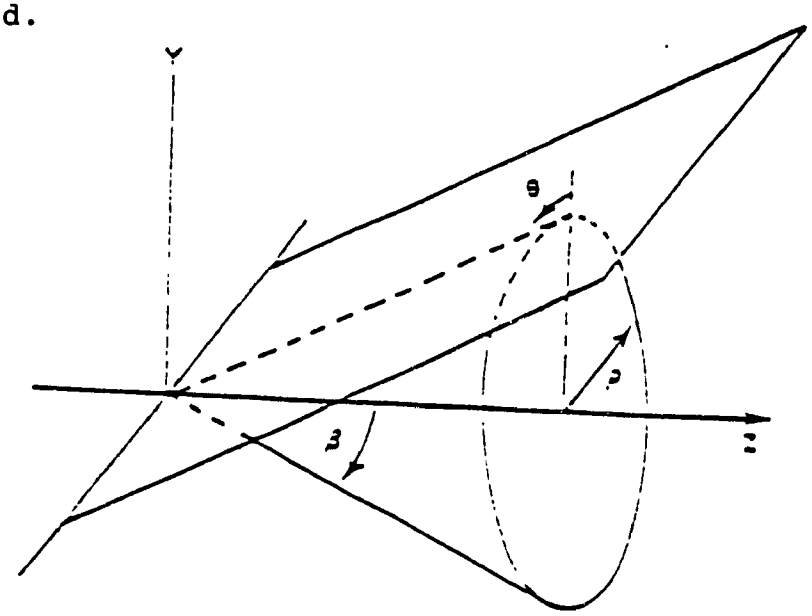


**Figure 7.2 Cone and Its Unrolled Plane**

## 7.3 Surface of Revolution

A point on the conical surface of the aircraft in AAPG is defined using the cylindrical coordinate system, where r represents the radius from the centroid of the aircraft, the angle from the vertical axis and the fuselage station of the point of concern.

The radius $\rho$ of any point on the cone can be obtained once the cone constant "K" is calculated. This constant is computed using any two known locations on the conical surface. For two points $\rho_1, \theta_1, Z_1, \rho_2, \theta_2, Z_2$, , K will be:

$$K = \frac{\rho_2 - \rho_1}{Z_2 - Z_1} \tag{7.3}$$

This constant is actually the slope of the conical surface which is constant. The relationship between $\rho$ and Z is therefore

$$\rho = K \cdot Z \tag{7.4}$$

Developing the cone shown in Figure 7.3 in a two dimensional plane in Figure 7.4, it is convenient to utilize polar coordinates as an intermediate system.

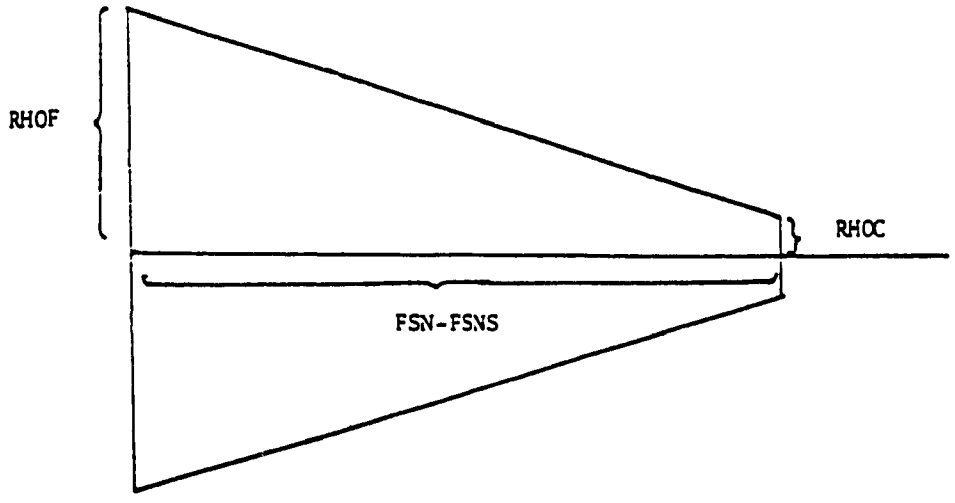


**Figure 7.3 Side View of a Three Dimensional Cone Illustrating The Nose of an Aircraft.**

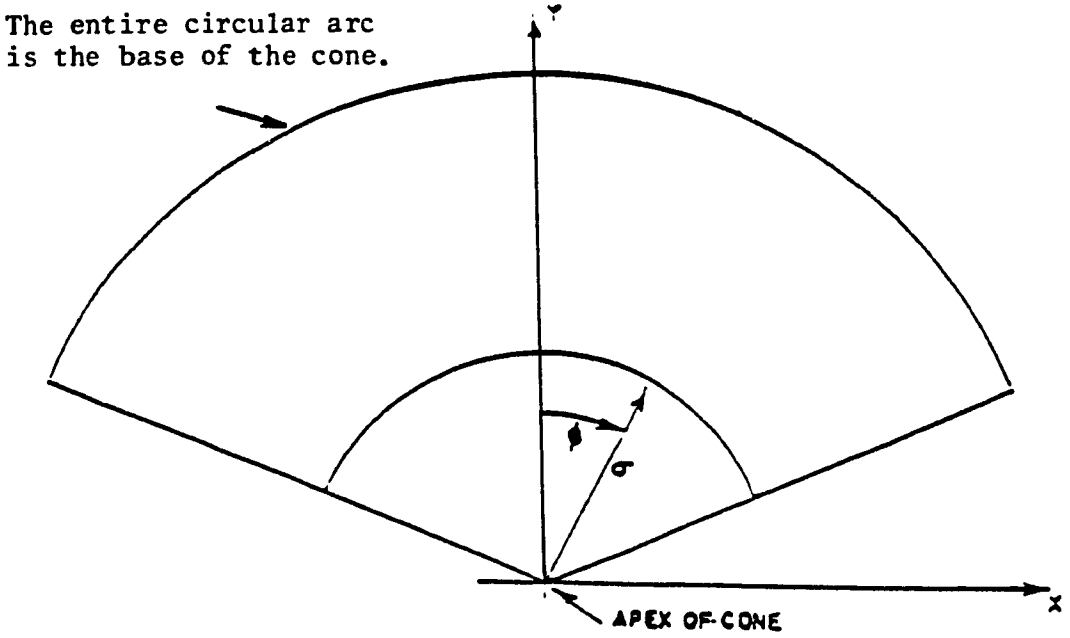


**Figure 7.4 The Three-Dimensional Cone Mapped Into Two Dimensions**

## 7.4 Mathematical Formulation

Since in AAPG, the aircraft is not necessarily modeled at the origin, the constant K is calculated as

$$K = (RHOF-RHOC)/(FSN-FSNS) \qquad (7.5)$$

The circular line shown in Figure 7.4 at a distance from the origin will represent the bulkhead of the aircraft and will be at RHOC/K.

Any point on the cone will have:

$$\sigma = Z^2 + \rho^2 \tag{7.6}$$

and replacing ρ by KZ as in equation (7.3) :

$$\sigma = Z \cdot \sqrt{1+K^2} \tag{7.7}$$

The angles $\phi$ and $\theta$ are related to each other as;

$$\phi\rho = \phi\sigma \tag{7.8}$$

Thus

$$\phi = \frac{\phi\rho}{\sigma} \tag{7.9}$$

replacing ρ by KZ as in Equation 7.4 and σ by the expression in Equation 7.7;

$$\phi = \Theta \frac{KZ}{Z\sqrt{1+K^2}} \tag{7.10}$$

$$\text{and} \quad \phi = \Theta \frac{K}{\sqrt{1+K^2}} \tag{7.11}$$

The polar coordinates are transformed into the orthogonal X,Y coordinates by the following Equation [6]

$$X = \sigma \, \text{Sin} \, \phi \tag{7.12}$$

$$Y = \sigma \, \text{Cos} \, \phi \tag{7.13}$$

substituting $\sigma$ and $\phi$ by equations 7.11 and 7.7 ;

$$X = Z\sqrt{1+K^2} \cdot \mathrm{Sin}\left(\theta \cdot \frac{K}{\sqrt{1+K^2}}\right) \qquad (7.14)$$

$$y = Z\sqrt{1+K^2} \cdot \mathrm{Cos}\left(\theta \cdot \frac{K}{\sqrt{1+K^2}}\right) \qquad (7.15)$$

The equations 7.13 and 7.14 map points from the 3-D cone into a 2-D, X,Y plane.

## 7.5 Software Implementation

The new mathematical formulation must be implemented within the AAPG code in order to improve the conical path distance measurement between two points on the cone portion of the aircraft.

The flowchart illustrating the new approach is included in this document as Appendix G and the program listing as Appendix H.

The function involved is called DCON, and utilizes the 3D to 2D mapping technique to calculate the distance on the cone.

## 7.6 Results

The new conical spiral distance calculation was programmed into AAPG and tested. Comparison between the new algorithm and the formal way to compute the distance has been done. It can be noted that in Figure 7.5, are two typical antenna locations on a Challenger C144 aircraft. The new formulation in Figure 7.5b is 139 wavelengths along with an EMI margin of -17.9 dB. This represents a path 9 wavelengths shorter than the old calculation shown in Figure 7.5, which was providing a distance of 148 wavelengths at-16.8 dB. This difference is significant especially when dealing with very sensitive systems.

When analyzing Figures 7.5, one may observe that the difference is in the surface shading where the loss is directly proportional to the distance.

Furthermore, the new technique of computing the conical spiral length will apply for any path on the cone. With the former algorithm, when two antennas were located at the same fuselage station, the calculation was switched over to the cylindrical spiral formulation.

Figure 7.6 illustrates a typical antenna location on the conical surface of an airframe. The two antennas being at the same fuselage station, they would be imposed as a

cylindrical spiral path by the initial AAPG conical path measurement.

It may be seen with the old algorithm in Figure 7.7, that the distance between the two antennas is 68 wavelengths which gives a cone a surface shading of -83.5 dB. The new method in turn, in Figure 7.7, provides a distance of 64 wavelength with a surface shading of -85.5 dB, 2 dB less than the formal way.

This improvement in the conical distance measurement is significant since the conical section of an aircraft contains numerous sensitive systems, where every decibel in the electromagnetic coupling could have a serious impact on the overall operation of the platform.

It must be mentioned that although the mathematical formulation provides more exact numbers, the graphics displaying the path on the cone remains to be updated so to reflect this new path. This will be mentioned in the recommendation for further development.

TRANSMITTER : RT-4 (RT-4TX ) RECEIVER : I3 (JAMRX )

| DESCRIPTION | HARMONIC NO 1 9.315 GHZ |
|---|---|
| TRANSMITTER POWER | 60.8 |
| XMTR CABLE LOSSES | 0.0 |
| XMTR ANTENNA GAIN | 33.0 |
| TRANSMISSION LOSS | -65.4 |
| SURFACE SHADING | -63.2 |
| EDGE SHADING | 0.0 |
| RCVR ANTENNA GAIN | -12.0 |
| RCVR CABLE LOSSES | 0.0 |
| RCVR SENSITIVITY | -30.0 |
| EMI MARGIN \ FIELD WARNING | -16.8 \ 148 |

| DESCRIPTION | HARMONIC NO 1 9.315 GHZ |
|---|---|
| TRANSMITTER POWER | 60.8 |
| XMTR CABLE LOSSES | 0.0 |
| XMTR ANTENNA GAIN | 33.0 |
| TRANSMISSION LOSS | -64.9 |
| SURFACE SHADING | -64.8 |
| EDGE SHADING | 0.0 |
| RCVR ANTENNA GAIN | -12.0 |
| RCVR CABLE LOSSES | 0.0 |
| RCVR SENSITIVITY | -30.0 |
| EMI MARGIN \ FIELD WARNING | -17.9 \ 139 |

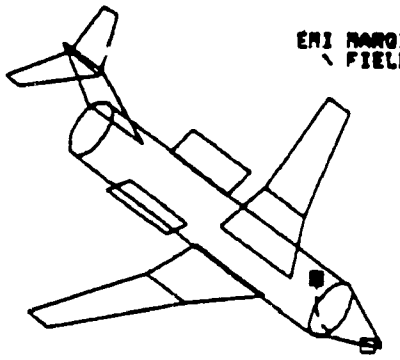

Figure 7.5 Conical Spiral Distance Comparison

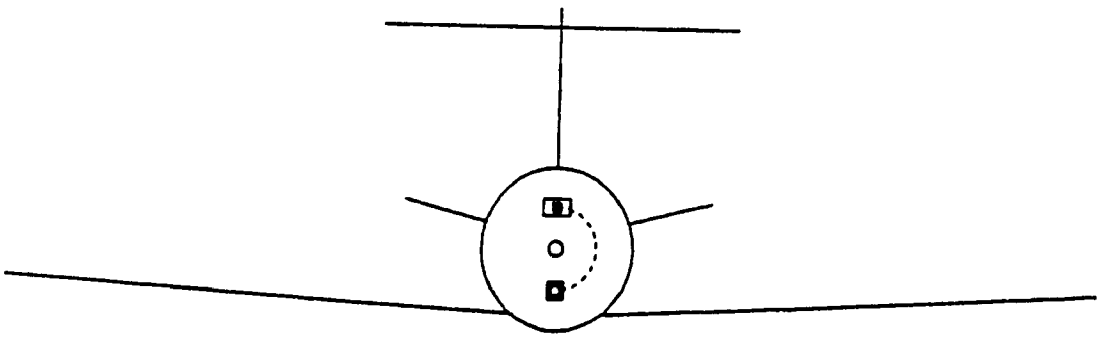

Figure 7.6 Front View of a Conical Spiral Path

TRANSMITTER : RT-4 (RT-4TX ) RECEIVER : IB (JANRX )

| DESCRIPTION | HARMONIC NO 1 9.315 GHZ |
|---|---|
| TRANSMITTER POWER | 60.8 |
| XMTR CABLE LOSSES | 0.0 |
| XMTR ANTENNA GAIN | 7.0 |
| TRANSMISSION LOSS | -58.7 |
| SURFACE SHADING | -83.5 |
| EDGE SHADING | 0.0 |
| RCVR ANTENNA GAIN | -12.0 |
| RCVR CABLE LOSSES | 0.0 |
| RCVR SENSITIVITY | -30.0 |
| EMI MARGIN \ FIELD WARNING | -56.3 \ 68. |

| DESCRIPTION | HARMONIC NO 1 9.315 GHZ |
|---|---|
| TRANSMITTER POWER | 60.8 |
| XMTR CABLE LOSSES | 0.0 |
| XMTR ANTENNA GAIN | 7.0 |
| TRANSMISSION LOSS | -58.1 |
| SURFACE SHADING | -85.5 |
| EDGE SHADING | 0.0 |
| RCVR ANTENNA GAIN | -12.0 |
| RCVR CABLE LOSSES | 0.0 |
| RCVR SENSITIVITY | -30.0 |
| EMI MARGIN \ FIELD WARNING | -57.8 \ 64. |

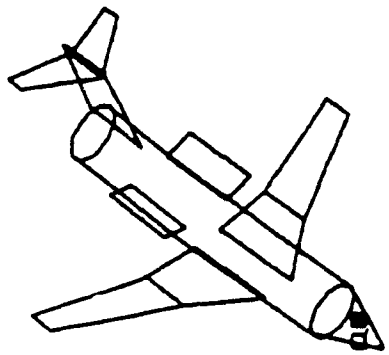

Figure 7.7 Conical Spiral

# CHAPTER 8

# CONICAL SPIRAL SHADING CALCULATION

## 8.1 Introduction

On modern aircraft, it is not unusual to count more than one hundred emittors and receptors points of which many are located on or around the conical geometry forming the nose of the airframe.

When the propagation path linking two emitting/receiving points is entirely or partly on the conical structure of the aircraft, AAPG version 7 does not take into consideration the varying radius of the curvature of the geometry. Instead, AAPG, taking the geometric mean of the radii of the two points of interest, approximates the curved surface shading loss by using the same mathematical formulation as the cylindrical shading loss. This cylindrical shading loss is computed using Equation 8.1.

$$L_{CS} = \frac{A}{\eta A + \xi}$$

where

$$A = \rho_S e_S^2 \sqrt{\frac{2\pi}{\lambda D_S}} \qquad (8.1)$$

$$\eta = \begin{cases} 0.005478 & \text{for } A < 26 \\ 0.003340 & \text{for } A \geq 26 \end{cases}$$

$$\xi = \begin{cases} 0.5083 & \text{for } A < 26 \\ 0.5621 & \text{for } A \geq 26 \end{cases}$$

$\rho_s$ = the geometric mean of the radii of the spiral end points, in meters = $\sqrt{\rho_1 \rho_2}$

$\theta_s$ = the angle spanned by the coupling-path spiral, in radians

$D_s$ = the length of the coupling-path spiral, in meters.

This equation, based on the work of Hasserjan and Ishimaru [15], approximates within 1 dB, the surface shading loss with measured data [20].

However, the above formulation assumes a right circular cylinder or geodesics of a constant curvature. This is not obviously satisfying when considering a conical geometry. Therefore, a new formulation is needed to address the problem of non constant radius of the curvature.

## 8.2 Arbitrary Curved Surface Diffraction Loss

When considering an emittor and receptor point in a lit region, where no obstacle between the two points exists, the radiated field propagates directly from the source to the field point along the incident ray of geometrical optics. However, when the observation pcint is located in the shadow region of a curved surface, the radiation from the source follows a surface ray or geodesic of the surface, to the diffraction point where tangential shedding along that geodesic may be observed.

Considering an infinitesimal magnetic current source $P_m$ at point Q which exists at point Q' on an arbitrary convex surface shown in Figure 8.1, the tangential magnetic field H at Q is expressed by Pathak and Wang [23] as in Equation 8.2.

$$\bar{H} = \bar{P}_m \cdot \left[ \hat{b}'\hat{b} \cdot \left\{ \left(1-\frac{j}{KS}\right)\cdot\tau V(\xi) + V^2\left(\frac{j}{KS}\right)^2 \cdot \left(\Lambda_S\tau^3 V(\xi)+\Lambda_C\tau V(\xi)\right) + T_o^2\left(\frac{j}{KS}\right)\cdot\left\{\tau^3 V(\xi)-\tau V(\xi)\right\}\right\} + \hat{t}'\hat{t}\cdot\left\{V^2\left(\frac{j}{KS}\right)\cdot\tau V(\xi)+\left(\frac{j}{KS}\right)\cdot\tau^3 V(\xi) - 2\left(\frac{j}{KS}\right)\cdot\left(\Lambda_S\tau^3 V(\xi)+\Lambda_C\tau V(\xi)\right)\right\} + \left(\hat{t}'\hat{b}+\hat{b}'\hat{t}\right)\cdot\left\{\left(\frac{j}{KS}\right)T_o\cdot\left\{\tau^3 V(\xi)-\tau V(\xi)\right\}\right\}\right] \cdot VG(S) \tag{8.2}$$

S.W. Lee derives a similar solution (4) in Equation [8.3].

$$\bar{H} = \bar{P}_m \cdot \left[ \hat{b}'\hat{b} \cdot \left\{ \left(1-\frac{j}{KS}\right)\cdot\tau V(\xi) - \left(\frac{1}{KS}\right)^2 \tau^3 V(\xi) + j(\sqrt{2}K\rho_g)^{-2/3}\tau V'(\xi) + j(\sqrt{2}K\rho_g)^{-2/3}\cdot\left(\frac{\rho_g}{\rho_b}\right)\tau^3 V'(\xi)\right\} + \hat{t}'\hat{t}\cdot\left\{\tau V(\xi)+\left(1-\frac{2j}{KS}\right)\cdot\tau^3 V(\xi) + j(\sqrt{2}K\rho_g)^{-2/3}\tau^3 V'(\xi)\right\}\cdot\frac{j}{KS}\right] \cdot VG(S) \tag{8.3}$$

where the parameters are:

$$\xi = \int \frac{m(S')}{\rho_g(S')}\, dS' \tag{8.4}$$

$$m(S') = \left[\frac{K\rho_g(S')}{2}\right]^{1/3} \tag{8.5}$$

$$\tau = \left[\frac{KS}{2m(0)m(S)\xi}\right]^{1/2} \tag{8.6}$$

$$V = \text{the divergence factor} \tag{8.7}$$

$$T_o = SGN\left[T(0)\right] \cdot SGN\left[T(S)\right] \sqrt{T(0)T(S)} \tag{8.8}$$

$$T(S) = \frac{Sin(2\alpha') \cdot \rho_g(S')}{2} \cdot \left(\frac{1}{\rho(S)} - \frac{1}{\rho(S')}\right) \tag{8.9}$$

$$\Lambda_S = \sqrt{\frac{\rho_2(0)}{\rho_1(0)} - \frac{\rho_2(S)}{\rho_1(S)}} \tag{8.10}$$

$$\Lambda_C = 1 - \Lambda_S \tag{8.11}$$

$$\rho_g = \sqrt{\rho_g(0)\rho_g(S)} \tag{8.12}$$

$$\rho_b = \sqrt{\rho_b(0)\rho_b(S)} \tag{8.13}$$

$$G(S) = K^2 \tag{8.14}$$

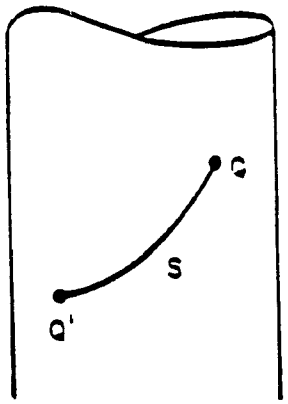


**Figure 8.1 Geodesic on a Convex Surface**

The similarity of these two expressions to determine the magnetic field at the observation point can be noted. The main factor differentiating the two equations is the torsion term $T_o$ used in equation 8.2.

Assuming a far field situation, a worst case polarization, an electrically large path length, and neglecting the torsion terms, the field is given as the lowest order term in inverse powers of the available length parameters according to either of the previous expressions as:

$$\bar{H} = P_m \cdot \hat{b}_1 \left[ \frac{KS}{2m(r')m(r)\xi} \right]^{1/2} \cdot DF \cdot V(\xi) \cdot G(S) \hat{b}_2 \qquad (8.15)$$

where H is the magnetic field induced at r by a magnetic dipole source, $P_m$ at r'. The unit vectors $b_1$ and $b_2$ lie in the tangent plane at r' and r respectively, oriented

perpendicular to the geodesic path. The term G(S) in Equation 8.16.

$$G(S) = \frac{KY_o}{2\pi j} \cdot \frac{e^{-JKS}}{S} \qquad (8.16)$$

dictates the behaviour of the field. The terms S, $Y_o$ and K are respectively the path length, free space admittance and wave number.

The Fock function $V(\xi)$ described in Chapter 2 of this document, is dependent on the curvature of the ray path over the geodesic.

The divergence factor DF, also dependent on the curvature of the path, is equal to unity for any surface which can be developed, such as a cone [24].

When analyzing Equation 8.4, one may note that the field resulting from a magnetic dipole on a curved surface, can be approximated asymptotically as the field attained at the same distance from the dipole on a flat surface, multiplied by a shedding factor that accounts for the curvature of the geodesic path.

This attenuation factor is the product of the terms defined in Equation 8.17 [25].

$$\tau = \left[\frac{KS}{2m(0)m(S)\xi}\right]^{1/2} \tag{8.17}$$

Since DF is unity for a cone geometry and using the approximation, good to within 1 dB, to calculate $V(\xi)$, used in version 7 of AAPG and given in Reference [8], the curved surface diffraction loss for an arbitrary convex surface is:

$$L_{CS} = -\frac{A}{\eta A + \xi'} + 20 \log\left\{\frac{KS}{2m(Q_1)m(Q_2)\xi}\right\}^{1/2} \tag{8.18}$$

with $A = \sqrt{2}\cdot\xi^{3/2}$

$$\eta = \begin{cases} 0.005478 & \text{for } A < 26 \\ 0.003340 & \text{for } A \geq 26 \end{cases}$$

$$\xi' = \begin{cases} 0.5083 & \text{for } A < 26 \\ 0.5621 & \text{for } A \geq 26 \end{cases}$$

where $\tau$ in the second term, can be defined as the attenuation due to the ray curvature.

## 8.3 The Ray Curvature On a Cone

The ray curvature term $\tau$ given in Equation 8.17, is a positive real for a convex surface and reduces to unity for the special case of a constant ray curvature.

the special case of a constant ray curvature.

The expressions $m(Q_1)$ and $m(Q_2)$ in Equation 8.18 are defined by [21].

$$m(Q) = \left[\frac{K\rho_g(Q)}{2}\right]^{1/3} \tag{8.19}$$

and depend on the radius of the geometry at points $Q_1$ and $Q'_2$.

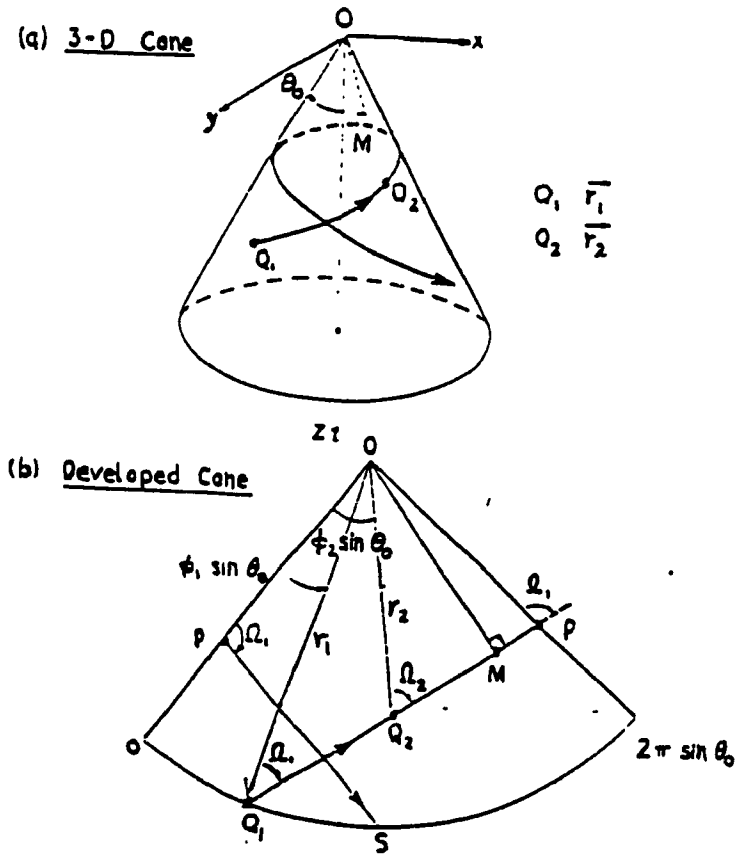


**Figure 8.2 3-D and Developed Cone**

In order to apply the formula of Equation 8.17 to a conical geometry, Green's function for a cone must be determined.

Given two points on a cone in spherical coordinates , with $\theta_0$ constant and equal to the half cone angle, as shown in Figure 8.2, the main contribution of the field at $Q_2$ comes from the shortest path described by [24].

$$r_1 \text{Sin}\ \Omega_1 = r_2 \text{Sin}\ \Omega_2 \tag{8.20}$$

as the ray propagates away from the source point $Q_1$ to the observation point $Q_2$ via the shortest path, the arc length is:

$$S = \left[ r_1^2 + r_2^2 - 2r_1 r_2 \text{Cos}[(\phi_1 - \phi_2)\text{Sin}\ \theta_o] \right]^{1/2} \tag{8.21}$$

The angles $\Omega_1$ at $Q_1$ and $\Omega_2$ being ;

$$\Omega_1 = \text{Sin}^{-1}\left[ r^2\ \text{Sin}\ [(\phi_2 - \phi_1)\text{Sin}\ \theta_o] \right] \tag{8.22}$$

while

$$\Omega_2 = \Omega_1 + (\phi_2 - \phi_1)\text{Sin}\ \theta_o \tag{8.23}$$

which derives from using the large parameter in the

asymptotic expansion of the Green's function [24]:

$$\xi = \left[\frac{1}{2} Kr_1 \text{Sin}\ \Omega_1\ \text{Sin}\ \theta_o\right]^{1/3} |\phi_2-\phi_1| \text{Cos}^{2/3}\phi_o \tag{8.24}$$

$$\tau = \left[\frac{KS}{\xi}\right]^{1/2} \cdot \left[2K^2 r_1 r_2\right]^{-1/6} \left\{\text{Sin}\ \Omega_1\ \text{Sin}\ \Omega_2\ \text{Cos}\ \phi_o\right\}^{1/3} \tag{8.25}$$

$\tau$ being the term related to the ray curvature.

The task to accomplish at this point is to translate Equations 8.9 through 8.15 into the appropriate computer code in order to calculate a more accurate conical spiral shading loss.

## 8.4 New Conical Spiral Loss Implementation

In the AAPG code, version 7, the conical spiral portion of the path is calculated in the subroutine LOSS. In this subroutine each path segment is verified for various types, ie: straight line, cylindrical spiral, conical spiral and edge diffraction, where each path length by type is kept in a specific variable. Once all path segments have been reviewed, each path length variable is used to calculate the total path loss as transmission loss for free space, surface shading for conical and cylindrical spirals and edge shading for edge diffraction.

The conical spiral segment in Version 7 was therefore included as part of the surface shading using the cylindrical spiral to approximate the loss.

The geometrical mean radius of the two points on the cone was utilized to perform this calculation.

The approach presented in the flowchart at Appendix J was used to code the new conical spiral loss calculation.

Appendix K contains the modified subroutine LOSS, containing the conical spiral shading calculation patch, as identified in the listing.

## 8.5 Conical Spiral Shading Results

The equation 8.25 formulation, for the case of two circumferential slots on a cone, has been extensively verified by S.W. Lee [24]. Figure 8.3 shows the coupling coefficient curve between two circumferential slots on a cone, as a function of frequency. One may notice that both theoretical results are in good agreement with the experimental data, with the present results being slightly better.

The implementation in AAPG was verified using the

Challenger aircraft model CE-144. When comparing Figures 8.4 through 8.6 it may be noted that for the same antenna system and locations, the new shading calculation presents an additional 8.9 dB loss which in turn presents a different total EMI margin. Figures 8.7 through to 8.9 also indicate an additional shading loss when using the new formulation, of 3.6 dB, which in this case also modifies the overall EMI margin.

Finally, Figures 8.10 through 8.12 illustrate an additional loss of 3.7 dB when using the new formulation, again changing the value of the overall EMI margin.

These new margins become more significant with the knowledge that some of the most sensitive and critical avionic systems are located on the conical portion of the airframe. These more accurate shading calculations will permit the avionic systems engineers to optimize the location of critical antennas thus improving the overall operation of the aircraft.

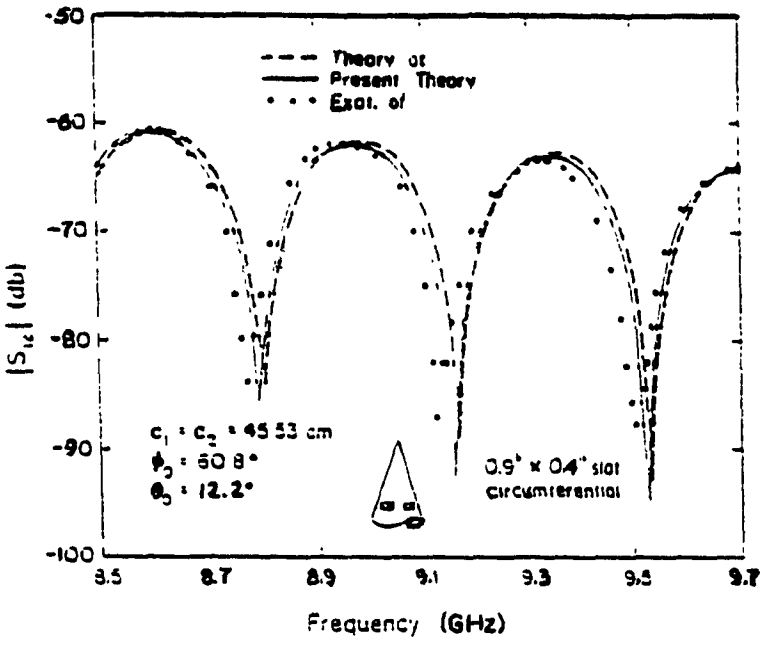


**Figure 8.3 Coupling Coefficient $S_{12}$ Between Two Circumferential Slots on a Cone as a Function of Frequency**

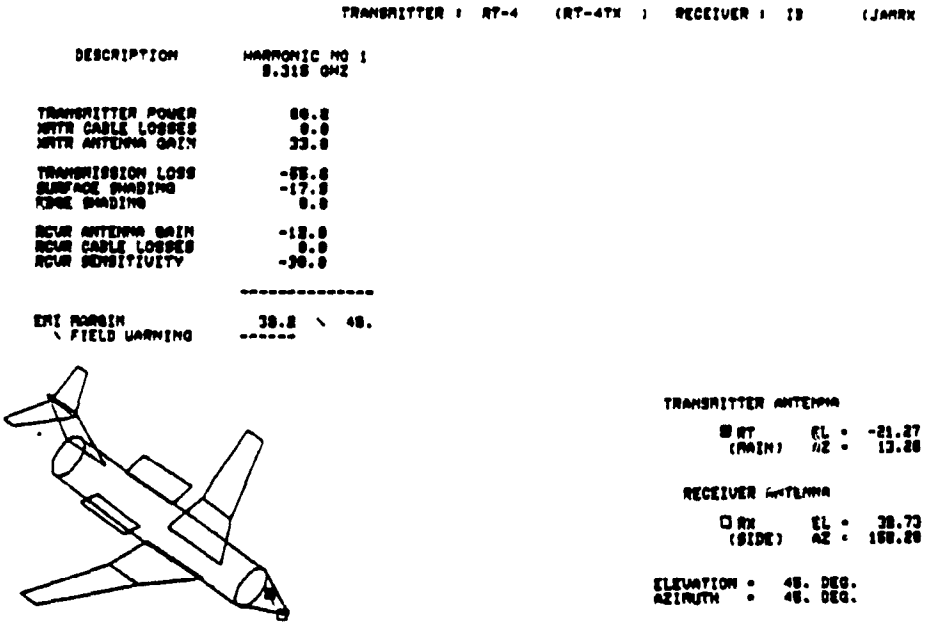


**Figure 8.4 Unmodified Path, Case 1**

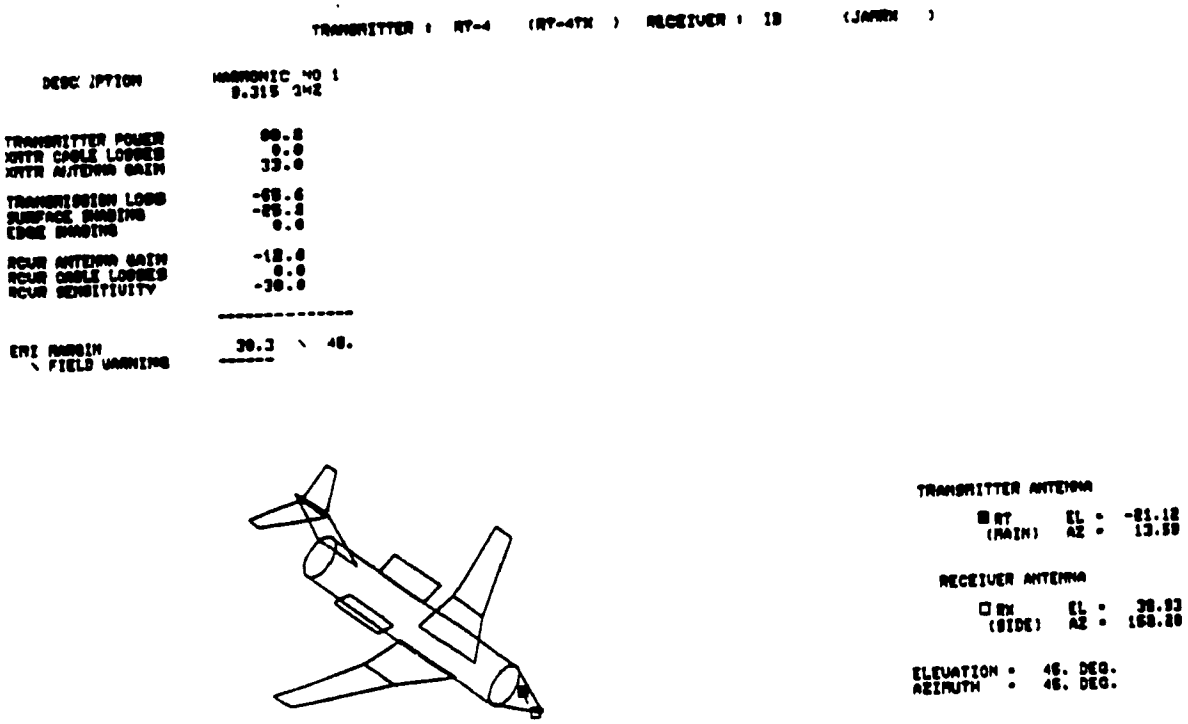


**Figure 8.5 Modified Path, Case 1**

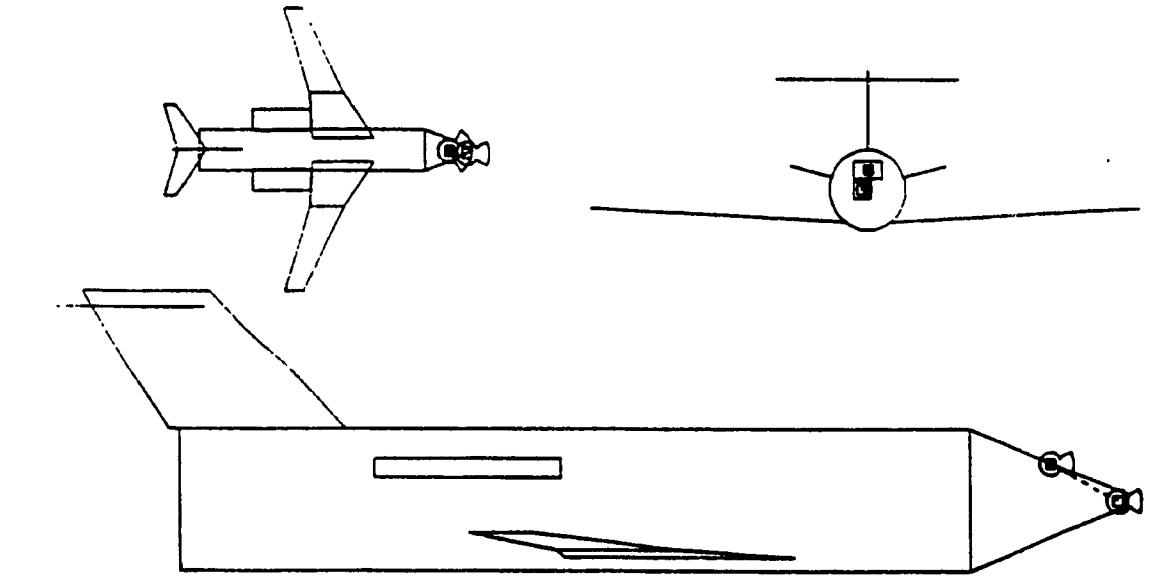


**Figure 8.6 Conical Path, Case 1-All View**

TRANSMITTER : RT-4 (RT-4TX ) RECEIVER : I8 (JAMRX )

| DESCRIPTION | HARMONIC NO 1<br>9.315 GHZ |
|---|---|
| TRANSMITTER POWER | 60.8 |
| XMTR CABLE LOSSES | 0.0 |
| XMTR ANTENNA GAIN | 33.0 |
| TRANSMISSION LOSS | -67.3 |
| SURFACE SHADING | -58.4 |
| EDGE SHADING | 0.0 |
| RCVR ANTENNA GAIN | -18.0 |
| RCVR CABLE LOSSES | 0.0 |
| RCVR SENSITIVITY | -36.0 |
| EMI MARGIN | 1.6 \ 60. |
| \ FIELD WARNING | ------ |

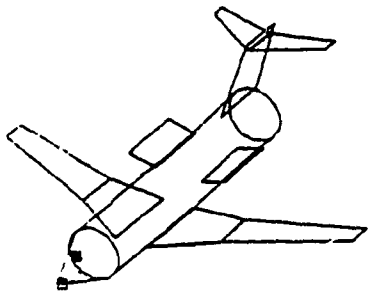

TRANSMITTER ANTENNA
RT (MAIN) EL : -10.80 AZ : -85.23

RECEIVER ANTENNA
RX (SIDE) EL : -11.33 AZ : -120.00

ELEVATION : 30. DEG.
AZIMUTH : -30. DEG.

Figure 8.7 Unmodified Path, Case 2

TRANSMITTER : RT-4 (RT-4TX ) RECEIVER : I8 (JAMRX )

| DESCRIPTION | HARMONIC NO :<br>9.315 GHZ |
|---|---|
| TRANSMITTER POWER | 60.8 |
| XMTR CABLE LOSSES | 0.0 |
| XMTR ANTENNA GAIN | 33.0 |
| TRANSMISSION LOSS | -67.3 |
| SURFACE SHADING | -56.0 |
| EDGE SHADING | 0.0 |
| RCVR ANTENNA GAIN | -18.0 |
| RCVR CABLE LOSSES | 0.0 |
| RCVR SENSITIVITY | -36.0 |
| EMI MARGIN | -8.0 \ 60. |
| \ FIELD WARNING | |

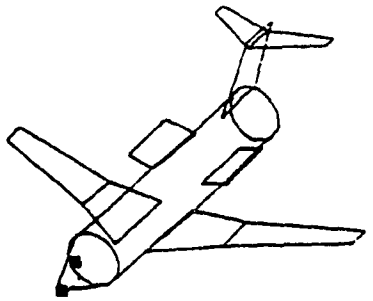

TRANSMITTER ANTENNA
RT (MAIN) EL : -00.15 AZ : -84.07

RECEIVER ANTENNA
RX (SIDE) EL : -11.36 AZ : -120.14

ELEVATION : 30. DEG.
AZIMUTH : -30. DEG.

Figure 8.8 Modified Path, Case 2

CONCYLTST1 PROPAGATION PATH DISPLAY CONCYLTST1
29-MAY-88

RECEIVER : IB (JAMRX ) TRANSMITTER : RT-4 (RT-4TX )
ANTENNA : RX (SIDE) ANTENNA : RT (MAIN)

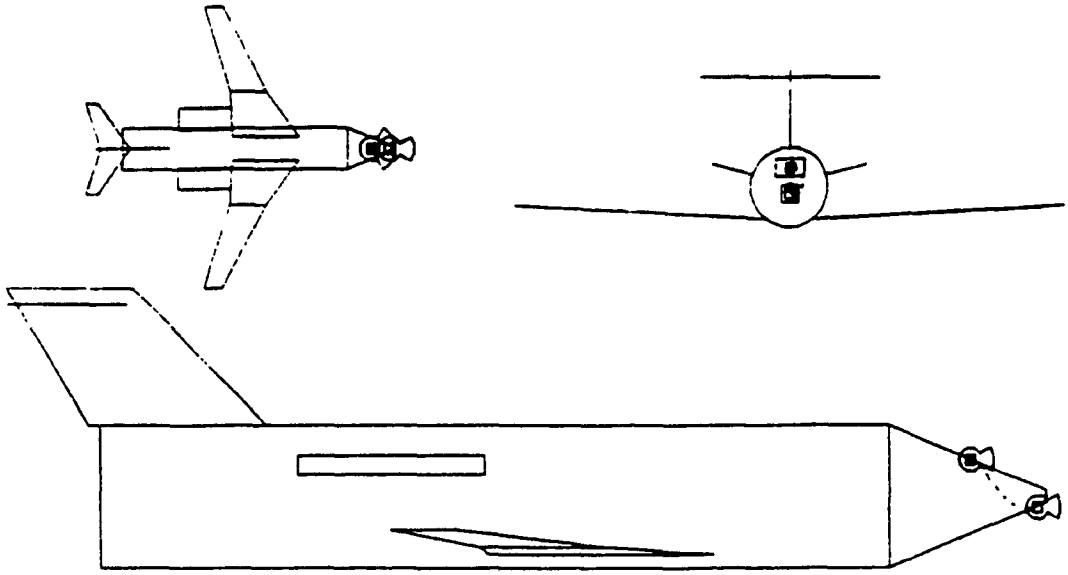

Figure 8.9 Conical Path, Case 2-All View

TRANSMITTER : RT-4 (RT-4TX ) RECEIVER : IB (JAMRX )

| DESCRIPTION | HARMONIC NO 1 9.315 GHZ |
|---|---|
| TRANSMITTER POWER | 60.8 |
| XMTR CABLE LOSSES | 0.0 |
| XMTR ANTENNA GAIN | 7.0 |
| TRANSMISSION LOSS | -58.7 |
| SURFACE SHADING | -86.8 |
| EDGE SHADING | 0.0 |
| RCVR ANTENNA GAIN | -18.0 |
| RCVR CABLE LOSSES | 0.0 |
| RCVR SENSITIVITY | -30.0 |
| EMI MARGIN | -80.6 |
| \ FIELD WARNING | \ 77. |

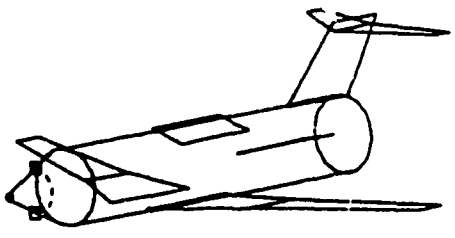

TRANSMITTER ANTENNA
■ RT (SIDE) EL : -4.63 AZ : -90.00

RECEIVER ANTENNA
□ RX (SIDE) EL : -3.78 AZ : -90.00

ELEVATION : 10. DEG.
AZIMUTH : -40. DEG.

Figure 8.10 Unmodified Path, Case 3

TRANSMITTER : RT-4 (RT-4TX ) RECEIVER : IB (JAMRX )

| DESCRIPTION | HARMONIC NO 1 8.315 GHZ |
|---|---|
| TRANSMITTER POWER | 60.8 |
| XMTR CABLE LOSSES | 0.0 |
| XMTR ANTENNA GAIN | 7.0 |
| TRANSMISSION LOSS | -59.7 |
| SURFACE SHADING | -90.3 |
| EDGE SHADING | 0.0 |
| RCVR ANTENNA GAIN | -18.0 |
| RCVR CABLE LOSSES | 0.0 |
| RCVR SENSITIVITY | -30.0 |
| EMI MARGIN \ FIELD WARNING | -64.3 \ 77. |

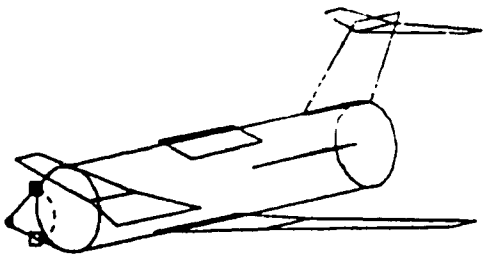

TRANSMITTER ANTENNA
RT (SIDE) EL : -5.22 AZ : -90.00

RECEIVER ANTENNA
RX (SIDE) EL : -3.71 AZ : -90.00

ELEVATION = 10. DEG.
AZIMUTH = -40. DEG.

## 8.11 Modified Path, Case 3

CONCYLTST1 PROPAGATION PATH DISPLAY

RECEIVER : IB (JAMRX ) TRANSMITTER : RT-4
ANTENNA : RX (SIDE) ANTENNA : RT

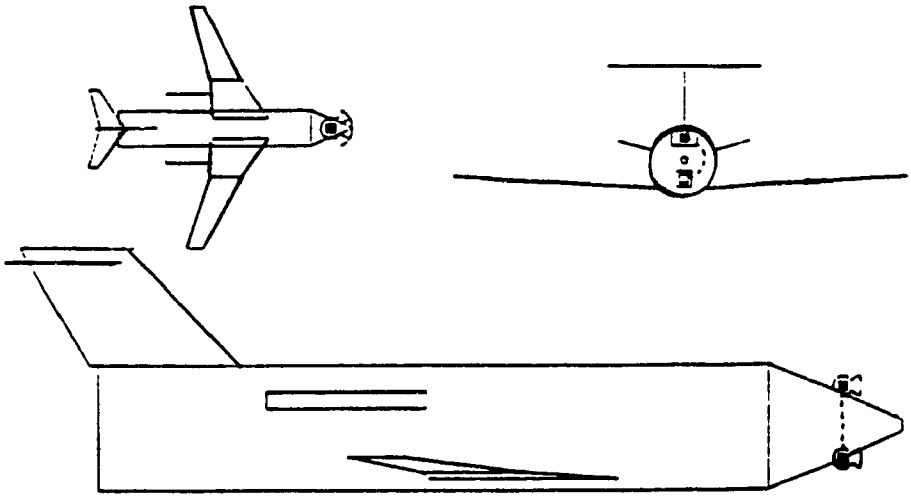

**Figure 8.12 Conical Path, Case 3-All View**

# CHAPTER 9

# SUMMARY AND CONCLUSION

## 9.1 Summary

In this thesis the analysis of one important method to calculate antenna coupling on an aircraft fuselage was reviewed. The basic concepts of this method, the Geometrical Theory of Diffraction (GTD) were presented in Chapter 2. The Antenna-to-Antenna propagation with Graphics (AAPG) computer code which uses the GTD technique to calculate electromagnetic interference is introduced in Chapter 3.

The importance of updating these analysis software programs is undeniable. The governments and industries using the codes expect a constant effort to upkeep these tools in order to ensure precise calculations and accurate EMI path predictions. These two important factors were the main objectives of this work.

Chapter 4 addressed a very important problem mainly concerning modern military aircraft, the determination of the proper wing diffraction point. The optimization approach presented, ensures that the exact diffraction point will be used, thus providing a more accurate diffracted field.

In Chapter 5 the difficulty in finding the proper cross- over point on the intercept line between the cone and cylinder portion of the airframe is studied. Here again an optimization method is introduced, which provides a much more accurate EMI path between two antennas located on either side of the cone/cylinder intercept line. Examples of improvement are provided and show a better adherence to the Fermat principle.

On the large majority of aircraft, both military and commercial, some of the most sensitive systems are located on the nose or conical portion of the fuselage. Chapter 6 examines a deficiency which existed in the previous version of the code, where difficulties were encountered when dealing with paths around the nose geometry. This concern applies to military aircraft in "close-flight" formation flying tactics. A new subroutine was developed and it was shown that the new algorithm greatly improves the EMI path prediction.

In Chapter 7, one could observe that the formal version of AAPG provided an incorrect conical spiral distance calculation. A three dimensional to two dimensional translation approach was introduced and proved to provide the proper conical path distances. The improvements are

supported by numerous examples.

It was also shown in Chapter 8, that the electromagnetic shading calculation previously done in AAPG was an approximation based on a constant radius of curvature, which is obviously not the case for a cone. A new approach was studied and coded in order to improve the shading loss determination thus providing a more accurate EMI figure when coupling takes place between two systems on the nose of the aircraft. Again, improvements are illustrated using examples on current airframes.

The work previously described has been implemented in a new version of the AAPG code and introduced to the industry and government departments using this tool. The tests done before the release of this new version indicated sound improvements in the EMC analysis of five aircraft types and have increased the engineering staff confidence in AAPG

## 9.2 Suggestions for Future Work

The new edition of AAPG provides accurate numerical values for the EMI margins and permits the visualization of the solution results. However, with the introduction of quite complex geometry on modern aircraft the graphics package requires a modification which would provide more flexibility in airframe representation to include such

technology as represented by the "stealth" design approach.

More research would also be necessary to improve the surface shading loss calculation where the radius of curvature is not constant. This new formulation could be necessary for EMC analysis of complex structures such as a space station or new technology such as the Concorde airframe.

Finally, research work to evaluate the present mathematical formulation in the presence of composite materials would be necessary. The utilization of this new construction technique is becoming more popular in the industrial world and presents a new challenge for the engineering staff who concentrate on EMC analysis.

Any effort to create and improve EMC analysis for aircraft will not only save money, but above all, may save lives.

## BIBLIOGRAPHY

[1] Electromagnetic News Report, Vol. 15, No. 5, January 1988.

[2] Girard T. Capraro, "An Intrasystem EMC Analysis Program", AGARD-LS-116, pp. 4-1/4-22, September 1981.

[3] Stanley J. Kubina, "Computer Graphics Aids to Weapon Systems EMC Analysis", AGARD-LS-116, pp. 5-1/5-13, September, 1988.

[4] Stutzman & Thiele, "Antenna Theory and Design", Wiley, 1981.

[5] J.B. Keller, "A Geometrical Theory of Diffraction", J. Opt. Soc. Am., Vol. 52, pp.116-130, 1962

[6] M. Kline, "An Asymptotic Solution of Maxwell's Equation", Comm. Pure and Appl. Math., Vol. 4, pp.225-263, 1951.

[7] R. Kouyoumjian & P. Pathak, "The Modern Geometrical Theory of Diffraction", Vol. 1 and 2, Report No. Nasa CR-2401, 1974.

[8] R. Kouyoumjian & P. Pathak, "A Uniform Theory of Diffraction for an Edge in a Perfectly Conducting Surface", Proc. IEEE, Vol. 62, pp. 1448-1461, 1974.

[9] R. Mittra, "Numerical and Asymptotic Techniques in EM", Springer-Verlag, 1975.

[10] P.H. Pathak, "Uniform GTD Solutions for a Class of Problems Associated with the Diffraction by Smooth Convex Surfaces", the Modern Geometrical Theory of Diffraction, Vol. 1, Course Note.

[11] L. James, "Geometrical Theory of Diffraction", IEEE Series, 1980.

[12] John F. Spina. "The EMC Concept for Weapon Systems", Lecture No. 2 NATO/AGARD Series 116 on EMC Fall 1981.

[13] H. Hodes, H. and P. Widmer, "The Solution of Real-World Aircraft EMC Problems Using the AAPG Computer Program", IEEE 1982.

[14] H.T. Friis, "A Note on a Simple Transmission Formula", Proc. IRE, Vol. 34, pp. 254-256, May 1946.

[15] Hasserjian and Ishimaru, "Excitation of a Conducting Cylindrical Surface of Large Radius of Curvature", IRE Trans. Aut. & Prop., Vol. AP10, pp. 264-273, May 1962.

[16] E. Durham, "Analysis and Measurement of EMI Coupling for Aircraft Mounted Antennas at SHF/EHF", IEEE Symposium on EMC, Atlanta, GA, August 1987.

[17] H.Pathak, D. Burnside, and J. Marhefka, "A Uniform GTD Analysis of the Diffraction of Electromagnetic Waves by a Smooth Convex Surface", Trans. IEEE on Antennas and Propagation, Vol. AP-28, No. 5, September 1980.

[18] H.P. Widmer, "A Technical Description of AAPG", Report ECAC-CR-83-048, Department of Defence, Annapolis, MD, November, 1983.

[19] Discussion with David Gaudine, Concordia University, EMC Department.

[20] H.P. Widmer, "A Technical Description of the AAPG Program", ECAC-CR-83-048, DOD ECAC, Annapolis, MD, November, 1983.

[21] R.J. Marhefka and Nan Wang, "GTD Curved Surface Applications", The Modern Geometrical Theory of Diffraction, OSU, Vol. 2, pp. B19-27.

[22] S.W. Lee, "Mututal Admittance of Slots on a Cone: Solution by Ray Teaching", IEEE, Trans. Antenna Prop., Vol, AP-26, pp. 768-773, 1978.

[23] P.H. Pathak & N. Wang, "Ray Analysis of Mutual Coupling Between Antenna on a Convex Surface", IEEE Transactions on Antennas and Prop., Vol. AP-29, pp. 911-922.

[24] S.W. Lee, "A Review of GTD Calculation of Mutual Admittance of Slot Conformal Array", Electromagnetics Journal, 1982, pp.. 85-127.

[25] P.E. Hussar & W.R. Klocko, "User's Manual for the Aircraft Inter-Antenna Propagation with Graphics (AAPG) Computer Program, Version 09", ECAC-UM-88-048, DOD ECAC, Annapolis, MD, February, 1988.

[26] J.L. Bogdamor, M.D., Siegel and G.L. Weinstock, "Intra-Vehicle Electromagnetic Compatibility Analysis", AFAAL-TR-71-155, PART I, McDonnell Aircraft Co., St. Louis, MO, July, 1971.

[27] K.E. Golden, G.E. Steward and D.C. Pridmore-Brown, "Approximation Techniques for the Mutual Admittance of Slot Antennas on Metallic Cones" IEEE Trans. Antenna Prop., Vol. AP-2, pp. 43-48, 1974.

[28] James Kozlowski, "Computation of the Geodesic of a Cone Using the Calculus of Variations", Electromagnetic Laboratory Technical Notes, EMC-78-01, 1978, Concordia University.

[29] S.W. Lee, "Differential Geometry for GTD Applications", Technical Report UILU-ENG-77-22, University of Illinois, 1977.

# APPENDIX A

## FLOWCHART SUBROUTINE WNGEDG

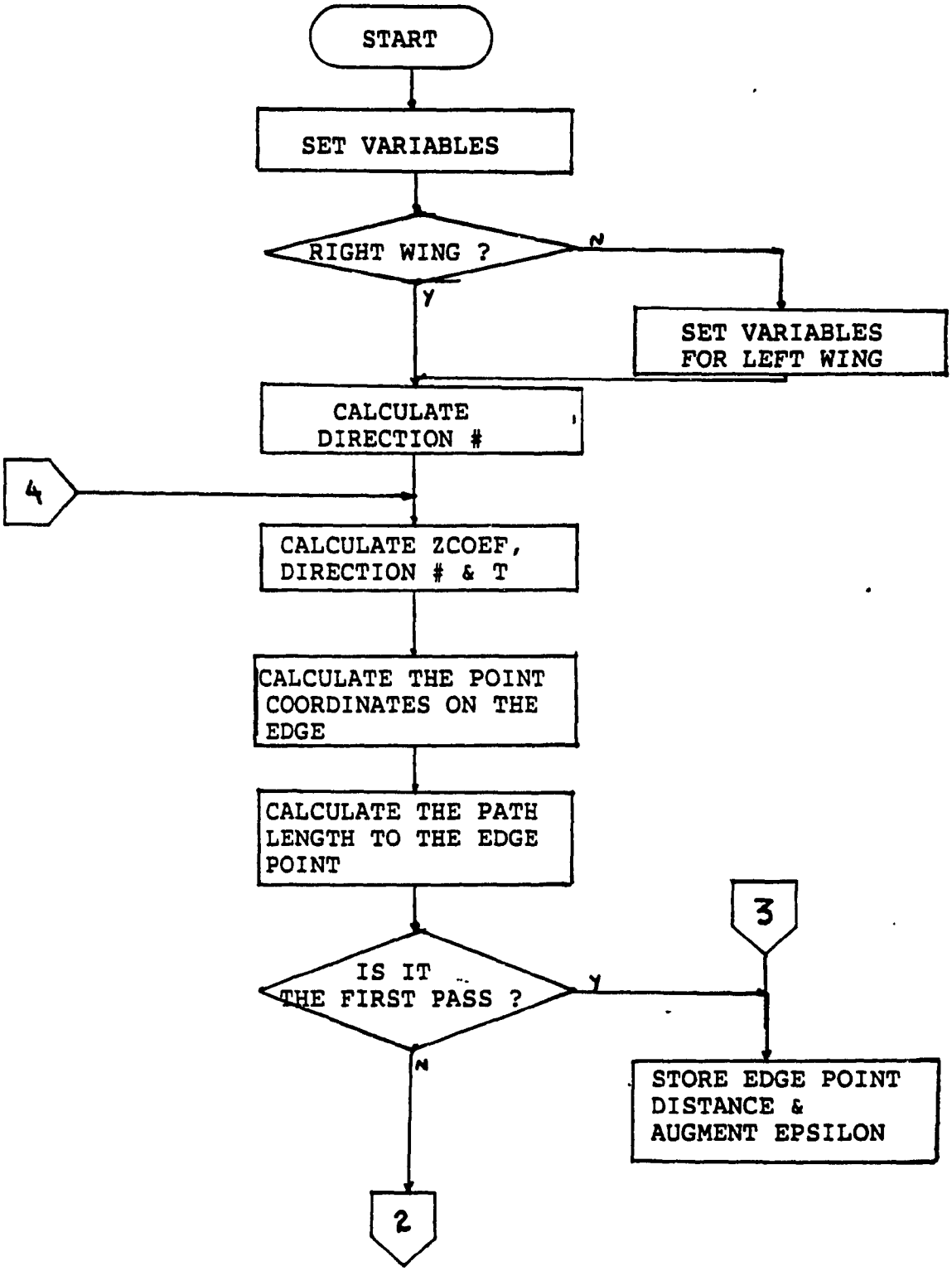

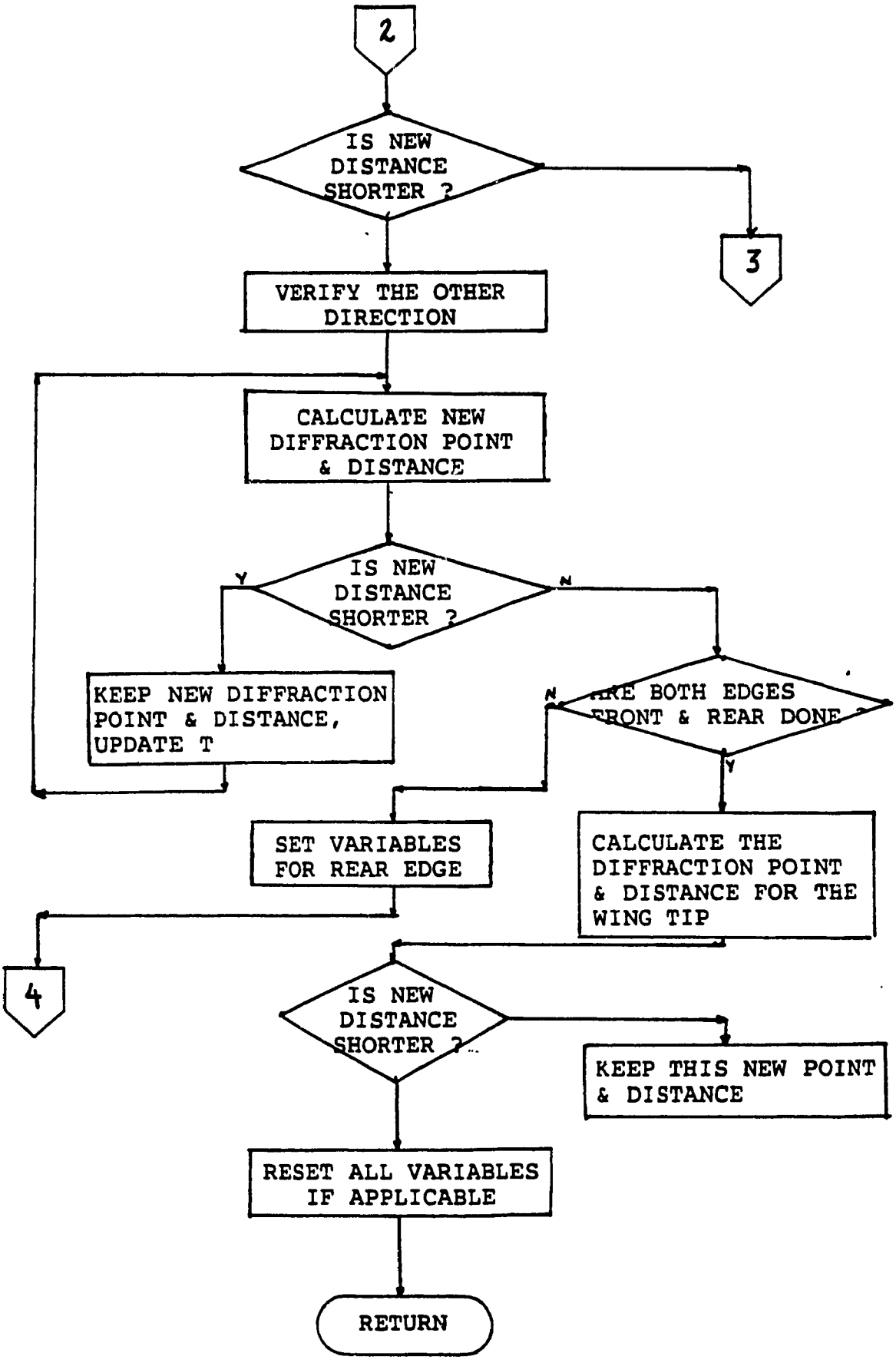
2
IS NEW DISTANCE SHORTER ?
3
VERIFY THE OTHER DIRECTION
CALCULATE NEW DIFFRACTION POINT & DISTANCE
IS NEW DISTANCE SHORTER ?
Y
N
KEEP NEW DIFFRACTION POINT & DISTANCE, UPDATE T
ARE BOTH EDGES FRONT & REAR DONE ?
N
Y
SET VARIABLES FOR REAR EDGE
CALCULATE THE DIFFRACTION POINT & DISTANCE FOR THE WING TIP
4
IS NEW DISTANCE SHORTER ?
KEEP THIS NEW POINT & DISTANCE
RESET ALL VARIABLES IF APPLICABLE
RETURN

## APPENDIX B

## MODIFIED SUBROUTINE WNGEDG LISTING

```
C     INCLUDE 'PSEUDO.OPS'
C     SUBROUTINE WNGEDG (RTWING,ANT1X,ANT1Z,ANT2X,ANT2Y,
C     ANT2Z,XINTR,YINTR,ZINTR,XWEDGE,YWEDGE,ZWEDGE,
C     IEDGE)
C     GIVEN THE COORDINATES OF THE POINT AT WHICH A NON-
C     DIFFRACTING PATH WOULD PIERCE A WING PLANE, THIS
C     SUBROUTINE COMPUTES THE THREE DIFFRACTION POINTS
C     ON THE FORWARD, AFT AND TIP OF THE WING.  THEN THE
C     PROGRAM FINDS THE OPTIMUM POINT SO THAT THE DISTANCE
C     FROM ANTENNA 1 TO ANTENNA 2 VIA THE DIFFRACTION POINT
C     IS OPTIMIZED.
C     ------------------------------------------------------
C      THE TECHNIQUE UTILIZED IS AS FOLLOWS;
C      WE FIRST FIND A POINT ON EACH EDGE BY TRACING A
C      LINE FROM THE PIERCING POINT TO EACH EDGE OF THE
C      WING, THEN WE ITERATE ALONG THE EDGE TO VERIFY IF
C      THIS POINT IS AY AN OPTIMUM POINT.  ONCE WE
C      ACCOMPLISH THIS TASK ON THE EDGES OF THE WING WE
C      HAVE THE OPTIMUM DIFFRACTION POINT OFF THE WING.
C     ------------------------------------------------------
C      PARAMETERS:  RTWING- LOGICAL FLAG DIRECTING THE
C                   SUBROUTINE TO FIND  A DIFFRACTION
C                   POINT ON THE APPROPRIATE WING.
C                          TRUE.  RIGHT WING
C                          FALSE.  LEFT WING
C      XINTR, YINTR AND ZINTR ARE THE COORDINATES
C      OF THE PIERCING POINTWEDGE, XWEDGE AND
C      ZWEDGE ARE THE ORTHOGONAL COORDINATES OF THE
C      DIFFRACTION POINT
C      IEDGE : DIFFRACTION POINT IS ON
C                       1-FORWARD WING EDGE
C                       2-WING TIP
C                       3-AFT WING EDGE
       INCLUDE 'ARCRFT.FCB'
       INCLUDE 'PLNSRF.FCB'
       LOGICAL RTWING, BOTH, ONCE

C      SET 'BOTH' TO INDICATE THAT BOTH THE FORWARD AND AFT
C      WING EDGE DIFFRACTION POINTS HAVE NOT YET BEEN
C      EVALUATED.  IF THIS COMPUTATION IS TO BE FOR THE LEFT
C      WING, NEGATE THE RIGHT WING BUTT LINE PARAMETERS, IF
C      NOT THEN WE WILL  GO DIRECTLY TO THE RIGHT WING
C      CALCULATIONS. EPSI REPRESENT EPSILONE OR THE SMALL
C      VALUE ADDED TO THE DIFRACTION POINT IN AN EFFORT TO
C      OPTIMIZE THE VALUE.
```

```
C
      BOTH = FALSE.
      EPSI = 0.001
      IF (RTWING) GO TO 25
C
C     HERE WE ADJUST THE PARAMETERS FOR THE LEFT WING WHERE
C     WE WILL TREAT THE LEFT WING FIRST
C
      PTBL(1)=-PTBL(1)
      PFBL(1)=-PFBL(1)
C
C     NOW WE WILL SET UP THE VARIABLES FOR THE RIGHT AND THE
C     LEFT WING CALCULATIONS
C
25    WFFS = PFFFS(1)
      WTFS = PTFFS(1)
      XCODE = PTBL(1)-RFBL(1)
      XCOEF = PTWL(1)-PFWL(1)
C
*************************************************************
C
C     THE FOLLOWING PART IS COMMON TO THE FORWARD AND THE AFT
C     WING DIFFRACTION POINT CALCULATION  HOWEVER WE START
C     WITH THE FORWARD WING AND FIND THE OPTIMUM  POINT GOING
C     ONE WAY, THEN WE WILL SEARCH THE OTHER WAY BY NEGATING
C     EPSILON
C
30   ZCOEF = WTFS-WFFS
C
     CONST = XCOEF*XINTR + YCOEF*YINTR + ZCOEFF*ZINTR
C
     PARAM = ( CONST - XCOEF*PFBL(1) - YCOEF*PFWL(1) -
     ZCOEF*WFFS) / (XCOEF**2 + YCOEF**2 + ZCOEF**2)
C
     T = PARAM
     ONCE = .TRUE.
     $$$$$$$$$$$$$$$$$$$$$$$$$$$$$$$$$
     ST=0
C
     $$$$$$$$$$$$$$$$$$$$$$$$$$$$$$$$$
C
     NOW WE CALCULATE THE DIFFRACTION POINT USING THE
     PARAMETRIC FORM FOR THE LINE
C
50   XEDGE = PFBL(1) + XCOEF * T
     XEDGE = PFWL(1) + YCOEF * T
     XEDGE = WFFS + ZCOEF * T
     $$$$$$$$$$$$$$$$$$$$$$$$$$$$$$$$$
C
C    HERE WE WANT TO CALCULATE THE DISTANCE BETWEEN ANTENNA 1
C    AND  ANTENNA 2 VIA THE DIFFRACTION POINT
C
     LEN1 = DSL(ANT1X,ANT1Y,ANT1Z,XEDGE,YEDGE,ZEDGE)
     LEN2 = DSL(XEDGE,YEDGE,ZEDGE,ANT2X,ANT2Y,ANT2Z)
```

```
      TLEN = LEN1+LEN2
C
C     IF WE ONLY WENT THROUGH THE SEQUENCE ONCE WE
      DO NOT WANT TO COMPARE, SO WE BYPASS

C     ---SECURITY TEST---
      ST=ST+1
C
      WRITE (7,*) ST,LEN1,LEN2,TLEN
C
      IF (ONCE) GO TO 100
C
C     WE VERIFY AT THIS POINT IF THE NEW CALCULATED VALUE
C     PROVIDE A BETTER DIFFRACTED POINT I.E. A SHORTER PATH
C
      IF ( TLEN .GE. ROUTE ) GO TO 150
C
C     IF THE NEW POINT IS GIVEN A SHORTER PATH THEN WE
C     WANT TO RETAIN THIS POINT AS THE DIFFRACTED POINT
C     THEN WE WANT TO INCREASE OUR PARAMETER TO
C     CALCULATE A NEW POINT
C
  100   ROUTE = TLEN
        T = T + EPS1
        ONCE = .FALSE.
        XWEDGE=XEDGE
        YWEDGE=YEDGE
        ZWEDGE=ZEDGE
C
C      $$$$$$$$$$$$$$$$$$$$$$$$$$$$$
         IF (ST.EQ.50) GO TO 150
         GO TO 50
C
C      **********************************************
C
C     HERE WE WILL VERIFY I.. THE OTHER DIRECTION
C
C     IF THE PATH LENGTH IS INCREASING WE ARE LIKELY GOING THE
C     WRONG WAY SO WE WILL TRY THE OTHER WAY BY CHANGING THE
C     SIGN  OF EPS1
C
150 T = PARAM
      EPS1 = -EPS1
C
C     $$$$$$$$$$$$$$$$$$$
C      ---SECURITY TEST---
      ST=0
C
200 XEDGE = RFBL(1) + XCOEF * T
      XEDGE = PFWL(1) + YCOEF * T
      XEDGE = WFFS + ZCOEF * T
C      $$$$$$$$$$$$$$$$$$$$$
C
C     HERE WE AGAIN CALCULATE THE DISTANCE FROM ANTENNA 1 TO
```

```
C    ANTENNA 2 VIA THE DIFFRACTION POINT
C    BUT THIS TIME WE ARE OF COURSE GOING THE OTHERC WAY
C
     LEN1 = DSL(ANT1X,ANT1Y,ANT1Z,XEDGE,YEDGE,ZEDGE)
     LEN2 = DSL(XEDGE,YEDGE,ZEDGE,ANT2X,ANT2Y,ANT2Z)
     TLEN = LEN1 + LEN2
     IF ( TLEN .GE. ROUTE ) GO TO 300
C
C    AGAIN WE WANT TO RETAIN THE LAST POINT IF THIS
C    POINT IS PROVIDING A SHORTER PATH
     ST=ST+1
C
 250 ROUTE = TLEN
      T = T + EPSI
      XWEDGE=XEDGE
      YWEDGE=YEDGE
      ZWEDGE=ZEDGE
C
      IF (ST.EQ.50) GO TO 300
C
      GO TO 200
C
C    ********************************************

C    AT THIS POINT WE HAVE THE OPTIMUM WING DIFFRACTION POINT
C    CALLED XEDGE, YEDGE, ZEDGE, AND THE TOTAL PATH LENGTH
C    FROM ANTENNA 1 TO ANTENNA 2 WHICH PASSES THROUGH THE
C    DIFFRACTION POINT AND WHICH IS CALLED 'ROUTE'
C    NOW WE WANT TO GO BACK AND EFFECTUATE THE SAME FOR THE
C    AFT EDGE, WE WILL SAVE OUR INFORMATION BEFORE SO NOT TO
C    LOOSE THE INITIAL POINT
C
300  IF (BOTH) GO TO 400
     RISEN = ROUTE
     IEDGE = 3
     BOTH = .TRUE.
C
C    HERE WE MUST INITIALIZE CERTAIN VARIABLES FOR THE
C    AFT WING
C
     WTFS = PTAFS(1)
C
     WFFS = PTAFS(1)
C
C    WE WILL NOW STORE THE OPTIMUM POINT FOUND
C    ON THE FRONT EDGE BEFORE WE GO ON TO THE
C    BACK EDGE
C
     XEDF=XWEDGE
     YEDF=YWEDGE
     ZEDF=ZWEDGE
C
     GO TO 30
C
```

```
C    NOW IF THE DIFFRACTION POINT ON THE AFT WING GIVES
C    A SHORTER PATH BETWEEN ANTENNA 1 AND ANTENNA 2 THEN
C    WE WILL RETAIN THIS POINT AS THE OPTIMUM POINT
C
400  IF ( ROUTE .GE. RISEN ) THEN
     XWEDGE = XEDF
     YWEDGE = YEDF
     ZWEDGE = ZEDF
     IEDGE = 1
      ELSE
      RISEN=ROUTE
      END IF
C     **************************************************
C    NOW LET'S DO THE SAME TYPE OF CALCULATIONS AS ABOVE
C    FOR THE DIFFRACTION POINT ON THE WING TIP.
C
     ZCOEF = PTAFS(1) - PTFFS(1)
     PARAM = (ZINTR-PTFFS(1))/ZCOEF
     ZEDGE = PTFFS(1) + ZCOEF * PARAM
     XEDGE = PTBL(1)
     YEDGE = PTWL(1)
     LEN1 = DSL(ANT1X,ANT1Y,ANT1Z,XEDGE,YEDGE,ZEDGE)
     LEN2 = DSL(XEDGE.YEDGE,ZEDGE,ANT2X,ANT2Y,ANT2Z)
     ROUTE = LEN1 + LEN2
C
C    HERE AGAIN WE VERIFY IF THE NEW POINT OBTAINED
C    WILL PROVIDE AN OPTIMUM VALUE, OF COURSE IF IT
C    DOES WE WILL RETAIN THIS NEW VALUE
C
     IF (ROUTE .GE. RISEN) GO TO 600
     RISEN = ROUTE
     XWEDGE = XEDGE
     XWEDGE = YEDGE
     ZWEDGE = ZEDGE
     IEDGE = 2
C   **************************************************
C    RESTORE THE POSITIVE WING BUTT LINE VALUES IF THEY WERE
C    NEGATED, AND RLTURN.
C
600  IF (RTWING) RETURN
     PTBL(1) = -PTBL(1)
     PFBL(1) = -PFBL(1)
     RETURN
     END
```

# APPENDIX C

## CONICAL/CYLINDRICAL SPIRAL CROSS OVER POINT IMPROVEMENT FLOWCHART

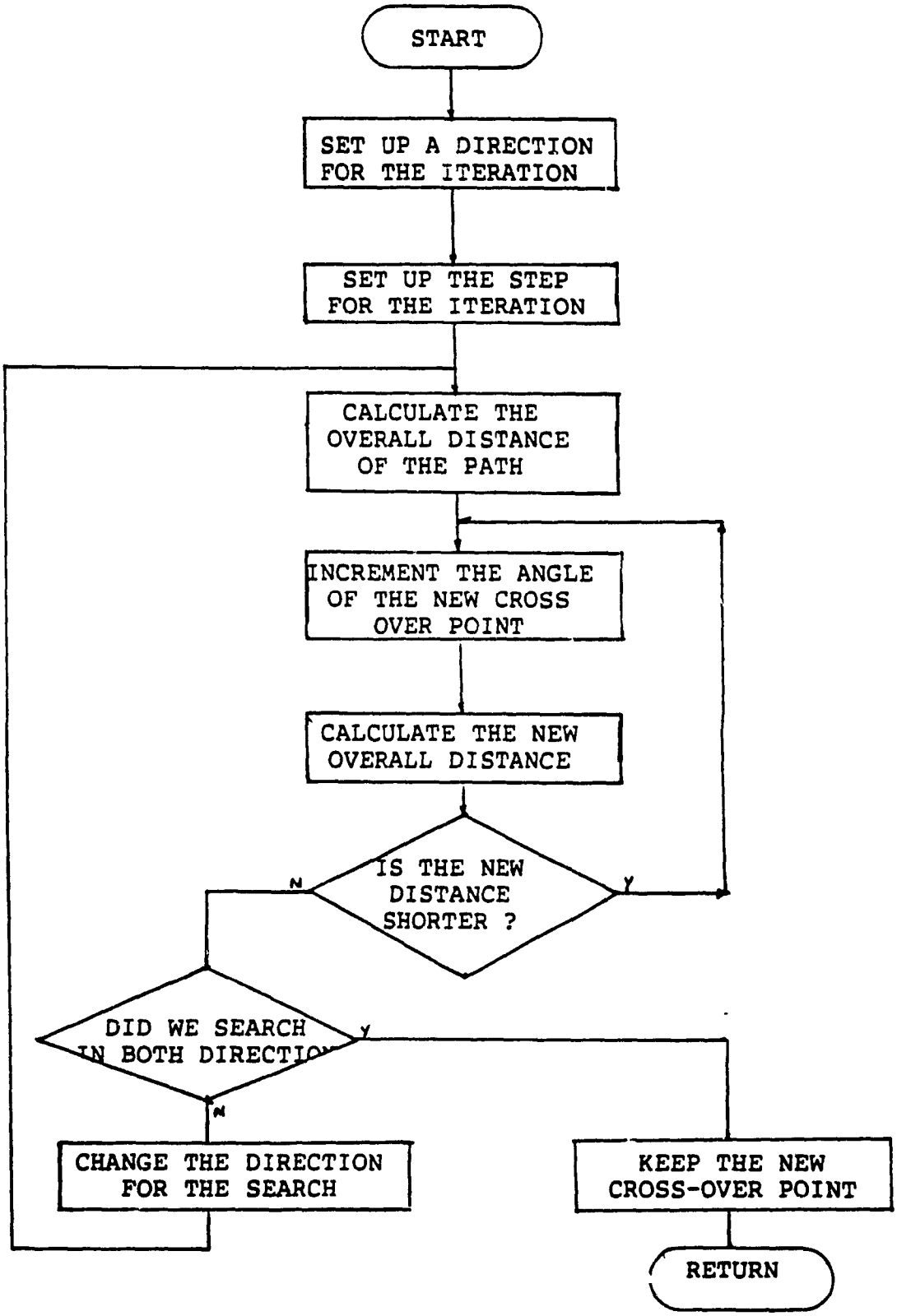

## APPENDIX D

## CONICAL/CYLINDRICAL SPIRAL MODIFICATION LISTING

```
C     THE FOLLOWING SUBROUTINE MODIFICATION UTILIZES AND
      ITERATIVE C    APPROACH
C     TO LOCATE THE OPTIMUM POINT AT WHICH THE GEODESIC
      CROSSES C THE CONE/CYLINDER INTERSECTION.  THIS APPLIES
      FOR A C    CYLINDRICAL/CONICAL SPIRAL PATH.
C
C     SIGN = -1.0
      STEP = 3.1415926 / 180.0
      NSTEP = ANGFSN / (STEP*2.0)
      A1 = AVCCCS(P1A)
      A2 = AVCCCS(P2A)
      AM = ANGFSN
      IF (P17.LT.P27) THEN
         DIST = DCON(P1R,A1,P1Z,RHOFSN,AM,FSN) +
                DCYL(RHOFSN,AM,A2,FSN,P2Z)
   &
      ELSE
         DIST = DCYL(P1R,A1,AM,P1Z,FSN) +
   &             DCON(RHOFSN,AM,FSN,P2R,A2,P2Z)
      END IF
C
C     DO 95 I=1,NSTEP
         AMC = AVCCCS(AM+SIGN*I*STEP)
         IF (P17.LT.P27) THEN
            DIST2 = DCON(P1R,A1,P1Z,RHOFSN,ANG,FSN) +
   &                DCYL(RHOFSN,ANG,A2,FSN,P2Z)
      ELSE
            DIST2 = DCYL(PLR,A1,ANG,P1Z,FSN) +
   &                DCON(RHOFSN,ANG,FSN,P2R,A2,P2Z)
      END IF
      IF (DIST2.GT.DIST) GOTO 95
      DIST = DIST2
      ANGFSN = ANG
95 CONTINUE
   IF (SIGN.EQ.-1.0) THEN
      SIGN = +1.0
      GOTO 80
C    END IF
C    RETURN
C    END OF COMMENTED SECTION.
```

# APPENDIX E

## SUBROUTINE CONINT FLOWCHART

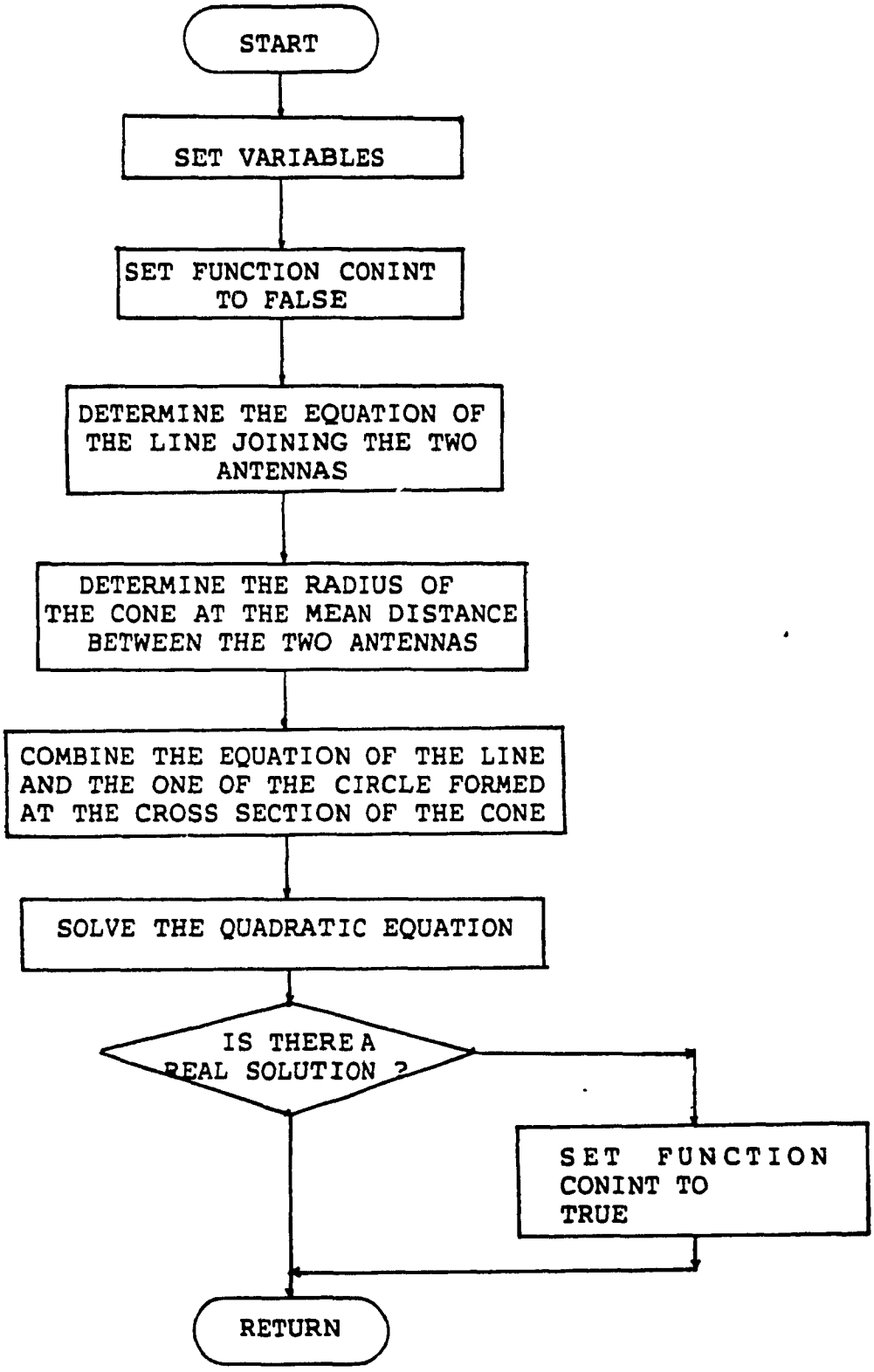

## APPENDIX F

## SUBROUTINE CONE LISTING

```
C     THIS SUBROUTINE IS TO FIND IF A STRAIGHT
C     LINE BETWEEN TWO ANTENNAS WILL
C     INTERSEPT THE CONE.
C
      INCLUDE 'PSEUDO.OPS'
      LOGICAL FUNCTION CONINT (SPR,SPA,P1Z,EPR,EPA,P2Z)
      LOGICAL REV
      INCLUDE 'ARCRFT.FCB'

C
C     WE FIRST SET CONINT TO FALSE ASSUMING THAT THE STRAIGHT
C     LINE BETWEEN THE TWO ANTENNAS WILL NOT INTERCEPT
C     THE CONICAL PORLTION OF THE AIRCRAFT AND WE WILL
C     CHANGE THE START AND END POINTS INTO XY COORDINATES.
C     CONINT= FALSE
      YDEB=ABS(P2Y-P1Y)
      YDEV=ABS(P2X-P1X)
      IF 9YDEV .LE. 1.0 .AND. XDEV .LE. 1.0 ) GOTO 200
C
C     HERE WE WILL PICK THE AXIS ON WHICH THE STRAIGHT
C     LINE WILL CROSS MOST RAPIDLY.
C
      REV=YDEV .GT. XDEV
      IF (REV) GOTO 130
      A1X=P1X
      A1Y=P1Y-WLC
      A2X=P2X
      A2Y=P2Y-WLC
      GOTO 150
130   A1X=P1Y-WLC
      A1Y=P1X
      A2X=P2Y-WLC
      A2Y=P2X
C
C     NOW WE CALCULATE THE SLOPE OF THE STRAIGHT LINE
C     JOINING  THE  TWO  ANTENNAS,  AND  THE  DISTANCE  FROM  THE
      ORIGIN C  TO THE CLOSEST POINT WHERE WE CROSS AN AXIS.
C
150 SLOPE=(A2Y-A1Y)/(A2X-A1X)
    YINTC=A1Y-A1X*SLOPE
C


C     IN ORDER TO WRITE THE QUADRATIC EQUATION INVOLVING
C     BOTH THE CIRCLE OF THE FUSELAGE AND THE STRAIGHT LINE,
```

```
C     WE MUST USE THE MEAN REDIUS BETWEEN THE TWO ANTENNA
      POINTS.
C
      DELX=ABS(P1X-P2X)
      DELZ=ABS(P2Z-P1Z)
      RAT=ABS(P1X/DELX)
      DEL=DELZ*RAT
      IF (P2Z .LE. P1Z) GOTO 170
      INTEZ=P2Z-DEL
      GOTO 190
170   INTEZ=P1Z-DEL
190   RADI=(RHOF/FSN)*INTEZ
C
C     NOW THAT WE HAVE THE RADIUS OF THE LOCATION
C     WHERE THE STRAIGHT LINE CROSSES THE CONE PORTION
C     WE CAN COMBINE THE TWO EQUATIONS, I.E. STRAIGHT
C     LINE AND CIRCLE OR CROSS SECTION CIRCLE OF THE
C     CONE PORTION
C
      A=1.0+SLOPE*SLOPE
      B=2 0*SLOPE*YINTC
      C=YINTC*YINTC-RADI*RADI
      ROOT=B*B-4.0*A*C
      IF (ROOT .LE. 0.0) GOTO 200
      T1=-0.5*B/A
      T2=0.5*SORT (ROOT)/A
      DO 195 I=1,2
      X=T1+T2
      IF(I .EQ. 2) X=T1-T2
      IF ((X .LE. A1X .AND. X .LE. A2X ) .OR.
     &    (X .GE. A1X .AND. X .GE. A2X )) GOTO 195
      Y=SLOPE *X+Y1NTC
      WB=WLBOT-(WLC+0.1)
      IF ( .NOT. REV .AND. Y .GT. WB) GOTO 198
      IF ( REV .AND. X .GT. WB ) GOTO 198
195   CONTINUE
      GOTO 200
198   CONINT = .TRUE.
200   RETURN
      END
```

# APPENDIX G

## CONICAL SPIRAL DISTANCE CALCULATION FLOWCHART

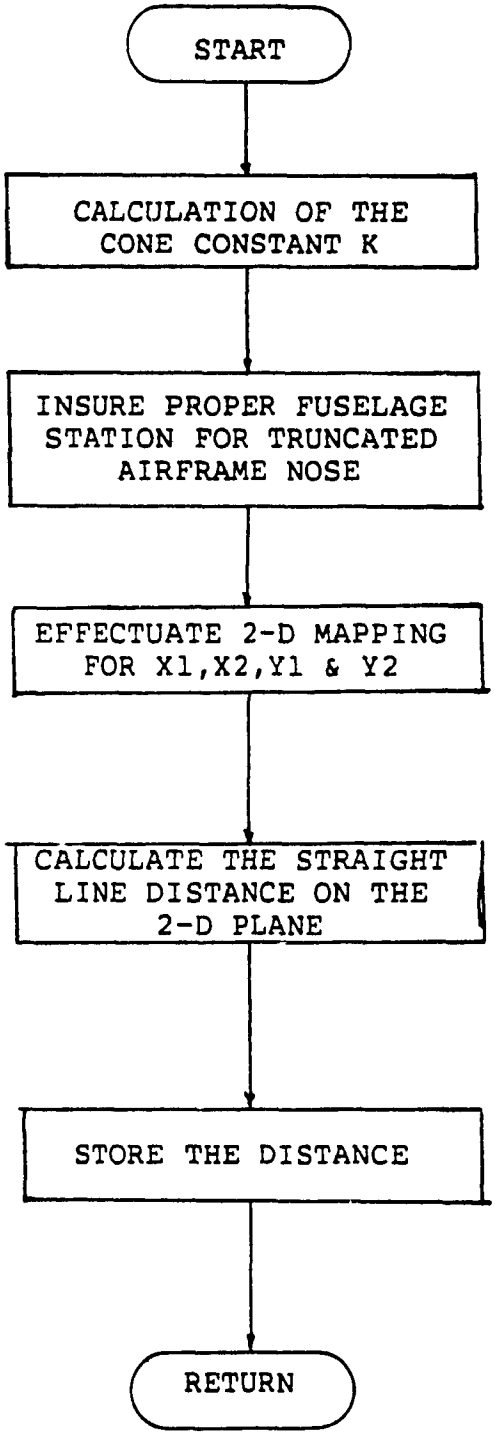

# APPENDIX H

## Subroutine DCON Listing

```
      INCLUDE 'PSEUDO,OPS'
      FUNCTION DCON (RH01, THETA1, Z1, RH02, THETA2, Z2)
C
C     THIS FUNCTION  RETURNS CONICAL SPIRAL DISTANCE
C     'DCON' BETWEEN TWO POINTS ON THE CONE SURFACE.
C     !!
C     !!    THIS SUBROUTINE HAS BEEN MODIFIED TO CALCULATE
C     !!    CALCULATE THE DISTANCE ON THE CONE USING THE
C     !!    3D TO 2D MAPPING.
C
C     PARAMETERS:
C
C          RH01, THETA1, Z1 - INITIAL POINT POSITION; AVCCCS
C             COORDINATES
C          RH02, THETA2, Z2 - FINAL POINT POSITION; AVCCCS
C             COORDINATES
C
      INCLUDE 'ARCRFT.FCB'
C     !!    HERE WE MUST ADJUST THE Z COORDINATE OF EACH POINT
C     !!    BECAUSE THE AIRCRAFT IS NOT NECESSARILY SITTING ON
C     !!    THE ORIGIN
C
C     CTA REPRESENT THE CONE CONSTANT
C     ZPLUS IS THE COMPENSATION MEASURE FOR THE
C     AIRCRAFT NOT SITTING ON THE ORIGIN
C     ZT1 AND Z12 ARE THE NEW Z COORDINATES FOR EACH
C     ANTENNA
C
C     CTA=(RHOF-RHOC)/FSN
      ZPLUS=RHOC/CTA
      ZT1=Z1+ZPLUS
      ZT2=Z2+ZPLUS
C
C     MAPPING PROCEDURE
C      PTX1=Z11*SQRT(1+CTA*CTA)*SIN(THETA1*
           (CTA/SQRT(1+CTA*CTA)))
      PTX2=Z12*SQRT(1+CTA*CTA)*SIN(THETA2*
           (CTA/SQRT(1+CTA*CTA)))
      PTY1=ZT1*SQRT(1+CTA*CTA)*COS(THETA1*
           (CTA/SQRT(1+CTA*CTA)))
      PTY2=ZT2*SQRT(1+CTA*CTA)*COS(THETA2*
           (CTA/SQRT(1+CTA*CTA)))
C
C     DISTANCE CALCULATION ON THE 2D PLANE
```

```
C
      DTE=SQRT(PTX2-PTX1)**2+(PTY2-PTY1)**2)
C
C     DCON IS THE VARIABLE RETURNED
C
C     DCON=DTE
C
      RETURN
C
      END
```

# APPENDIX J

## CONICAL SHADING IMPROVEMENT FLOWCHART

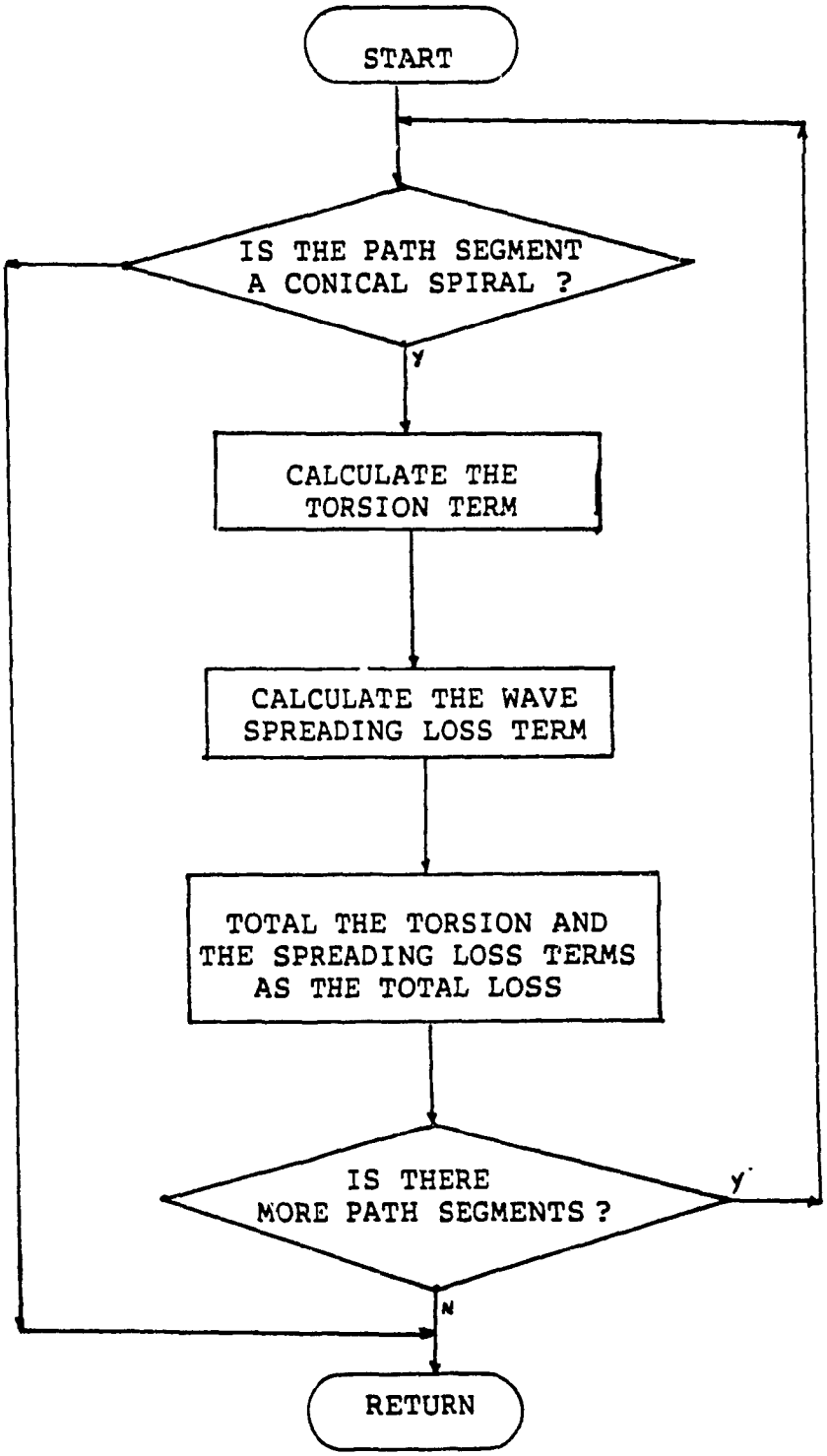

## APPENDIX K

## SUBROUTINE LOSS LISTING

```
      INCLUDE 'PSEUDO.OPS'
      SUBROUTINE  LOSS(IUPCNT,FREQ,EDGSHD,SURSHD,PROPLS,
      GR,GX,IR,IX)
C     ******************************************
C     SUBROUTINE LOSS.MD CONTAINING MODIFICATIONS
C     ******************************************
C     SUBROUTINE 'LOSS' COMPUTES THE EDGE SHADING, SURFACE
C     SHADING, AND PROPAGATION LOSS FOR THE EMI PROPAGATION
C     PATH
C     CONTAINED IN THE 'PATH' AND 'ISHADE' ARRAYS.  THESE
C     ARRAYS MUST BE COMPRESSED.
C     IUPCNT - UP COUNTING POINTER INDEXING 'PATH' ARRAY.
C     IN THIS CASE, THE  NUMBER OF PATH INTERSECTION
C     POINTS.
C     FREQ    - FREQUENCY AT WHICH LOSSES ARE TO BE
C     COMPUTED
C     EDGSHD - RETURNED / EDGE SHADING IN DECIBELS
C     (NEGATIVE)
C     SURSHD - RETURNED / SURFACE SHADING IN DECIBELS
C     (NEGATIVE)
C     PROPLS - RETURNED / PROPAGATION LOSS IN DECIBELS
C     (NEGATIVE)
C     GR      - RETURNED / RECEIVER ANTENNA GAIN IN
C     DECIBELS
C     GX      - RETURNED / TRANSMITTER ANTENNA GAIN IN
C     DECIBELS
C     IR      - RETURNED / 'GR' MAIN BEAM OR SIDE LUBE
C     FLAG
C     IX      - RETURNED / 'GX' MAIN BEAM OR SIDE LOBE
C     FLAG
C
C       INTEGER 1
        LOGICAL  MNBEAM
        INCLUDE 'ANTANG.FCB'
        INCLUDE 'ANTENA.FCB'
        INCLUDE 'PATH.FCB'
        INCLUDE 'ARCCAL.FCB'
        INCLUDE 'ARCRFT.FCB'
        INCLUDE 'RADIAN.FCB'
        LOGICAL  MNBMR, MNBMX
C
C     INITIALIZATION OF SHADINGS, DISTANCES AND ANGLES;
```

```
C
C     DISTOT  -  TOTAL PATH DISTANCE
C     DTSFCY  -  TOTAL DISTANCE OF PATH SEGMENTS PROCEEDING
C                ALONG FUSELAGE
C     ATSFCY  -  TOTAL CHANGE IN ANGLE OF PATH SEGMENTS
C                PROCEEDING ALONG FUSELAGE SURFACE.
C     DTSFCN  -  TOTAL DISTANCE OF PATH SEGMENTS PROCEEDING
C                ALONG CONE
C     ATSFCY  -  TOTAL CHANGE IN ANGLE OF PATH SEGMENTS
C     PROCEEDING ALONG CONE
C
      EDGSHD = 0.0
      SURSHD = 0.0
      DISTOT = 0.0
      DTSFCY = 0.0
      ATSFCY = 0.0
      DISFCN = 0.0
      ATSFCN = 0.0
C
C
C     THIS DO-LOOP IS EXECUTED ONCE FOR EVERY PATH
C     INTERSECTION POINT.  THE FIRST PORTION SUMS THE PATH
C     SEGMENT DISTANCES, AND FUSELAGE DISTANCES AND ANGLES
C     FOR PATH SEGMENTS PROCEEDING ALONG THE FUSELAGE.
C
C     THIS IS TO PRINT THE TWO ARRAYS PATH AND ISHADE
C
         DO 470  I = 1, IUPCNT
C
         DISTOT = DISTOT + PATH(IPASS,4,I)
         IPTYPE = ISHADE(IPASS,2,I)
         IF ( IPTYPE.NE.0 ) THEN
            DIST = PATH(IPASS,4,I)
            ANG = AVCCCS ( PATH(IPASS,2,I) -
                  PATH(IPASS,2,I-1) )
            IF (IPTYPE.EQ.1) THEN
C
C           THIS IS A CYLINDRICAL SEGMENT.  ADD THE DISTANCE
C            AND ANGLE TO THE TOTAL OF ALL CYLINDRICAL
C           SEGMENTS, BUT CYLSHD WILL USE THE MOST RECENT
C           VALUE FOR PHOFUS WHICH MAY NOT BE IDEAL.
C
               DISFCY=DISFCY+DIST
               ATSFCY=ATSFCY+ANG
             ELSE
C
C        THIS IS A CONICAL SEGMENT.  ADD THE DISTANCE   AND
C        ANGLE TO THE TOTAL OF ALL CONICAL  SEGMENTS, BUT THE
C        RADIUS USED WILL ONLY BE VALID FOR THE FINAL SEGMENT
C        (OK SINCE ONLY  ONE IS ALLOWED IN THE CURRENT, AND
C        FORSEABLE FUTURE, VERSIONS OF AAPG).
C
               DTSFCN=DTSFCN+DIST
C
```

```
C               ATSFCN=ATSFCN+ANG
C               RHCONE = SQRT (PATH(IPASS,1,I) *
C               PATH(IPASS,1,I-1))
             ENDIF
          ENDIF
C

  500     IF ( ISHADE(PASS,3,I) .NE. 1) GO TO 460
          IF ( I .EQ. 1 .OR. I .EQ. IUPCNT ) GO TO 460
C
C     THE CURRENT PATH INTERSECTION POINT IS A WING EDGE
C     DIFFRACTION POINT, THUS SUBROUTINE 'XY' RETURNS THE
C     POINT IN ORTHOGONAL COORDINATES SO THAT ITS BUTT LINE
C     CAN BE CHECKED TO DETERMINE WHICH WING IT IS ON.  THEN
C     FUNCTION  'WNGSHD' IS CALLED TO DETERMINE THE EDGE
C     SHADING FOR THE APPROPRIATE WING, AND THIS VALUE IS
C     ADDED TO PREVIOUS EDGE SHADING VALUES.
C
            CALL XY ( I, PNTX, PNTY, PNTZ )
            IF ( PNTX .LT. 0.0 ) GO TO 490
C
            EDGSHD = EDGSHD + WNGSHD (I, IUPCNT,
                     IEDGE(IPASS,2), .TRUE., FREQ)
            GO TO 460
C
  490       EDGSHD = EDGSJD + WMGSJD(I,IUPCNT,IEDGE(IPASS,1),
                     .FALSE.,FREQ)
C
C  >>>>>>>>>>>>>>>>>>>>>>>>>>>>>>>>>>>>>>>>>>>>>>>>>>>>>>>>>>>>
C
C   !!  THIS SECTION IS TO CALCULATE THE CONICAL SPIRALS
C       SHADING LOSS
C   !!  1982 AVAILABLE AT MCGILL U. ENG. LIB.
C
  400 IF (IPTYPE.NE.-1) GO TO 470
C
      ALF=(RHOF-RHOC)/FSN
      TETAZ=ATAN(ALF)
      IF (ISHADE(IPASS,L,I).NE.0) THEN
      WRITE(Z,*)'WRONG COORDINATE SYSTEM ??!!'
      WRITE(7,*)'PLEASE VERIFY..'
      ENDIF
C
      ER1=PATH(IPASS,1,I-1)/SIN(TETAZ)
      ER2=PATH(IPASS,1,1)/SIN(TETAZ)
      TERM=SORT(1+ALF*ALF)
C
C   !!  IN ORDER TC AVOID DIVISION BY ZERO
C
      IF (PATH(IPASS,2,I-1).EQ.0.0) PATH(IPASS,2,1-1)=01
      IF (PATH(IPASS,2,I).EQ.0.0) PATH(IPASS,2,I)=.011
C
      PHII=PATH(IPASS,2,I-1)
      PHIF=PATH(IPASS,2,I)
```

```
      ANGDI=ABS(PHIF-PHII)
C
      ARGU=ER2/PATH(IPASS,4,I)
C
      BREAK=ARGU*SIN(ANGDI*SIN(TETAZ))
      IF (BRAK.GT.1.0)BRAK=BRAK-1.
      OMG1=ABS(ASIN(BRAK))
C

      OMG2=ABS(OMG1+(PHIF-PHII)*SIN(TETAZ))
      CA=2+3.141592*FREQ
C
      CHA1=(.5*CA*ER1*SIN(OMG1)*SIN(TETAZ))**(1./3.)
      CHA2=ABS(PHIF-PHII)
      CHA3=COS(TETAZ)**(2./3.)
      CHAI=CHA1*CHA2*CHA3
C
      TTTE=((CA*PATH(IPASS,4,I)/CHAI)**(.5))
      TAU=TTTE*(2*(ca)**2,*ER1*ER2)**(-/16667))*
     &(SIN(OMG1)*SIN(OMG2)*COS(TETAZ))**(.3334)
C
      CSHD=20.*ALOG10(TAU)
      TEMP=RHOFUS
      RHOFUS=SQRT(PATH(IPASS,1,I-1)*PATH(IPASS,1,I))
C
      PERT=CYLSHD(PATH(IPASS,4,I),ANG,FREQ)
C
C !!  NOW THE TOTAL CONE SHADING WILL BE A COMBINATION
C !!  OF ASSERJIAN & INSHIMARU FORMULATION PLUS THE LEE
C !!  TERM
C
      SURSHD=SURSHD+CSHD+PERT
C
C >>>>>>>>>>>>>>>>>>>>>>>>>>>>>>>>>>>>>>>>>>>>>>>>>>>>>
C
      RHOFUS=TEMP
 470  CONTINUE
C
C  FUNCTION 'CYLSHD' IS CALLED TO COMPUTE THE SURFACE
C  SHADING IF THERE IS A LENGTH OF PATH ALONG THE FUSELAGE,
C  AND THEN THE PRUPAGATION LOSS IS CALCULATED, BUT ONLY IF
C  THE TOTAL PATH DISTANCE IS NOT MINISCULE (<1 MIL).
C
        . IF ( DISTOT .LE. 1.E-3 ) GO TO 475
C
          IF ( DTSFCY .NE. 0.0 ) SURSHD = CYLSHD ( DTSFCY,
          ATSFCY, FREQ )
C
.........................................................
C
C    >>> THE PART BETWEEN THE '...' IS COMMENTED OUT IF THE
C          ABOVE MOD.
C    >>> IS BEING USE <<
C  NOW REPEAT FOR THE CONE.  USE 'CYLSHD', TEMPORARILY
```

```
C  REPLACING  'RHOFUS' WITH 'RHCONE'.
C
C          TEMP = RHOFUS
C          RHOFUS = RHCONE
C          IF (DTSFCN.NE.0.0) SURSHD = SURSHD + C
C          YLSHD(DTSFCN,ATSFCN,FREQ)
C          RHOFUS = TEMP
C ..................................................

C
      PROPLS = 2.0 * ALOG10 (9.3895EB / ( FREQ * DISTUT ) )
C
C     LOGICAL FUNCTION 'MNBEAM' RETURNS .TRUE. IF THE EMI
C     PROPAGATION PATH GOES THROUGH THE ANTENNA'S MAIN
C     BEAM.  IT IS CALLED ONCE FOR THE RECEIVER ANTENNA AND
C      ONCE FOR THE TRANSMITTER ANTENNA.  IF THESE ANTENNAS
C     HAVE BEEN REVERSED (DURING THE SECOND PATHCOMPUTATION
C     PASS), AN ALTERNATE SET OF 'MNBEAM' CALLS IS
C     EXECUTED.
C
 475       IF ( RFIRST ) GO TO 510
C
           MNBMX = MNBEAM (1, 2, THTX1, THTX2, PHIX2 )
           MNBMR = MNBEAM ( IUPCNT, IUPCNT-1, THTR1, THTR2,
                   PHIR1, PHIR2 )
C
           GO TO 520
C
 510       MNBMX = MNBEAM ( IUPCNT, IUPCNT-1, THTX1, THTX2,
                   PHIX1, PHIX2 )
           MNBMR = MNBEAM (1, 2, THTR1, THTR2, PHIR1, PHIR2)
C
C     THE RECEIVER ANTENNA GAIN 'GR' IS SET TO EITHER ITS
C     MAIN BEAM VALUE OR SIDE LOBE VALUE, AND THE MAIN BEAM
C     - SIDE    LOBE FLAG 'IR' IS SET APPROPRIATELY,
C     DEPENDING ON WHETHER 'MNBMR' IS .TRUE. OR .FALSE..
C
 520   IF ( MNBMR ) GO TO 430
C
       GR = GMSLR
       TR = 1
       GO TO 440
C
 430   GR = GMBR
       IR = GMBR

C
C   THE SAME FOR THE TRANSMITTER ANTENNA GAIN 'GX' AND FLAG
C   'IX'
C
 440    IF ( MNBMX ) GO TO 450
C
        GX = GMSLX
        IX = 1
```

```
      RETURN
C
 450  GX = GMBX
      IX = 0
      RETURN
C
      END
```